Delevitation modelling of an active magnetic bearing supported rotor

Thesis submitted for the degree *Philosophiae Doctor*
at the Potchefstroom campus of the North-West University

Jan Jacobus Janse van Rensburg

Promoter: Prof. G. van Schoor
Co-promoter: Dr. P.A. van Vuuren
10 June 2014

"The more original a discovery,

the more obvious it seems afterwards."

Arthur Koestler

Acknowledgements

For “Oupa” Jan Jacobus Nel (1928 - 2013)

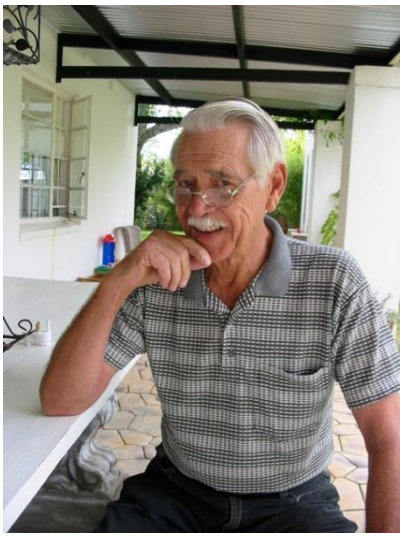

I would like to thank my promoters, Prof. George van Schoor and Dr. Pieter van Vuuren, for their help and motivation. To my wife Angelique, thank you for your support and understanding. To Janik Bessinger, a special thanks for his willingness to always listen. I would also like to thank Christian Vanek for his help during his visit to South Africa. I would also like to thank Prof. Izhak Bucher for the use of the rotor dynamics software RotFE. Lastly I would like to thank my parents, thank you for your support and the privilege of growing up in a loving home.

What a journey!

Abstract

The problem addressed in this thesis is the delevitation modelling of an active magnetic bearing (AMB) supported rotor. A system model needs to be developed that models the highly non-linear interaction of the rotor with the backup bearings (BBs) during a delevitation event. The model should accurately predict forward and backward whirl as well as the system forces experienced. To this end, the severity of rotor delevitation events should be characterised.

The contributions of the research include a more comprehensive model of a cross-coupled flexible rotor-AMB-BB system, a method to obtain repeatable experimental results, two methods for quantifying the severity of a rotor-drop (RDQ and $Vval$) and the simulation of forward whirl.

A simulation model (BBSim) was developed to predict the behaviour of a rotor in rolling element BBs in an AMB system during a rotor delevitation event. The model was validated using a novel rotor delevitation severity quantification method ($Vval$) to compare experimental and simulated results. In this study the force impulse values as the rotor impacts the BBs are seen as critical to monitor, as an indication of rotor drop severity. The novel quantification method was verified by comparing the impulse values of delevitation events to the values obtained for the same delevitation events using the novel quantification method.

The simulation model (BBSim) was developed by integrating and cross coupling various simpler models to obtain a model that could accurately predict the behaviour of a rotor during a delevitation event. A plethora of simulation results were generated for various initial conditions. The simulation results were used to perform a parametric study, from which the effects that certain design parameters have on the severity of rotor delevitation events are determined.

The novel quantification method results presented in this research compared well to the impulse values. Since most AMB systems that have BBs do not have force measurement capabilities, the development of the novel quantification method enables the quantification of rotor drop severity solely based on position data.

The simulation model BBSim was found to accurately predict the behaviour of a rotor during a delevitation event. The parametric study completed using BBSim revealed that the severity of rotor delevitation events is less sensitive to the bearing stiffness than the bearing damping. The parametric study also found that the severity of a delevitation event is slightly sensitive to the angle of delevitation. The friction factor between the rotor and the inner-race of the rolling element bearings moderately influences the severity of the rotor delevitation event.

The inertia of the rolling element bearing's inner-race and balls influences the behaviour in a complex manner, where the inertia should be kept as low as possible for actively braked rotors, and should be higher for free running rotors. The unbalance of the rotor plays a major role in the severity of rotor delevitation events. A rotor with a high unbalance usually tends to go into forward whirl, whereas low unbalance could promote the development of backward whirl if the inertia of the inner-race and the friction factor between the inner-race and the rotor are excessively large.

Some of the recommended future work to be done on BBSim Include investigations into load sharing, various failure modes of AMBs, the effect that rotor circularity has on the stability of AMB control and an investigation into forward whirl. Envisaged improvements that can be made to BBSim are the inclusion of an axial rotor AMB and BB model, cross-coupled with the existing BBSim model. Other improvements could be the inclusion of thermal modelling and the ability to simulate other

types of BBs. Future experimental work could include a comparison of simulated and experimental results of larger systems and using the developed quantification methods to refine the defined threshold values for the safe operation of AMB systems.

Keywords: Backup bearing; Auxiliary bearing; Catcher bearing; Retainer bearing; Modelling; Quantification; Physical system modelling; Rotor drop; Rotor delevitation; Active magnetic bearing

Contents

List of figures

List of tables

List of symbols

$\alpha_{Bearing_{Friction}}$	Bearing deceleration caused by rolling friction
$\alpha_{Bearing_{Total}}$	Total acceleration of the bearing inner-race
$\alpha_{InnerRace}$	Acceleration of the inner-race
$\alpha_{levitated}$	Deceleration of levitated rotor
α_{Rotor}	Rotational acceleration of the rotor
$\alpha_{Rotor_{Brake}}$	Deceleration of the rotor due to braking torque
$\alpha_{Rotor_{Total}}$	Total acceleration of the rotor
BF	Bouncing factor
C_{AMB}	AMB damping
C_{BB}	Damping constant of the BB
C_{Static}	Static load rating of the angular contact bearing
$D_{Mean_{Bearing}}$	Mean diameter on the angular contact bearing
$Dval$	Non-dimensionalised distance
e	Eccentricity
E_k	Kinetic energy
F_{AMB}	AMB force
$F_{centripetal}$	Centripetal force
$F_{contact}$	Contact force
$F_{friction}$	Friction force
$F_{max_{BB}}$	Maximum rated force of the backup bearing
F_{normal}	Normal force / Force caused by the deformation of the backup bearing
$F_{Preload}$	Axial preload force present on the angular contact bearings
$F_{u,x}$	Unbalance force in the x direction
$F_{u,y}$	Unbalance force in the y direction
I	Impulse
I_b	Bias current
$I_{InnerRace\&Balls}$	Polar moment of inertia of the inner-race and rolling elements of the backup bearing
I_p	Polar moment of inertia
$I_{perSecond}$	Impulse-per-second
I_{ref}	Reference current
I_{Rotor}	Polar moment of inertia of the rotor
K_{AMB}	AMB stiffness
K_{BB}	Stiffness of the BB
K_q	Constant describing the relationship between impulse and $Vval$
m	Mass
$M_{friction}$	Moment caused on the inner-race due to contact friction
m_{rotor}	Mass of the rotor

μ	Friction factor of the rotor on the inner-race of the bearing
n	Window size
n_{total}	Total number of samples
ω	Rotational speed
ω_{BB1}	Rotational speed of the inner-race of backup bearing one
ω_{BB2}	Rotational speed of the inner-race of backup bearing two
ω_{COM}	Rotational speed of the centre of mass of the rotor
ω_{factor}	Rotational speed factor
$\omega_{InnerRace}$	Rotational speed inner-race
ω_{Rotor}	Rotational speed of the rotor
R_{airgap}	Radius of the airgap
$R_{InnerRace}$	Radius of the inner-race
R_{rotor}	Radius of the rotor
RDQ	Rotor drop quality factor
s_{rotor}	Magnitude of the translational distance of the geometric centre of the rotor from the centre of the airgap
t	Time
τ_{air}	Aerodynamic torque
$\tau_{bearings}$	Bearing deceleration torque
$\tau_{braking}$	Deceleration torque on the rotor (aerodynamic and bearing)
$\tau_{BrakingTorque}$	Braking torque
θ	Phase angle of unbalance
v	Velocity
$v_{InnerRace}$	Surface speed of the inner-race
v_{rotor}	Surface speed of the rotor
$Vvala$	Non-dimensionalised velocity of the geometric centre of the rotor (averaged)
$Vval$	Non-dimensionalised velocity of the geometric centre of the rotor (maximum)
X_{rotor}	Rotor position in the backup bearing clearance in the Cartesian direction of x
Y_{rotor}	Rotor position in the backup bearing clearance in the Cartesian direction of y

List of abbreviations

AMB	Active magnetic bearing
ANEAS	Analysis of non-linear AMB systems
BB	Backup bearing
BBSim	Backup bearing simulation tool
BEAST	Bearing simulation tool
HBM	Harmonic balance method
PMB	Passive magnetic bearing
Rotor/BB	Rotor and backup bearing
TMM	Transfer matrix method
ZCAB	Zero clearance auxiliary bearing

Chapter 1

Introduction

1.1 Motivation

In recent years active magnetic bearings (AMBs) have become more popular due to their efficiency and ability to operate in extreme conditions [1]. In a conference paper presented in 2011 [2], Schweitzer states that the non-linear dynamics of rotor bearing interaction should be investigated. One of the reasons why the commercial use of AMBs in the industry is not more prolific [3], is the fact that the safety of AMBs cannot be guaranteed [4]. While this safety can also not be guaranteed with conventional bearings, the uncertainty regarding the safety has been clarified.

The failure of AMBs results in a highly non-linear interaction of the rotor with the backup bearings (BBs) [4-7]. The uncertainty of AMB failure safety lies mainly in this non-linear interaction between the rotor and BBs [7]. As stated in [2], touch-down dynamics are inherently non-linear and need to be investigated. Based on these statements, a need is identified to simulate the non-linear interaction of the rotor and BBs in order to clarify some of the uncertainty encountered during AMB failure.

The uncertainty encountered during AMB failure pertains to the forces involved, the rotor behaviour and the frequencies excited. The uncertainties lead to the question of selecting the appropriate BB. To answer this question, the conditions the BB are subjected to, need to be characterised. The conditions that the BBs are subjected to can be characterised by developing an accurate model for rotor delevitation events. The following paragraphs state some of the requirements of the model.

The model should be representative of the real life interaction of the rotor and BBs. In order to predict the behaviour of a highly non-linear system, the initial conditions play an important role since the initial conditions of the rotor system are primarily determined by the AMBs, an AMB model should also be included in the model.

The inclusion of a flexible rotor model enables the model to predict the critical frequencies of the system and accounts for the interaction of these critical rotor frequencies on the BB system. Lastly, a BB model enables the model to predict the forces experienced due to impacts and dynamic behaviour of the rotor.

The prediction of forward and backward whirl is also a major concern [1,2,8-14]. Simulations in the literature predict backward whirl while in the experimental work, forward whirl is observed [8,10,12]. The fact that the simulation models in the literature do not accurately predict the development of forward and backward whirl indicates some unmodelled phenomena [15].

The objective of this research is to accurately predict the behaviour of a rotor during a delevitation event in order to improve the safety of AMB levitated rotors. A reliable simulation of BBs could also eliminate the need for destructive testing and enable the optimisation of the system parameters before commissioning to make AMBs more economical.

BB-modelling research mainly focuses on either frequency-domain solving [6,16-26] or finite element method (FEM) analysis [7,11,15,16,27-47].

In frequency-domain solutions, the transient behaviour of the rotor and BB (rotor/BB) system is not modelled and in the case of rotor delevitation events, the transient behaviour of the rotor is especially important. While FEM analysis does model the transient behaviour of the rotor, this method is computationally intensive and the cross-coupling of the rotor/BB system is not clear.

In order to select appropriate BBs for a specific application, the fundamental physics responsible for specific rotor behaviour should be understood. The possibility exists to develop a model to transiently solve the dynamics of the rotor/BB interactions using fundamental physics. Using these fundamental formulae, conclusions can be made as to what parameters cause certain rotor behaviour and forces.

An explanation for forward whirl based on simulation results is required. Previous explanations relied on educated guesses [8,10,12]. Forward whirl has only been simulated recently (2013) [48], and is attributed to the contact force at the axial BB. Thus if the model can simulate forward whirl, an alternative explanation for this phenomena could be deduced since this model does not include the contact forces of the axial BB.

The integration of a flexible rotor model, an AMB model and a BB model integrated into a cross-coupled model has not been reported. The integration of the AMB model into the system model creates possibilities for simulating all of the failure modes of an AMB and the interaction this will have on the rotor/BB system.

Currently, the dynamic behaviour of rotor/BB interaction is not satisfactorily modelled and there is no quantitative method to determine the severity of a rotor delevitation event.

1.2 Problem statement

This thesis focuses on the delevitation modelling of an active magnetic bearing supported rotor. A system model needs to be developed that models the highly non-linear interaction of the rotor with the backup bearings during a delevitation event.

The model should accurately predict forward and backward whirl as well as the system forces experienced. To this end, the severity of rotor delevitation events should be characterised.

1.3 Research objectives

This study is divided into the following main research objectives:

Literature overview. The literature investigation focuses on the modelling and simulation of BBs to identify the current methods and assumptions. The spectrum of literature considered includes rotordynamics, AMBs, physical systems and modelling.

Develop a simulation model. After the detailed literature investigation on BB-modelling, a BB model is developed incorporating the components identified in the literature investigation.

Determine the unknown parameters using empirical methods. Since some of the parameters of the physical system cannot be measured directly, empirical methods are employed to determine these parameters.

Obtain simulation results. The developed simulation model is used to produce simulated results for varying initial conditions and system parameters.

Develop a severity quantification method for rotor delevitation events. The need to quantify rotor delevitation event severity arises from the fact that the rotor delevitation events are not perfectly repeatable. To enable quantitative comparison between experimental rotor delevitation events and simulated rotor delevitation events, a method to quantify the severity of each drop is required.

Validate developed quantification method. The developed quantification method should be validated using the simulated results.

Obtain experimental results. Various experimental results should be obtained by delevitating the rotor at various initial conditions.

Compare simulated and experimental data. The experimental and simulated results are compared in order to validate the simulation model.

Conduct a parametric study. Using the validated BB simulation model, a parametric study is done to determine the sensitivity of the rotor delevitation event severity to various parameters.

1.4 Research methodology

In order to address the objectives listed, the methodology as portrayed in the flowchart in Figure 1 is employed. Following the figure, each section is discussed in detail. Although some of the processes are iterative, only the final iteration is presented in the thesis.

1.4.1 Literature overview

After the investigation into BBs, the possible contributions are identified. The literature overview also serves as background for the development of a simulation model.

1.4.2 Develop a simulation model

The model is developed in Matlab® - Simulink® using the SimScape® solver environment. The model includes the translational movement of a point mass within the airgap of the BB, the rotational speed of the bearing inner-race and the friction between the bearing inner-race and the rotor.

Without inclusion of a flexible rotor model, the BB model as mentioned above is not a true representation of the rotor bearing system. The rotor model used is RotFE, a Matlab® toolbox created by Izak Bucher [49,50]. RotFE is however, not suitable for use within the Simulink® environment. RotFE is adapted by means of an S-function making the model speed-dependent. The rotor model is adapted to integrate the BB model mentioned in the previous paragraph. With the inclusion of a flexible rotor model, the BB model no longer simplifies the rotor as a point mass.

Concurrent with this research, a new nonlinear AMB model [51] was developed. This model is used in conjunction with the BB model. The proposed model now includes a flexible rotor, a BB model and an AMB model. The AMB model however is too computationally intensive to be included in the BB model and the model is simplified to a linear AMB model. The possibility to use the non-linear model is however, still available.

The sub-models mentioned above need to be coupled so that an event at one of the sub-models influences the behaviour in the other sub-models and vice versa. The sub-models are coupled using a combination of a friction model and the rotor model. The AMBs work in parallel to the BBs, but the BBs only start acting on the rotor when the airgap is exceeded. The parallel functioning of the BB and AMB sub-models enables load-sharing simulations. The Coulomb-friction model is used to determine the bearing inner-race speed-up and the slow-down of the rotor.

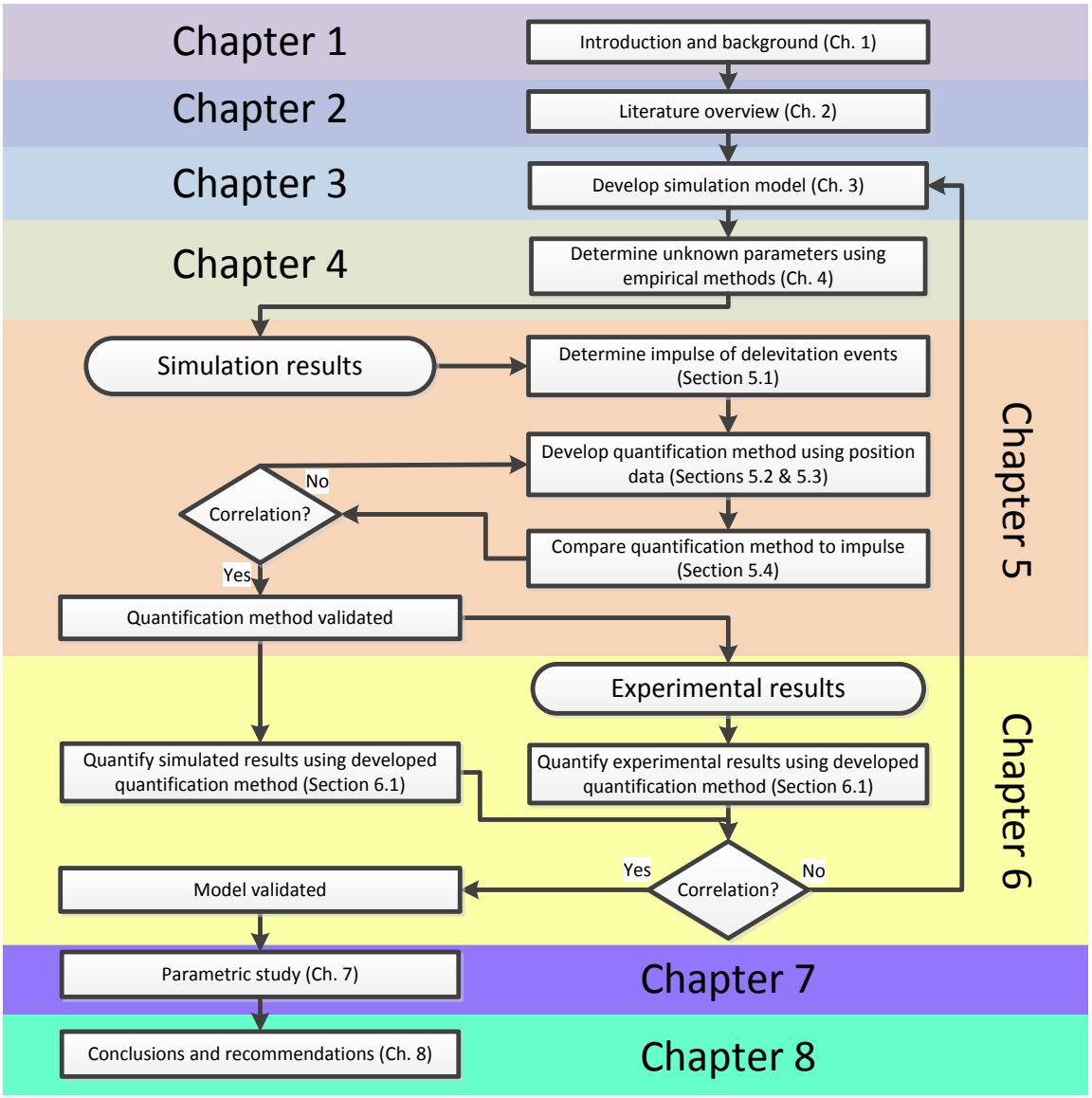

Figure 1: Flowchart of the research methodology and chapter breakdown

1.4.3 Determine the unknown parameters using empirical methods

The unknown parameters are determined using various empirical methods. The parameters determined using empirical methods are the BB clearances, the friction factor between the rotor and the inner-race of the bearings, the unbalance present on the rotor, the windage braking, internal bearing friction and the rotor circularity at the sensing locations. The empirical studies are conducted using the system as described in [52] but modified to use rolling element BBs. A detailed description of the system used to conduct the empirical studies can be found in Section 4.1.

1.4.4 Obtain simulation results

Simulation results are obtained for various initial conditions. The rotational speed of the rotor at the moment of delevitation is varied as well as the position of the rotor in the BB clearance.

1.4.5 Develop a quantification method for rotor delevitation events

The quantification should be a representation of the damage\degradation and the energy transferred to the BBs during the rotor delevitation event. Since most experimental systems do not have force measurement capabilities, the quantification method should utilize only the position data.

1.4.6 Validate developed quantification method

The quantification method is validated by comparing the impulse values for each of the simulated rotor delevitation events to the value of the developed quantification method that only uses the position data. If there is a good correlation between the impulse values and the developed quantification method, the quantification method is validated.

1.4.7 Obtain experimental results

The experimental results are obtained using the system as described in [52] but modified to use rolling element BBs. The results are produced for the whole operating speed range of the system and with each delevitation event repeated at four different locations within the BB clearance.

1.4.8 Compare simulated and experimental data

The experimental results are compared to the results obtained using the developed integrated BB simulation tool (BBSim). Results are compared by using the quantification method proposed in the previous paragraph. A secondary comparison is done by visually comparing the orbital plots and general behaviour of the rotor in the BBs.

1.4.9 Conduct a parametric study

Using the previously generated simulation results, a parametric study is completed to determine the sensitivity of the rotor delevitation severity to bearing stiffness, bearing damping, delevitation angle, friction between rotor and inner-race of the bearing, the inertia of the inner-race and balls of the bearing and the unbalance of the rotor.

1.5 Contribution of research

The contribution of the research towards BB knowledge is:

- A more comprehensive model of a cross-coupled flexible rotor-AMB-BB system [53]
- A method to obtain repeatable experimental results [54]
- Two methods for quantifying the severity of a rotor-drop (RDQ and $Vval$) [54,55]
- Simulation of forward whirl [53]

A detailed discussion on the contributions can be found in Section 8.5

1.6 Thesis layout

Chapter 2 gives a literature overview on the relevant literature namely magnetic bearings, rotor dynamics and BBs. The literature is then investigated on the current types of BBs available. The advantages and disadvantages of each are discussed. The next section in this chapter deals with the modelling of BBs. An investigation into the state of the art is done in order to highlight the current shortfalls of the research in the literature.

Chapter 3 deals with the conceptualisation of the BB model. The sub-models of an AMB/BB system are identified and developed. The sub-models discussed include the translational bearing model, the rotational bearing model, the AMB model and the rotor model. The integration and coupling of the various sub-models as well as the refinements of the model are discussed.

Chapter 4 discusses the empirical techniques used to determine some of the unknown parameters of the bearing model. The parameters discussed are the BB clearances, the friction factor between the inner-race of the bearing and the rotor, the unbalance present on the rotor, the aerodynamic losses, the internal bearing frictional losses and the rotor circularity.

Chapter 5 deals with the quantification of rotor delevitation events. Three different quantification methods are discussed namely the impulse of a rotor delevitation event, the rotor drop quality factor (*RDQ*) and the non-dimensionalised velocity of the geometric centre of the rotor (*Vval* and *Vvala*). *RDQ*, *Vval* and *Vvala* are validated by comparing these quantification methods to the impulse of rotor delevitation events.

Chapter 6 deals with the validation of the simulation model. The simulation model is validated by using the quantification methods developed in Chapter 5 and comparing simulated results to experimental results. The model is also validated by comparing various simulation and experimental orbit plots.

Chapter 7 presents a range of parametric studies done on the validated model. The parametric studies include the rotor sensitivity towards bearing stiffness, bearing damping, the angle of delevitation, the friction between the inner-race and rotor, the inertia of the inner-race and balls of the bearing and the unbalance of the rotor. The parametric results can be useful when designing AMB/BB systems.

Chapter 8 provides conclusions about the simulation model, the quantification methods and the method of model validation. The contribution of the research is highlighted and future work on this research topic is discussed.

Chapter 2

Literature overview

This chapter serves to familiarise the reader with the field of backup bearing (BB) modelling and the current state of the art in BB modelling and simulation. The broader background includes magnetic bearings, BBs and rotor dynamics. The literature overview is followed by a section on the guidelines currently stated in the literature when selecting an appropriate BB. Finally, the state of the art of BB modelling is discussed and a few shortcomings are highlighted.

2.1 Magnetic bearings

The levitation of rotors became a practical reality in the 1960s [56]. Magnetic bearings levitate rotors by means of magnetic forces [57]. There are two main types of magnetic bearings: passive magnetic bearings (PMBs) and active magnetic bearings (AMBs) [58]. In PMBs, permanent magnets are used to levitate a rotor while AMBs utilise electromagnets.

Figure 2 shows the basic layout of an AMB and BB system. In AMBs, levitation is achieved by controlling the reluctance forces generated by the electromagnets. The currents in the coils are controlled in relation to the rotor position.

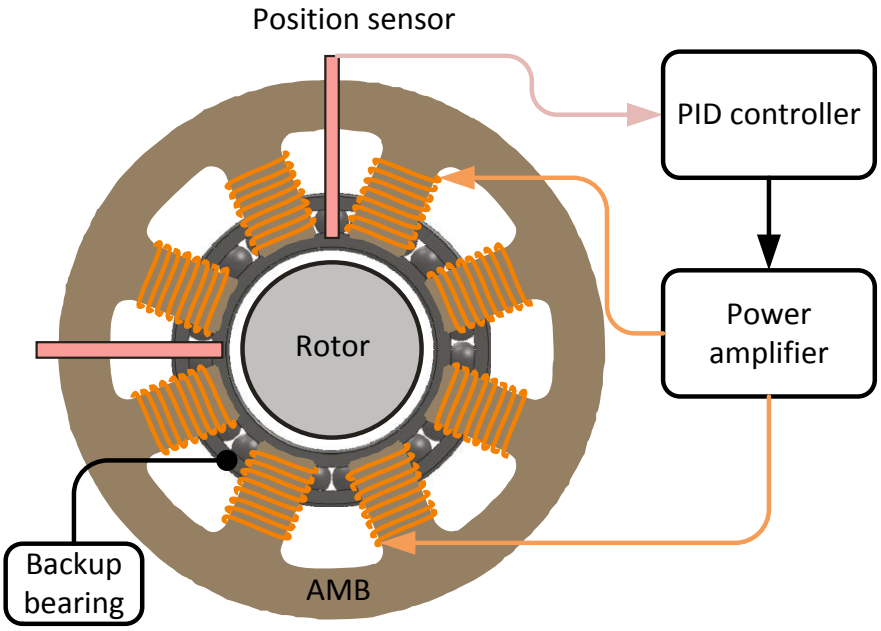

Figure 2: Illustration of the basic layout of an AMB and BB system

The position of the shaft is monitored by sensors which produce position signals that are fed to a controller. The controller generates an appropriate control signal for the power amplifiers which in turn provides the desired current to the electromagnets. The attractive force generated by the electromagnets then corrects the error as sensed by the position sensors [59]. The illustration shown in Figure 2 also shows the location of the BBs.

AMBs have several advantages when compared to rolling element bearings [58]. Some of these advantages are that AMBs do not have any mechanical wear, the bearing characteristics are

adjustable and the friction is very low. AMBs also offer the ability to monitor the system online and the ability to control vibration. The unique features of AMBs enable a diverse range of applications [57].

2.2 Backup bearings

BBs are used to protect the AMBs in the event of a system failure. Safety as defined by Schweitzer [4] "*is the quality of a unit to represent no danger to humans or environment when the unit fails*". BBs are used to improve the safety of AMB systems. AMBs can fail due to a fault in the AMB system or due to an overload imposed on the AMB.

A BB is set up with a clearance from the rotor. Currently using half the airgap of the AMB is the norm in BB design [8,12,13,60-62]. BBs are divided into five main types according to their physical layout [63]. The five types of BBs are plain BBs, rolling element BBs, planetary BBs, zero clearance BBs (ZCAB) and hydro-dynamic BBs.

Table 1 gives a comparison of the different types of BB technologies. As stated in [64] rolling element bearings and plain bearings are the most commonly used bearing types. This thesis focuses on rolling element bearings since it could be easily simplified to represent a plain bearing. Thus by developing a model for rolling element BBs the model can later be simplified to also represent plain BBs.

Table 1: Advantages and disadvantages of BB technologies [63,65]

BB type	Advantages	Disadvantages
Plain BBs	• Low-cost • Passive, no moving parts in bearing • Reduced potential for deterioration in standby mode • Condition, wear may be assessed by measuring clearance with AMBs	• Higher friction coefficients and heat generation during rundown
Rolling element BBs	• Low-cost • Low friction coefficients and heat generation during rundown • Potentially minimum volume with combined radial/thrust bearing	• Potential for bearing/cage damage during acceleration • Potential for deterioration in standby mode, contamination must be avoided • Windage induced rotation must be prevented in standby mode
Planetary BBs	• Reduced DN for given rotor diameter and speed • Low friction coefficients and heat generation during rundown	• Greater complexity and cost • Contamination must be avoided • Windage induced rotation must be prevented in standby mode • Potential for acceleration damage (reduced relative to rolling element bearings)
Zero clearance BBs	• Eliminates rotor-bearing gap during rundown • Extended run time capability • Reduced DN for given rotor diameter and speed • Low friction coefficients, heat generation during rundown	• Greatest complexity and cost • Actuation failures should be considered • Contamination must be avoided • Windage induced rotation must be prevented in standby mode • Potential for acceleration damage

BB type	Advantages	Disadvantages
Ceramic BBs	• High temperature operation • High harness • Low inertia (lower density) • Low coefficient of heat expansion • Self-lubricated ceramics have been shown to perform well	• Lower life than rolling element BB • Expensive • Theory not yet proven as in rolling element bearings • Inconsistent performance • Ceramics are porous • Non-uniform mechanical properties of the ceramics
Gas/Compliant-foil/hydrodynamic BBs	• The process fluid is used as the lubricant • Very low friction • Low noise • Low vibration • High and low temperature • High rotational precision • Long life	• Low weight bearing capability at low speeds • Impurities in working fluid could cause major damage, thus the reliability is reduced • Requires very high machining tolerances • Expensive

During a rotor delevitation event, the rotordynamics of the rotor plays a major role in the behaviour of the rotor. The complexity of rotordynamics is made worse in rotor drop situations because more non-linearities are added to the system. For instance, while the rotor is in contact with the BBs, the stiffness on the critical speed map will be at a relatively high value and when the rotor is not in contact, the value of the stiffness will be zero. The stiffness of the supports have a great influence on the behaviour of the rotor and the mode shapes of the critical frequencies as can be seen in Figure 3 and Figure 4.

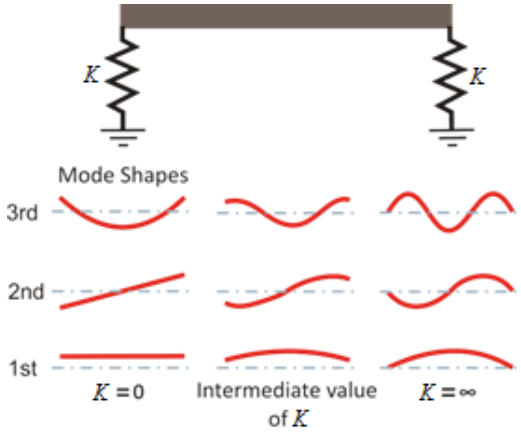

Figure 3: Effect of bearing support stiffness K on lateral vibration modes of a uniform shaft [66]

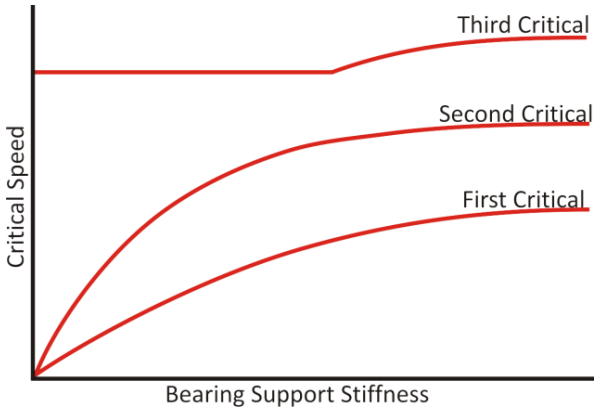

Figure 4: Critical speed map for three modes [66]

2.3 Design guidelines

When designing or selecting BBs, low friction is essential since higher friction forces could cause the development of destructive backward whirl. Good results have been obtained with ball bearings with coated rollers or rollers made of ceramics. No caging of the balls to reduce the inertia is also good practice. The lower inertia is essential when the bearing elements have to be accelerated toward the touchdown rotor speed. Selecting bearings with higher internal clearance to allow for thermal expansion is a good practice [4].

The landing sleeve should be made of high strength material and have a surface with low friction and great hardness. The support-structure should be rigid to maintain alignment, and the BB should be kept clean from contamination. Special components should be designed for impact damping, such as the corrugated ribbon design used in [8,13,14], or a damping ring as used in [9] or alternatively, a compliant mount as used in [67]. Contact time has to be kept short to avoid overheating of the BBs and the rotor should be actively slowed down or recovered by control actions [4].

However, the optimal design of BBs still relies mostly on experience and "*a systematic, generally accepted design procedure has yet to be developed"* [2]. According to Schweitzer [4], "*safety can only be improved, never guaranteed"*. He also states that further research is required for guidelines on the design of BBs. To gain insight into the selection of BBs, a simulation model is required.

2.4 Modelling techniques

In this section, various modelling techniques from the literature are described. The aim is to give an overview of the state of the art. Each paragraph gives a short description of the modelling technique used and some of the conclusions made based on the results that the model delivered. A summary of all the models discussed is given in Table 3 including all the modelled and unmodelled effects.

In [68], Karpenko *et al.* investigate the dynamics of a non-linear and discontinuous rotor system. They examine the effect of bearing clearances on the system dynamics. They use Poincare maps and other visualization tools to represent the results. The model is non-dimensionalised and includes unbalance and bearing clearances. The model proved the existence of periodic and quasi-periodic motions. These motions indicate that the behaviour of the rotor in the BBs is not chaotic.

Kirk *et al.* [69] describe the use of the commercial bearing and rotor dynamic bearing analysis program, DyRoBeS, to analyse the ISO NEDO test rotor and other bearing systems with more than two bearings.

The proper design of any AMB system requires the knowledge of all the dynamic loads that the system will experience in its planned life. The forces acting on a rotor system before and after failure of a bearing system are given in Table 2. The three columns summarise all the forces acting on the rotor. The first column are the forces produced by the AMBs. The second column displays forces that are always present, namely the rotor unbalance and gravity. The last column is a summary of the forces produced by the interaction of the rotor and BBs after AMB failure.

Table 2: Forces acting on rotor before and after AMB failure [69]

Forces before AMB failure	Forces independent of failure	Forces after AMB failure
Magnetic bearing force $F_{AMB} = K_{AMB} s_{rotor} + C_{AMB} \dot{s}_{rotor}$	Unbalance $F_{u,x} = me\omega^2 \cos(\omega t + \theta)$ $F_{u,y} = me\omega^2 \sin(\omega t + \theta)$	Contact force between rotor and bearing (Hertzian or Coulomb) $F_{friction} = f(F_{contact}, \mu)$
Bias current load (Preload)	Gravity $F_g = Ma_g$	Inner-race contact dynamics As the inner-race starts to rotate, the sliding friction will transform into static friction or bearing friction
		BB stiffness and damping The stiffness and damping is a function of the deformation of the BB
F_{AMB} AMB force, K_{AMB} AMB stiffness, s_{rotor} Rotor position, C_{AMB} AMB damping, $F_{u,x}$ unbalance force in the x direction, $F_{u,y}$ unbalance force in the y direction, m mass, e eccentricity, ω rotational speed, t time, θ phase angle of unbalance, $F_{friction}$ Friction force, $F_{contact}$ Contact force, μ Friction factor of the rotor on the inner-race of the bearing		

Flowers *et al.* [27] investigate the steady-state behaviour of a rotor by using the finite element method. The results are discussed for a wide range of input variables, i.e. rotor-imbalance, the support stiffness and damping. It is assumed that the BBs are identical in terms of stiffness, damping and friction. In this paper, the authors found that clearance plays a significant role in the behaviour of the rotor. The authors also found a correlation between the value of the imbalance and some sub harmonics which does not correlate to any of the system's critical frequencies.

In [45], Orth and Nordmann investigates ANEAS (**A**nalysis of **N**onlin**E**ar **A**MB **S**ystems). ANEAS is a modelling tool for non-linear dynamics of AMB systems. ANEAS is a fairly complete simulation tool that has the following features:

- Friction
- Simplified stator dynamics
- Rotor deceleration due to bearing friction
- Inner-race acceleration
- Non-linear damping
- An AMB model
- Simulates more than one BB
- Transient simulation
- Simulates plain and rolling element BBs
- A flexible rotor model

Although the included features are quite comprehensive, ANEAS lacks the following features:

- Unbalance simulation
- Active braking of the rotor
- The AMB model does not include non-co-location of the sensors and the AMBs
- Load-sharing between the AMBs and the BBs
- Thermal analysis
- Impact analysis
- Dynamics of the rotor during non-contact with the BBs
- BB defects

The unmodelled dynamics of the rotor-bearing system means that ANEAS cannot provide an accurate simulation of real world situations.

In [6], Zu and Ji improve on the transfer matrix method and implement it on non-linear rotor-bearing systems. The rotor is described using Timoshenko beam theory. The bearing model utilises cubic non-linear spring characteristics and a linear damping coefficient. The model only includes a rigid rotor model and thus the high excitation frequencies caused by a flexible rotor remains unmodelled. The model also does not include a friction model. As will be shown later in Section 7.3 and 7.4, the friction between the rotor and the BBs influences the rotor behaviour as well as the acceleration of the inner-race of the BB. Friction also contributes to the occurrence of whirl [37] and thus the model can't be used to accurately predict the forces in the system and the behaviour of the rotor.

Cuesta *et al.* [7] describe a simple model for the behaviour of a rotor in contact with the BBs. A non-linear model is proposed to model the highly non-linear behaviour of the rotor during contact. The model is separated into two regimes: one for levitation and one for a contact situation. Rigid body theory for planar collision is considered for the description of the impacts between the BB and the rotor.

Sopanen and Mikkola present a model of a deep-groove ball bearing including defects [19,20]. The modelled bearing is a six-degree-of-freedom bearing. The model includes descriptions of non-linear Hertzian contact deformation and elastohydrodynamic fluid film. Although this model was not intended to be used as a model for a BB, the same principles can be used to model defects in a BB. The model was implemented in a commercial product named MSC.ADAMS. This thesis however will not discuss the modelling of BB defects.

In [29], Sahinkaya *et al.* present an alternative modelling technique for a rotor in contact with the BBs. The authors state that highly non-linear normal contact forces can be estimated using Hertzian theory. This model uses Coulomb friction modelling.

In [36], Sahinkaya *et al.* discuss the performance of some linear controllers while the AMBs are still active. The authors also state that during contact with the BBs, some controllers may worsen the rotor response. The reason for the worsening of the response is attributed to phase shifts in the measured vibration response. Thus the need is identified to be able to simulate AMB-BB load-sharing. The simulation of load-sharing can be used to optimize controllers for load-sharing situations. The ability to simulate AMB/BB load-sharing is viewed as essential for the proposed model as discussed in Chapter 3.

In [37], Sun *et al*. present a detailed ball bearing model for BB applications. The results of this publication reveal that the friction coefficient, support damping and side loads are critical parameters in the simulation of BBs and the prevention of backward whirl.

Ji *et al.* [22] introduce a method of obtaining approximate solutions and chaotic motions of a piecewise nonlinear-linear oscillator. This type of nonlinear characteristics (stiffness and damping) are frequently encountered in mechatronic systems with clearances. The behaviour of the rotor is explained with the use of bifurcation diagrams, Lyapunov exponents, Poincare maps, phase portraits and basins of attraction. It was found that the initial conditions play a significant role in the resultant motion of the system. Because the initial conditions play such a big role in the resultant motion of the rotor, the initial conditions need to be accurately modelled to simulate the resultant motion of the rotor accurately.

Půst [38] investigates the dynamic effects of a rotor suspended by passive magnetic bearings and in contact with the BBs. This model neglects the inertia of the inner-race of the BB. As shown later in Section 7.4, the inertia of the inner-race of the BB needs to be taken into account since it will determine the acceleration of the inner-race. The acceleration of the inner-race in turn determines the time the inner-race takes to reach the same surface speed as the rotor and this influences the presence of contact friction that can contribute to the occurrence of whirl as discussed later in Section 7.3.

Villa *et al.* [23] present another reduction method using the invariant manifold approach applied to the non-linear dynamics of a rotor-bearing system. The invariant manifold approach brings the concept of modal analysis to nonlinear problems. The solution of the Eigen problem of a rotor is a computationally intensive problem. The strategy presented is to allow the determination of the linear invariant manifolds for several spin speeds based on only a few calculated ones.

Sun [31] presents a detailed bearing and damper model. The model is determined using the material, geometry, speed and preload with the nonlinear Hertzian load–deflection formula. The thermal growths of bearing components during the rotor drop are estimated using a 1D thermal model. This work is a continuation of the work done in [37] with the addition of a non-linear damper model and the inclusion of thermal growth.

Amer and Hegazy [24] model the vibration of a rotor subjected to a periodically time-varying stiffness by using a coupled second order non-linear ordinary differential equations with quadratic and cubic non-linearities. The authors found that different shapes of chaotic motion exist and it is shown that the system parameters have different effects on the non-linear response of the rotor. The non-linearities introduce phenomena not found in linear systems. These include jumping, multiple solutions, modulations, shift in natural frequencies, generation of combination resonances, evidence of period multiplying bifurcations and chaotic motions.

Kärkkäinen *et al.* [32] present the transient simulation of a rotor drop onto BBs. The authors state that the design parameters have a significant influence on the behaviour of the rotor during a drop event. The model includes a detailed ball bearing model including damping, stiffness, the oil film properties and the friction between the races and rolling elements. The model also includes the combined inertia of the rotating parts, unbalance and the stiffness and damping of the support.

Keogh and Cole [70] present a paper on the effect of misalignment of the BBs has on the ability of AMBs to recover the rotor. The authors find that the results obtained for alignment and misalignment are comparable. This is contradictory to the findings of Kärkkäinen *et al.* in [11].

Kärkkäinen *et al.* [39] describe the simulation of a flexible rotor during a drop onto BBs. The paper focuses on the effect the chosen number of modes used in the component mode synthesis has on the accuracy of the simulation. The paper also describes the effect of different friction models and concludes that Coulomb friction is sufficient for simulating rotor drop events. As shown in Chapter 3, Coulomb friction is also used for the proposed model within this thesis.

Popprath and Ecker [40] examine the dynamics of a rotor in contact with an elastically suspended stator. The model is deduced for a Jeffcott-rotor having intermittent contact with the stator. This model implicates the stator model only when contact occurs. The sub-model of the stator is an additional vibratory system. The results illustrate the importance of modelling the stator dynamics. The stator dynamics can have a significant influence on the resultant motion of the rotor and the

forces experienced by the BBs. Based on these results, the stator dynamics is also included in the model presented in Chapter 3.

In [34], Braut *et al.* model blade-loss in rotor-dynamic systems. This paper does not concern itself with BBs but with normal bearings in a sudden unbalance situation. This sudden unbalance can occur with AMB systems and should be included in any BB-rotor model. Although the model presented in Chapter 3 has the ability to model sudden blade-loss, this thesis does not investigate the phenomena and is included in future work.

Ransom *et al.* [15] present a paper about a numerical tool able to account for flexible rotor and stator dynamics, BB stiffness and the damping in the system. Testing and modelling is done on a vertical rotor. The authors state that in a vertical machine, forward/backward whirl is more likely because of the absence of the stabilizing gravity force present in horizontal machines.

Xie *et al.* [44] present a detailed model of the AMB supported rotor BBs. This model includes discontinuous stiffness caused by the bearing clearance. The bearings can be modelled in compliant mounts or rigid mounts. Nonlinear Hertzian contact stiffness and Coulomb friction forces are included. Gyroscopic effects can have a major influence on the critical frequencies of flexible rotors but were neglected. As shown in Chapter 3, the gyroscopic effects are included in the presented model by using a flexible rotor model.

Ishida and Inoue [43] present a model of a vertical rotor system's radial BB operating above the first two bending modes. The mathematical models for contact and friction forces which exist during contact were considered. The rotation of the inner ring of the BB is also considered and modelled.

2.5 Shortcomings

The non-linear nature of BBs complicates the modelling of BBs and rotor delevitation events. The literature has a plethora of different models available, as shown in Table 3. The models currently available in the literature cover a wide range of influencing factors although these factors are not simultaneously investigated. Most of these models ignore many of the transient effects present on the rotor or bearing. These transients experienced by the bearings and the rotor could influence the rotor's behaviour in an unpredictable manner.

The frequency-domain simulations are useful for predicting the steady state behaviour of the rotor, but the critical time-transient bearing forces experienced during a rotor delevitation event is not modelled. Modelling of the transient forces is necessary to select appropriate BBs. The models currently in the literature are still fairly incomplete. The models do not include all of the influencing factors necessary to realistically model a rotor delevitation event.

A summary of the models currently in the literature is given in Table 3. The models are divided into two groups, analytical and numerical. These two groups are summarized and two of the most complete models in each category are broken down in detail. The table marks the factors that are included in the model with a ☑ and the factors not included are marked with an ☒.

The most complete models available in the analytical field are those utilizing the transfer matrix method (TMM) and the harmonic balance method (HBM). The most complete numerical models are BEAST (**BEA**ring **S**imulation **T**ool) and ANEAS (**A**nalysis of **N**onlin**E**ar **A**MB **S**ystems). As shown in Table 3, these models are still fairly incomplete.

The developed BB and rotor model (BBSim) is also shown with all the factors that are included in this model. The factors not included in BBSim are a rigid rotor model, thermal modelling, a steady state simulation and BB defects.

The inclusion of a rigid rotor model is not deemed necessary since a flexible rotor model is included. The thermal analysis of the rotor delevitation event may be important in certain situations but for the sake of simplicity and solving time, a thermal analysis was not included. The inclusion of thermal modelling is seen as future work.

A steady state solution for the behaviour of the rotor is not done, since the forces of interest are the transient forces, a steady state solution would be unnecessary.

BB defects is an important factor in determining the behaviour of a rotor in worn or near to replacement BBs. In this simulation, the assumption is made that the behaviour of the rotor in new, well manufactured BBs is similar to the behaviour of the rotor in a bearing with no defects.

The percentages shown in the last row of Table 3 reflect the percentage that the particular factor has been included in the models in the literature. Most of the factors are included in less than 30% of the models. The factors included in BBSim have never been simultaneously simulated to determine the effect these factors have on each other and the rotor behaviour.

Table 3: Current simulations and models in the literature

Type of model	Effects	Flexible rotor model	Rigid rotor model	Unbalance	Friction	Rotor braking	Simulation of the stator	Rotor deceleration due to RE-BB friction	Inner-race acceleration	Non-linear damping	Non-co-location	AMB model	Capable of simulating load sharing	Ability to simulate more than one coupled BBs	Ability to simulate non-identical coupled BBs	Thermal analysis	Transient simulation	Steady state simulation	Can simulate plain BBs	Can simulate rolling element BBs	Impact analysis	Capable of simulating contacting and non-contacting state	Simulates BB misalignment	Includes BB defects	Non-linear bearing stiffness	Sudden unbalance (blade loss) simulation	Vertical machines	Horizontal machines	References
Analytical		☑ 3(S)	☑	☑ 5	☑	☒	☒	☒	☒	☑ 3	☒	☑ (VS)	☑	☒	☒	☒	☒	☑ 9	☑ 5	☑ 2	☒	☑	☑	☑ 2	☑	☒	☑	☑ 5	[16-25]
TMM (A)		☒	☑	☑	☒	☒	☒	☒	☒	☒	☒	☒	☒	☑	☑	☒	☒	☑	☒	☒	☒	☒	☒	☒	☑	☒	☒	☒	[6]
HBM (A)		☑ (S)	☒	☑	☒	☑	☒	☒	☒	☒	☒	☒	☒	☑	☑	☒	☒	☑	☒	☒	☒	☒	☒	☒	☒	☒	☒	☒	[6,25,26]
Numerical		☑ 7	☒	☑ 18	☑ 14	☑	☑ (S)	☑ 5	☑ 7	☒	☒	☑ 7(S)	☑ 6	☑ 6	☑ 4	☑ 2	☑ 15	☑ 3	☑ 13	☑ 7	☑ 10	☑ 14	☑	☒	☒	☑ 5	☑ 3	☑ 13	[7,11,15,16,27-44]
ANEAS (N)		☑	☑	☒	☑	☒	☑	☑	☑	☑	☒	☑	☒	☑	☑	☒	☑	☒	☑	☑	☒	☒	☒	☒	☑	☑	☒	☒	[45]
BEAST (N)		☒	☒	☒	☑	☒	☒	☒	☒	☑	☒	☒	☒	☒	☒	☑	☑	☒	☒	☑	☑	☒	☒	☑	☑	☒	☒	☒	[46,47]
BBSim (Presented model)		☑	☒	☑	☑	☑	☑	☑	☑	☑	☑	☑	☑	☑	☑	☒	☑	☒	☑	☑	☑	☑	☑	☒	☑	☑	☑	☑	Key: (S) – Simplified model (VS) – Very Simple model
Percentage of models that include this feature		28%	5%	63%	43%	5%	5%	15%	20%	13%	0%	23%	18%	23%	18%	8%	43%	35%	48%	28%	28%	38%	5%	8%	10%	15%	10%	45%	

NOTE: The percentage below the ☑ represents the proportion of the models referenced in the last column that include this feature

2.6 Conclusion

From the literature presented in Chapter 2 the following conclusions can be made. Firstly, the literature is divided on whether the behaviour of the rotor is chaotic [2,22,24,27,60] or not [68]. Secondly, it is necessary to include the ability to simultaneously model multiple bearings [69]. Thirdly, to accurately model the behaviour of the rotor during a delevitation event, the model should include the modelling of all the forces acting on the rotor as shown in Table 2. Lastly using a Coulomb friction model is sufficiently accurate for use in transient rotor delevitation event simulation [39].

The conclusions drawn from the literature are used to determine the effects to be modelled in the proposed model. The effects included in the model are shown in Table 3. An important observation made from the literature is that all the effects mentioned in Table 3 have never been simultaneously modelled. Secondly, the simulation of non-co-located BBs, AMBs and position sensors has not yet been implemented.

In Chapter 3, the conceptualisation of this model and the breakdown of the model into simpler models are discussed. Then each of these simpler models are investigated. After the discussion on each of the sub-models, the integration and cross-coupling of these models are investigated.

Chapter 3

Model conceptualisation

From the investigated literature given in Chapter 2, the need for a more complete backup bearing (BB) model was identified. In this chapter, the conceptualisation of this model is presented. The chapter provides the rationale behind the formulation of the sub-models and the integration and coupling of these sub-models into the final BB simulation (BBSim) model.

3.1 BBSim modelling principles

The stiff nature of any BB model requires the initial values before the delevitation of the rotor to be accurately modelled (i.e. the events prior to the delevitation of the rotor should also be modelled). In the case of BBs, the factors that determine the initial values are the AMBs and the rotor unbalance. This means that the unbalance should be known and accurately modelled. This also requires the AMB model to be an accurate representation of the real-world equivalent.

Following the delevitation of the rotor, the next step in the modelling of the event is the determination of when contact occurs between the rotor and the bearing inner-race. The size of the airgap needs to be known for each individual bearing. Although the airgap is specified during the design of the system, manufacturing tolerances on both the bearing and the rotor influence the size of the airgap. Should the stator be modelled, the BB moves relative to the housing after the first impact. This motion of the BB has to be taken into account to determine if contact is occurring.

The forces on the rotor during contact need to be determined. These forces are highly dependent on the stiffness and damping of the bearing and the stator. this means that the stiffness and damping of both the bearing and the stator have to be determined with great accuracy. After initial contact occurs, the rotational motion of the rotor will impart a torque on the inner-race of the BB and this torque will cause the bearing inner-race to accelerate. The acceleration of the bearing inner-race will continue while there is contact and until the surface speeds of the rotor and the bearing inner-race are equal. When the surface speeds are equal, the friction force of the bearing on the inner-race will, in effect, be zero since there is no relative motion between the rotor and the inner-race. There are however, still rolling and internal bearing friction present when the surface speeds of the rotor and the bearing inner-race are equal.

The contact between the inner-race and the rotor also causes the rotor to experience a translational force. The translational force causes the rotor to move inside the BB airgap radius. The translational movement of the rotor at the bearing locations is highly cross-coupled. Consequently, the translational movement at each bearing location influences the translational movement at all other bearing locations. The rotor model should accurately represent the real-world rotor to accurately cross-couple the BBs.

The foregoing principles are discussed in greater detail in the rest of this chapter. Firstly, the overall BBSim concept is presented. Secondly, an explanation of the translational model with focus on the contact and stator model is presented. Next, the rotational model is presented with a focus on the friction model, the rotational dynamics of the inner-race and rotor and the modelling of the circularity of the sensing surface. This is followed by the introduction of the AMB and rotor models used in BBSim. Lastly, the cross-coupling of all of the sub-models is discussed.

3.2 BBSim model concept

The concept of the BBSim model is the division into simpler sub-models of the complex interaction between the rotor, the AMBs and the BBs. The main sub-models include a rotor-model, AMB-models and BB/stator-models in the translational direction and the rotational direction. A representation of the rotor, AMB and translational BB sub-models are shown in Figure 5. Figure 6 shows a representation of the rotational BB model. Detailed discussions of the translational BB model, the rotational BB model, the AMB model and the rotor model are given in Sections 3.3, 3.4, 3.5 and 3.6 respectively.

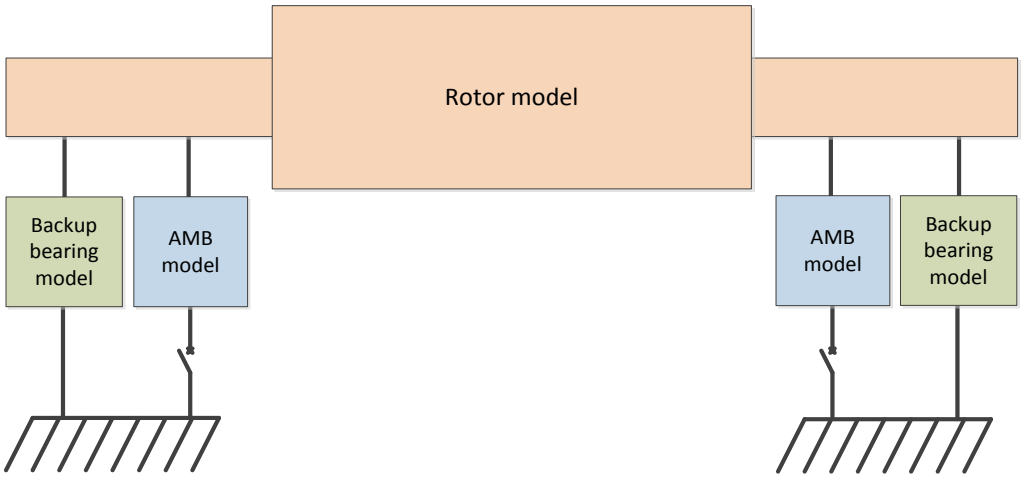

Figure 5: Schematic of the translational model concept

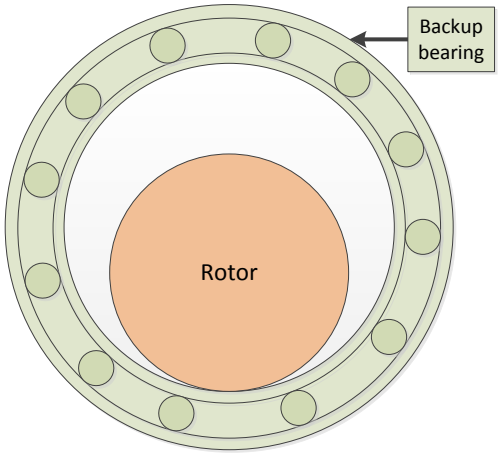

Figure 6: Schematic of the rotational model concept

3.3 The translational BB sub-model

This section focuses on the translational BB sub-model shown in green in Figure 5. Firstly, it is important to note that each BB is divided into two models: an x-axis and a y-axis model. The coupling of the x-axis and y-axis models is explained in Sections 3.4.1 and 3.7.

3.3.1 Airgap and contact modelling

The airgap can be defined as a span of co-ordinates where there is no force acting on the rotor. Should the airgap be exceeded, the Newtonian mechanics differential equations as shown in (3.1) are valid.

$$F_{normal} = \begin{cases} 0 & if \quad s_{rotor} < R_{airgap} \\ K_{BB} \cdot (s_{rotor} - R_{airgap}) + C_{BB} \cdot \dfrac{d(s_{rotor} - R_{airgap})}{dt} & if \quad s_{rotor} \geq R_{airgap} \end{cases} \tag{3.1}$$

with F_{normal} the magnitude of the normal force experienced by the BBs, K_{BB} the stiffness of the BB, s_{rotor} the magnitude of the translational distance of the geometric centre of the rotor from the centre of the airgap, R_{airgap} the radius of the airgap and C_{BB} the damping constant of the BB.

Determining the airgap is problematic since the cartesian components of the airgap cannot be represented with constants. If X_{airgap} and Y_{airgap} (as illustrated in Figure 7) were constants, the boundary produced would be square.

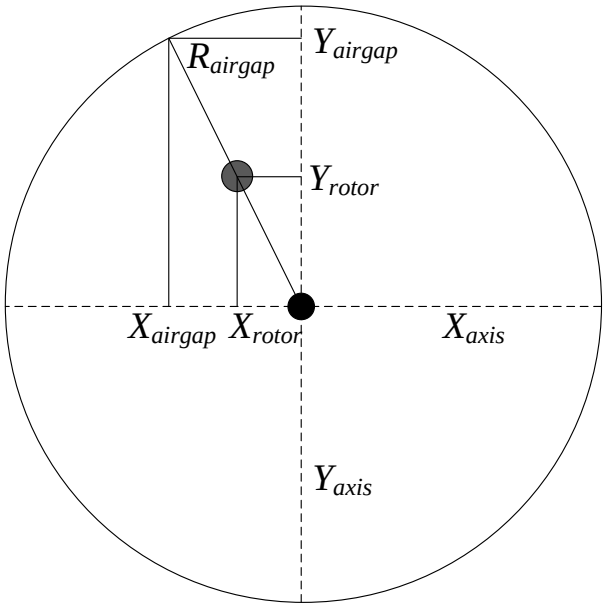

Figure 7: Illustration defining the airgap calculation

From Figure 7, it can be deduced that the triangle 0-X_{rotor}-Y_{rotor} is congruent to triangle 0-X_{airgap}-Y_{airgap}. with X_{rotor} and Y_{rotor} known, R_{rotor} is solvable using (3.2).

$$R_{rotor} = \sqrt{X_{rotor}^{\ 2} + Y_{rotor}^{\ 2}} \tag{3.2}$$

The two triangles will always be congruent. This means that the relationship shown in (3.3) is always true.

$$\frac{X_{rotor}}{R_{rotor}} = \frac{X_{airgap}}{R_{airgap}} \rightarrow \frac{Y_{rotor}}{R_{rotor}} = \frac{Y_{airgap}}{R_{airgap}} \rightarrow \frac{X_{rotor}}{Y_{rotor}} = \frac{X_{airgap}}{Y_{airgap}} \tag{3.3}$$

Using (3.3) we determine X_{airgap} and Y_{airgap} shown in (3.4). Keep in mind that the values of X_{airgap} and Y_{airgap} are calculated for each time-step.

$$\begin{aligned} X_{airgap} &= R_{airgap} \times \frac{X_{rotor}}{R_{rotor}} = R_{airgap} \times \frac{X_{rotor}}{\sqrt{X_{rotor}^{\ 2} + Y_{rotor}^{\ 2}}} \\ Y_{airgap} &= R_{airgap} \times \frac{Y_{rotor}}{R_{rotor}} = R_{airgap} \times \frac{Y_{rotor}}{\sqrt{X_{rotor}^{\ 2} + Y_{rotor}^{\ 2}}} \end{aligned} \tag{3.4}$$

Rewriting (3.1) into the forms shown in (3.5), (3.6) and (3.7) gives equations of the normal force experienced by the BBs in the direction of the cartesian axes.

$$F_{normal} = \sqrt{F_{normal_x}^2 + F_{normal_y}^2} \tag{3.5}$$

$$F_{normal_x} = \begin{cases} 0 & if \quad |X_{rotor}| < X_{airgap} \\ K\cdot(|X_{rotor}| - X_{airgap}) + C\cdot\dfrac{d(|X_{rotor}| - X_{airgap})}{dt} & if \quad |X_{rotor}| \geq X_{airgap}, \; X_{rotor} > 0 \\ -\left(K\cdot(|X_{rotor}| - X_{airgap}) + C\cdot\dfrac{d(|X_{rotor}| - X_{airgap})}{dt} \right) & if \quad |X_{rotor}| \geq X_{airgap}, \; X_{rotor} \leq 0 \end{cases} \tag{3.6}$$

$$F_{normal_y} = \begin{cases} 0 & if \quad |Y_{rotor}| < Y_{airgap} \\ K\cdot(|Y_{rotor}| - Y_{airgap}) + C\cdot\dfrac{d(|Y_{rotor}| - Y_{airgap})}{dt} & if \quad |Y_{rotor}| \geq Y_{airgap}, \; Y_{rotor} > 0 \\ -\left(K\cdot(|Y_{rotor}| - Y_{airgap}) + C\cdot\dfrac{d(|Y_{rotor}| - Y_{airgap})}{dt} \right) & if \quad |Y_{rotor}| \geq Y_{airgap}, \; Y_{rotor} \leq 0 \end{cases} \tag{3.7}$$

Furthermore, substituting (3.4) into (3.6) and (3.7) gives equations that determine the normal contact force in the cartesian directions, dependent only on the position of the rotor within the BB clearance (X_{rotor} and Y_{rotor}), and the constants K (bearing stiffness), C (bearing damping) and R_{airgap} (airgap radius). These normal forces can then be used to determine the friction forces in the cartesian directions - more on this in Section 3.4.1.

3.3.2 Backup bearing and stator modelling

The BB and stator are modelled using damping, stiffness and mass. The differential equations for stiffness, damping and mass are given by (3.8), (3.9) and (3.10) respectively.

$$F_{stiffness} = K\cdot s \tag{3.8}$$

$$F_{damper} = C\cdot\frac{ds}{dt} \tag{3.9}$$

$$F_{mass} = m\cdot\frac{d^2 s}{dt^2} \tag{3.10}$$

with s the displacement, K the stiffness constant, C the damping constant and m the mass of the respective elements.

The BB and stator are modelled using these basic elements as shown in Figure 8. The stator is modelled as a rolling element bearing mounted on a damper. The stator and the bearing translational models are inseparable. The vibrational characteristics of the BB and the BB-housing are dependent on each other.

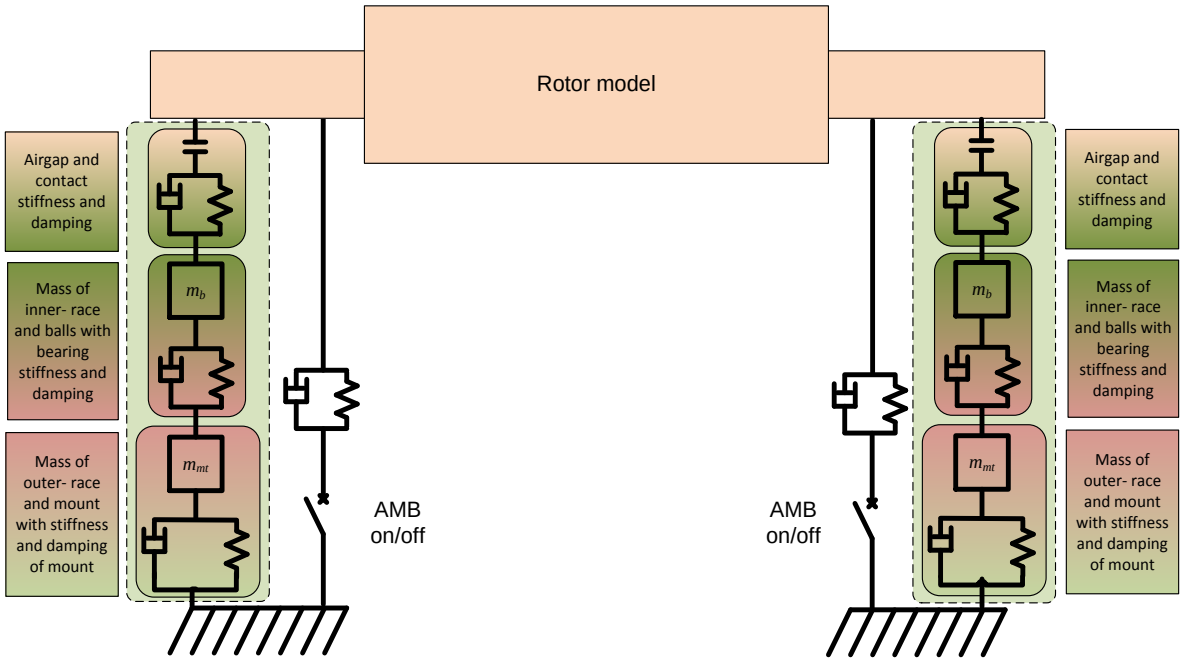

Figure 8: Schematic of the BBSim model highlighting the BB and stator sub-model

The rotor model receives the force exerted by the AMBs (if the AMBs are active) and the force caused by contact with the BB (if the airgap is exceeded). The rotor model uses these forces and determines the new position of the rotor within the airgap clearance. This means the BB model determines the force exerted on the rotor for a certain translational displacement and velocity. The force determined by the BB model is used as input by the rotor model to determine the new position of the rotor.

3.4 The rotational BB sub-model

This model focuses on the bearing rotor and friction forces experienced in the rotational axis. Some of these effects couple directly back to the translational BB model and will be explained in detail. The rotational model is illustrated in Figure 9.

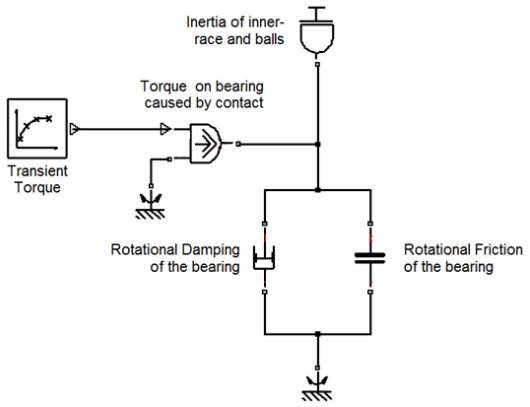

Figure 9: Simplified schematic of the rotational BB model

3.4.1 Friction between rotor and inner-race

The friction model used in the rotor BB model is standard Coulomb friction model (3.11). Coulomb friction is independent of the magnitude of the relative speed between the surfaces in contact. When the relative speed between these surfaces is not equal to zero, the friction force is proportional to the normal force. If there is no relative motion between these surfaces, there is no friction force.

$$F_{friction} = \begin{cases} 0 & if \quad v_{relative} = 0 \\ F_{normal} \cdot \mu & if \quad v_{relative} \neq 0 \end{cases} \qquad (3.11)$$
$$\text{with} \quad v_{relative} = v_{rotor} - v_{inner-race}$$

The normal force (F_{normal}) experienced by the rotor is simply the vector sum of the forces in each of the translational directions as shown in (3.5). The friction force ($F_{friction}$) is tangential to the contact point and opposite to the rotational direction as shown in Figure 10. The friction force can be transposed to the midpoint of the rotor by transforming the force into a force-moment pair as illustrated in Figure 10. $M_{friction}$ is defined as the product of the friction force and the radius of the rotor as shown in (3.12) with the direction of this moment as shown in Figure 10.

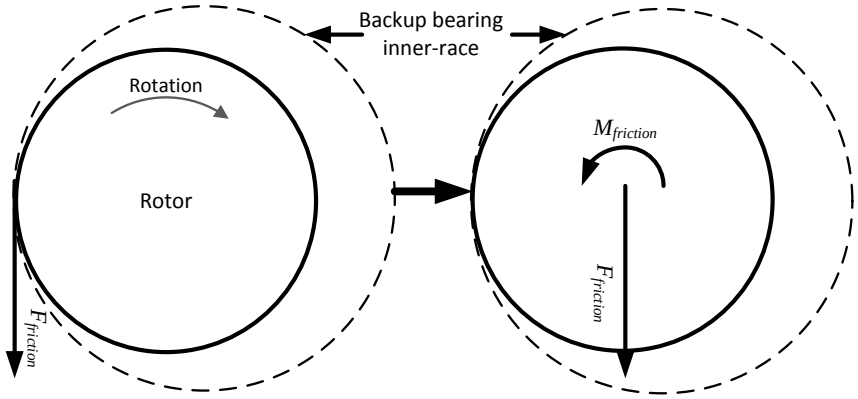

Figure 10: Force-couple transformation

$$M_{friction} = F_{friction} \times R_{rotor} \qquad (3.12)$$

The friction force couples the *x* and *y* directions of the translational BB model. The normal forces in the respective directions (*x* and *y*) are perpendicular. This means that the friction force in the *x* direction influences the total force in the *y* direction. This inter-dependency between the friction forces and normal forces are given by (3.13).

$$\begin{aligned} F_{friction_x} &= F_{normal_y} \cdot \mu \\ F_{friction_y} &= F_{normal_x} \cdot \mu \end{aligned} \quad \therefore \quad \begin{aligned} F_{Total_x} &= F_{normal_x} + F_{normal_y} \cdot \mu \\ F_{Total_y} &= F_{normal_y} + F_{normal_x} \cdot \mu \end{aligned} \qquad (3.13)$$

where F_{normal_x} and F_{normal_y} are the normal forces in the *x* and *y* directions respectively, $F_{friction_x}$ and $F_{friction_y}$ the friction forces in the *x* and *y* directions respectively, F_{Total_x} and F_{Total_y} the total forces in the *x* and *y* directions respectively and μ the friction factor between the two contacting surfaces.

The friction force determined using the normal force in the *x* direction is added to the translational BB model in the *y* direction and vice versa. This couples the *x* and *y* axes so that forces experienced in one direction influences the behaviour of the rotor in the other direction. This is illustrated in Figure 11 .

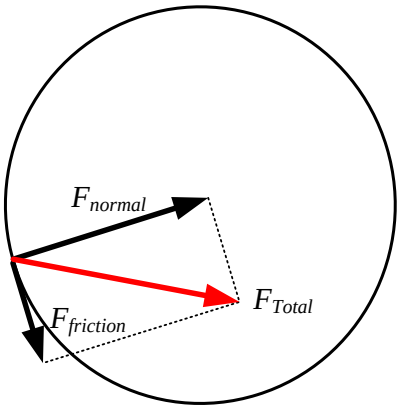

Figure 11: Total force on the rotor

Firstly, the surface speeds of both the rotor and the inner-race of the BB should be determined. Should the surface speeds of the rotor and the inner-race of the BB be equal, the friction force is zero. The equations to determine the surface speed are given in (3.14)

$$\begin{aligned} v_{rotor} &= \omega_{rotor} \cdot R_{rotor} \\ v_{InnerRace} &= \omega_{InnerRace} \cdot R_{InnerRace} \end{aligned} \tag{3.14}$$

with v_{rotor} and $v_{InnerRace}$ the surface speeds of the rotor and inner-race contacting surfaces respectively, ω_{rotor} and $\omega_{InnerRace}$ the rotational speeds of the rotor and inner-race respectively and R_{rotor} and $R_{InnerRace}$ the radii of the rotor and inner-race respectively.

The equations for the total force experienced are thus dependent on the relative speed of the rotor and the bearing inner-race as shown in (3.15). It has to be noted that when the rotor speed is less than the inner-race speed, all the friction forces change direction.

$$\left.\begin{aligned} F_{Total_x} &= F_{normal_x} + F_{normal_y} \cdot \mu \\ F_{Total_y} &= F_{normal_y} + F_{normal_x} \cdot \mu \end{aligned}\right\} \quad if \quad v_{rotor} - v_{inner-race} \neq 0$$
$$\left.\begin{aligned} F_{Total_x} &= F_{normal_x} \\ F_{Total_y} &= F_{normal_y} \end{aligned}\right\} \quad if \quad v_{rotor} - v_{inner-race} = 0 \tag{3.15}$$

This means that the rotor will experience a force causing it to move in the direction perpendicular to the normal force until the bearing inner-race and the rotor have the same surface speeds at which point the rotor will only experience the reaction force to the normal force.

3.4.2 Inner-race acceleration and rotor deceleration

While the rotor and bearing are in contact, the bearing speeds up to the rotor speed. When the rotor and bearing are not in contact, the bearing will decelerate according to the bearing friction. The acceleration of the inner-race ($\alpha_{InnerRace}$) is calculated using (3.16)

$$\alpha_{InnerRace} = \frac{M_{friction}}{I_{InnerRace\&Balls}} = \frac{F_{Total} \cdot \mu \cdot R_{InnerRace}}{I_{InnerRace\&Balls}} \tag{3.16}$$

with $I_{InnerRace\&Balls}$ the moment of inertia of the inner-race and rolling elements of the BB and $M_{friction}$ the moment caused on the inner-race due to contact friction.

The braking of the rotor due to the contact is calculated in a similar way, but has the opposite direction. The deceleration of the rotor is usually very small due to the fact that the rotor moment of inertia is much larger than that of the inner-race and balls. The equation for the deceleration of the rotor is given in (3.17).

$$\alpha_{Rotor} = \frac{-F_{Total} \cdot \mu \cdot R_{Rotor}}{I_{Rotor}} \tag{3.17}$$

The bearing deceleration caused by rolling friction ($\alpha_{Bearing_{Friction}}$) is dependent on the bearing parameters. The bearing inner-race decelerates due to bearing rolling friction. To determine this deceleration in angular contact bearings (3.18) [71] can be used.

$$\alpha_{Bearing_{Friction}} = -\left[\frac{F_{Total} + F_{Preload}}{C_{Static}}\right]^{\frac{1}{3}} \cdot \frac{Z \cdot \left(F_{Total} + F_{Preload}\right) \cdot D_{Mean_{Bearing}}}{I_{InnerRace\&Balls}} \tag{3.18}$$

where $F_{Preload}$ is the axial preload force present on the angular contact bearings, C_{Static} the static load rating of the angular contact bearing, Z the bearing parameter constant defined in [71] as 0.001 and $D_{Mean_{Bearing}}$ the mean diameter on the angular contact bearing.

If the rotor is actively braked (e.g. by means of a resistor bank), the rotor has a constant braking torque ($\tau_{BrakingTorque}$) applied to it. The formula for this is shown in (3.19).

$$\alpha_{Rotor_{Brake}} = \frac{-\tau_{BrakingTorque}}{I_{Rotor}} \tag{3.19}$$

With all the accelerations known, the total acceleration and deceleration of the inner-race and rotor can be determined as given by (3.20).

$$\begin{aligned} \alpha_{Bearing_{Total}} &= \alpha_{InnerRace} + \alpha_{Bearing_{Friction}} \\ \alpha_{Rotor_{Total}} &= \alpha_{Rotor} + \alpha_{Rotor_{Brake}} \end{aligned} \tag{3.20}$$

The rotor and the bearing both have different initial speeds. The rotor is at the operating speed and the bearing is usually stationary. Rotational speed is obtained by integrating the acceleration. The rotational speed loss is subtracted from the initial rotational speed as shown in (3.21).

$$\begin{aligned} \omega_{Rotor} &= \omega_{Initial_{Rotor}} - \omega_{Rotor_{TotalLosses}} \\ \omega_{BB1} &= \omega_{Initial_{Bearing1}} + \omega_{Bearing1_{Speedup}} \\ \omega_{BB2} &= \omega_{Initial_{Bearing2}} + \omega_{Bearing1_{Speedup}} \end{aligned} \tag{3.21}$$

The resulting rotational speed of the rotor is then used as the rotational speed for the next time-step. The rotational speed of the BB is used to determine the magnitude and direction of the friction force.

3.4.3 Non-circularity of the sensing surface

The non-circularity of the sensing surface has an influence on the behaviour of the AMB. An AMB controls the position of the rotor by measuring the distance to the surface of the rotor and then

assuming that the centre of the rotor is a fixed distance from the surface. This, however, is invalid since the rotor is not perfectly circular. The non-circularity at the sensing location is illustrated in Figure 12.

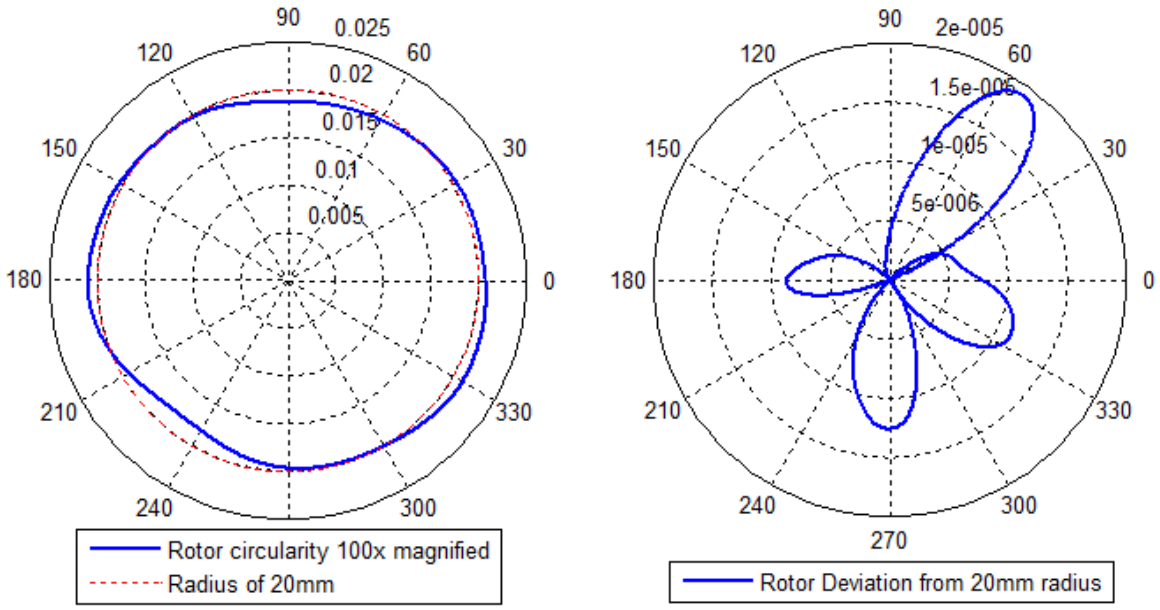

Figure 12: Rotor non-circularity at sensing location 1 (Left – Rotor circularity magnified 100x, Right – Absolute rotor circularity)

The non-circularity of a rotor influences the behaviour of the AMB by introducing additional frequencies of vibration into the system. The non-circularity of the rotor contact surface can also influence impacts on the BBs. It is therefore necessary to include the non-circularity of the rotor in the rotational model. The method used to incorporate the non-circularity of the rotor is shown in Figure 13.

The data obtained from the non-circularity of the rotor sensing surface (Figure 12) is superimposed on the position data based on the current rotational angle of the rotor. The offset value is determined by using measured data in a lookup table. Adding the non-circularity at this location has an effect on both the AMB model and the BB model. This will facilitate further research on the effect that non-circularity has on the rotordynamic behaviour of the system during levitation and AMB failure.

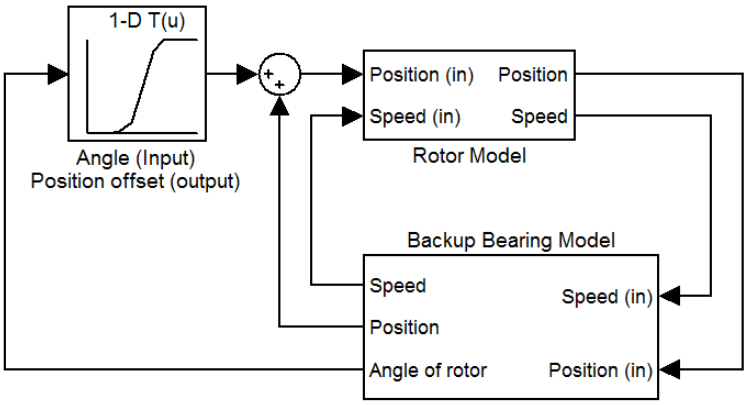

Figure 13: Schematic showing the method of incorporating the non-circularity of the rotor into the BBSim model

3.5 The active magnetic bearing sub-model

The AMB model is based on the model in [51] but simplified to ease the computational intensity of the BBSim model. The AMB model as shown in Figure 5 is only representative of the bearing stiffness and damping. The actual model is more complex. A representation of the model for one axis of one AMB is shown in Figure 14.

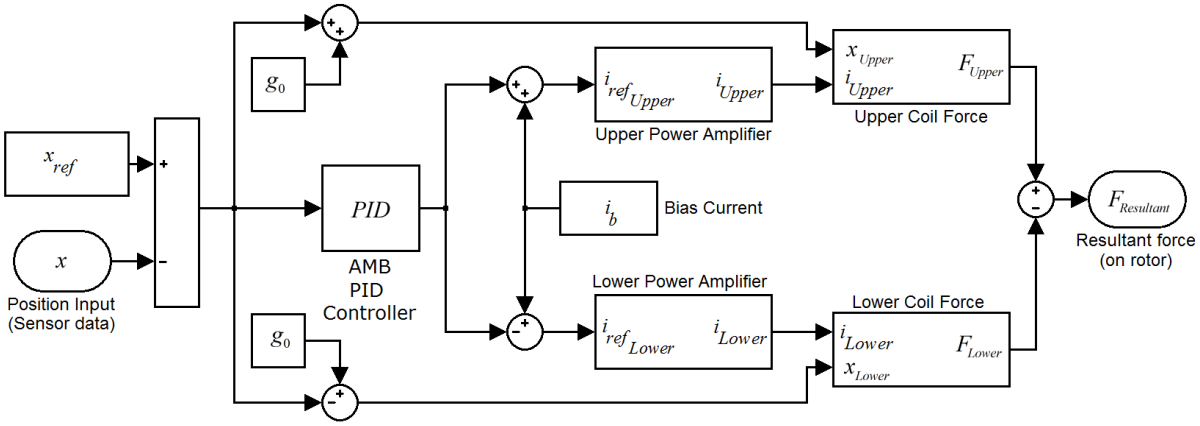

Figure 14: Block diagram of the AMB model

An error signal is produced by subtracting the rotor position (x) from the reference position (x_{ref}). This error signal is sent to the PID controller. The PID controller produces a reference current signal (i_{ref}) which is added and subtracted from the bias current (i_b) to produce the reference current for the upper ($i_{ref_{Upper}}$) and lower ($i_{ref_{Lower}}$) power amplifier (PA) respectively. The reference current is the input to the PA block. The PA blocks produce the true current (i_{Upper} and i_{Lower}) that the PAs deliver for that specific reference current. The currents are transformed into forces using (3.22).

$$\begin{aligned} F_{Upper} &= \frac{K_m \cdot i_{Upper}^2}{x_{Upper}^2} \\ F_{Lower} &= \frac{K_m \cdot i_{Lower}^2}{x_{Lower}^2} \\ F_{Resultant} &= F_{Upper} - F_{Lower} \end{aligned} \tag{3.22}$$

with K_m the electromagnet constant, x_{Upper} the position error signal (x_{ref} - x) added to the nominal airgap (g_0) and x_{Lower} the position error signal subtracted from the nominal airgap. The resultant force is determined by subtracting the lower force from the upper force. The resultant force on the rotor is the output of the AMB model.

3.6 The rotor sub-model

The rotor is modelled using the finite element method RotFE [50], an add-on to Matlab® was used for this purpose. RotFE is a two-dimensional finite element based rotor model that is capable of modelling solid and hollow shafts with rigid discs and/or point masses. RotFE also includes the capability to model linear stiffness, viscous damping and multi-plane unbalance forces. Transient external forces can be applied to the rotor in any of the defined nodes, and the transient displacement of any node can be determined. The rotor model is not discussed in great detail. Only the changes made to the standard RotFE code and the coupling of the rotor model are discussed. An example of a rotor modelled in RotFE is shown in Figure 15.

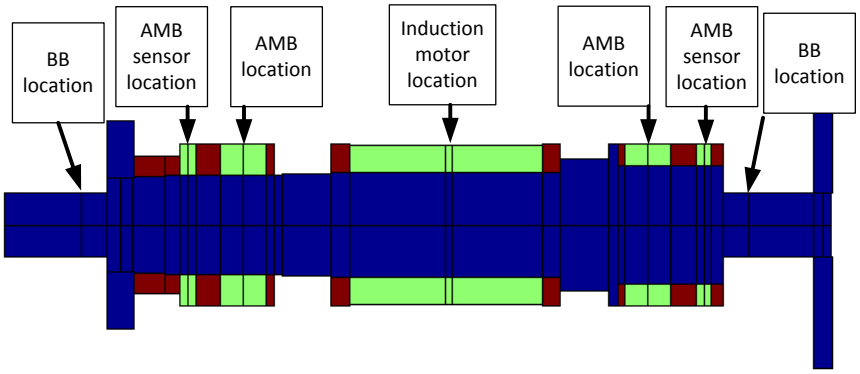

Figure 15: Graphical illustration of a typical rotor model

Figure 15 shows a typical layout for a rotor, with the positions for the AMB, BB, induction motor and position sensors. The position sensors are not in the same location as the AMBs and therefore the measurement of the position is not accurate for bending modes and conical modes. The AMB controller uses the position data measured at the sensor locations and applies force at the AMB locations. This is represented in Figure 16.

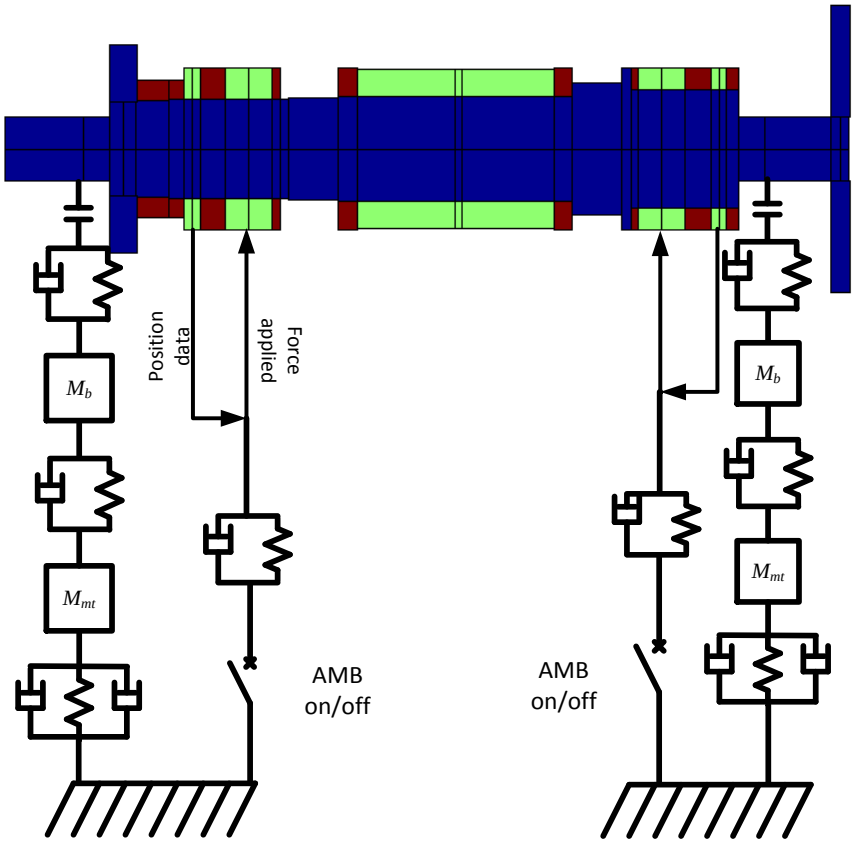

Figure 16: Illustration showing the locations where position data is obtained and where the AMB force is applied

Table 4: Rotor model input and output

Rotor model inputs		Rotor model outputs	
Input	**Signal originates from**	**Output**	**Signal sent to**
Rotor rotational speed	BB rotational and friction model	Rotor position @ AMB sensor locations	AMB model
AMB force	AMB model		
BB force	BB translational model and friction model	Rotor position @ BB locations	BB translational model
Gravity force	BB translational model		

In Table 4, the rotor model inputs and outputs are given. The rotor model inputs are stated in the first column and the second column states from where that particular signal originates. The third column states the rotor model output and the fourth column states the destination of that particular signal. This table should be read while referring to Figure 16. The rotor model determines the position of each of the nodes in the rotor model.

3.7 Coupling of the sub-models

The sub-models discussed in 3.2 to 3.6 are all interconnected. This section explains how and to what each of these models is coupled. Coupling of each of these sub-models is illustrated in Figure 17. The signals represented by each of the connecting lines are described in the paragraphs following Figure 17.

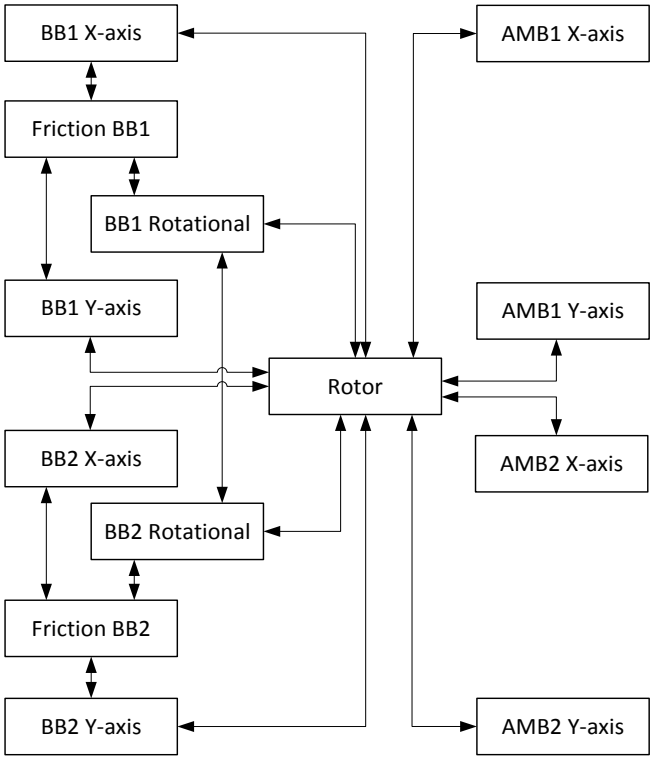

Figure 17: Sub-model coupling

The translational BB models receive the current position of the rotor from the rotor model. The BB model also receives the friction force from the friction model determined from the normal force on the other axis. The BB models further send the forces determined by each BB model to the rotor model.

The friction models receive the normal forces acting on the rotor and use them to determine the friction forces. They also receive the current bearing speed from the rotational BB model and send the current friction factor to the rotational model.

The rotational BB model receives the perpendicular forces from the friction model and determines the speed-up torque of the bearing as well as the slow-down torque of the rotor. It also receives the current friction factor from the friction model.

The AMB model receives the current position of the rotor at the sensor locations and sends the forces acting on the rotor at the AMB locations to the rotor model.

The rotor model receives the forces acting on the rotor (from AMBs and BBs) and sends the current position of the rotor to the AMBs and BBs. It receives the current rotational speed from the rotational BB model.

3.8 Conclusion

This chapter explained the conceptualisation of the model "*Backup Bearing Simulation"* (BBSim). The sub-models were identified and explained. The sub-models were discussed and the relevant governing equations were presented. The integration of these sub-models was explained. The coupling of all the sub-models produces a model that addresses most of the shortcomings that were identified in Chapter 2.

In the next chapter, some of the empirical studies performed on an experimental workbench [52] are presented. To validate the BBSim model, the parameters for the various constants within the model need to be determined first.

Chapter 4

Empirical studies

Some of the parameters used during the simulation of a rotor delevitation event that are critical in determining the behaviour of the rotor in the BB clearance, need to be determined by using empirical methods. This chapter deals with these parameters and the methods used to determine them. These parameters are the BB clearances, the friction factor between the inner-race and the rotor, the unbalance present on the rotor, the windage braking of the rotor, the bearing rolling friction and the rotor circularity.

4.1 System used for empirical studies

As mentioned in Section 1.4.3, the system described in [52] is used to perform the empirical studies. Figure 18 is an illustration of the system with modifications which allows for the use of rolling element bearings.

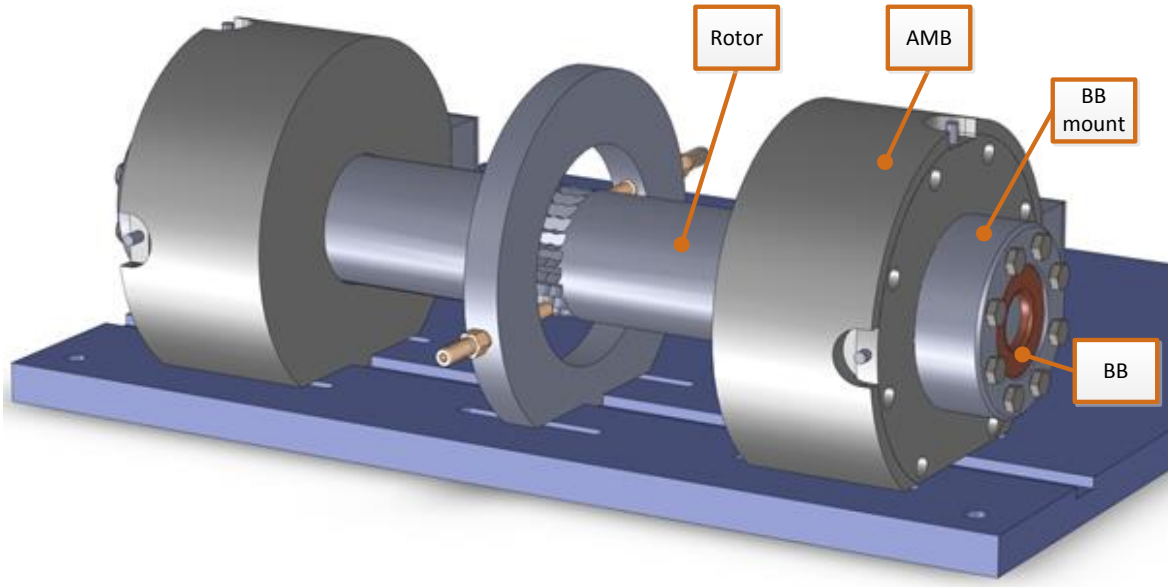

Figure 18: Illustration of the system used to perform the empirical studies

The system consists of two radial AMBs each with two eddy current probes to measure the displacement of the rotor. It is important to note that the rotor is not axially suspended. The system was modified by adding two back-to-back angular contact rolling element BBs to both of the AMBs. The system is rotated by means of a Pelton wheel and compressed air. The rotational speed of the rotor is measured optically.

4.2 BB clearances

The BB clearance is important because it determines where the point of first contact will be, whether the two bearings will experience contact simultaneously or which one will make contact first. To determine the BB clearances, the rotor was left in a delevitated state and moved to the extremities of the clearance. This data was captured using the eddy current probes. The result of this experiment is shown in Figure 19. As seen in the figure, the two clearances are not exactly the same. This is due to manufacturing tolerances on the rotor.

Circles are fitted on the captured data and the respective radii determined. The fitted circles are shown in Figure 19 with the dashed lines. The fitted circle for the left bearing has a radius of $290\ \mu m$ and the right fitted circle has a radius of $268\ \mu m$. To determine the radius on other systems where the rotor is too heavy to be moved manually or where the rotor is difficult to reach, the AMBs of the system can be used to move the rotor in the same manner.

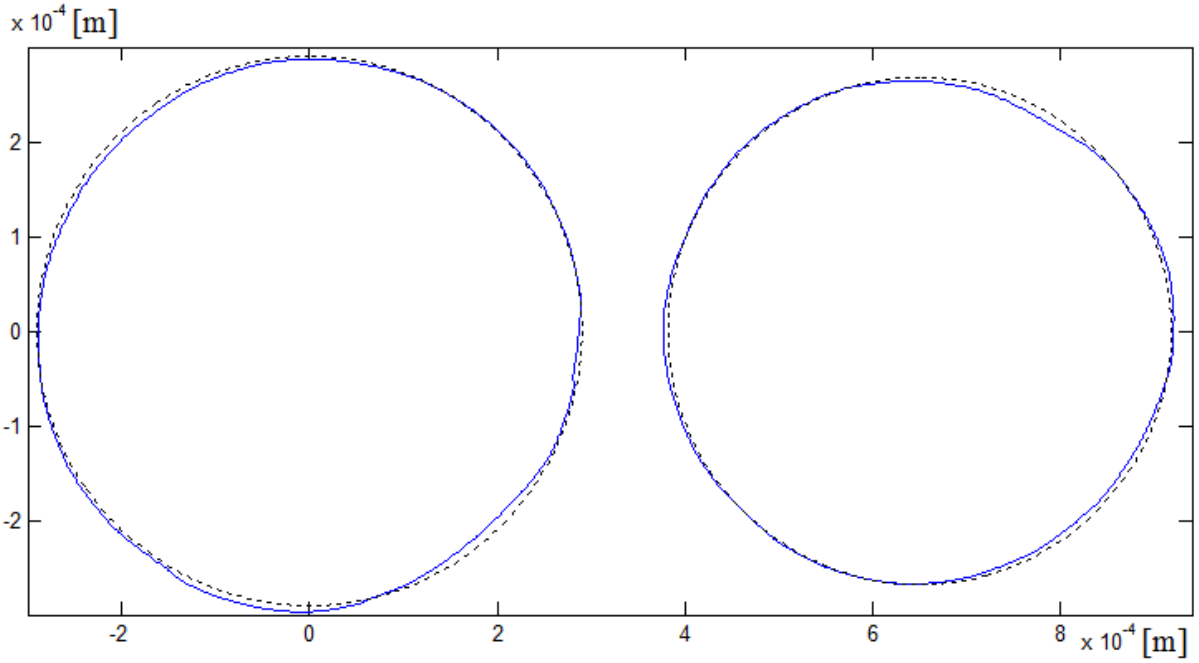

Figure 19: Bearing clearances

4.3 Friction factor

The friction factor between the rotor and the inner-race of the BB is very important. The friction factor between the surfaces in contact is determined by preventing the inner-race from rotating during a rotor delevitation event at slow speed. The inner-race of the bearing is stationary and the friction force is the only force braking the rotor. The previous statement relies on the assumption that, at lower speeds, the windage (aerodynamic) losses of the rotor is negligible. From (4.1), μ can be solved and the result of (4.2) obtained.

$$\tau_{friction} = I_{Rotor} \cdot \alpha_{Rotor} \quad , \quad F_{friction} = \frac{\tau_{friction}}{R_{rotor}} \quad , \quad \mu = \frac{F_{friction}}{m_{rotor} \cdot g} \tag{4.1}$$

$$\mu = \frac{I_{Rotor} \cdot \alpha_{Rotor}}{R_{rotor} \cdot m_{rotor} \cdot g} \tag{4.2}$$

where m_{rotor} is the mass of the rotor, I_{Rotor} the moment of inertia of the rotor, α_{Rotor} the rotational acceleration of the rotor, R_{rotor} the radius of the rotor at the bearing location, g the gravitational acceleration and μ the friction factor between the rotor and the inner-race of the bearings. Using (4.2) and the data from rotor delevitation events performed using plain bearings, the friction factor obtained was 0.204. This value is expected for steel-on-steel contact [72,73].

4.4 Unbalance

The unbalance of the rotor has a big influence on the initial conditions of the rotor upon AMB failure. The unbalance also plays a role in the behaviour of the rotor after AMB failure, where a large

unbalance can force the rotor into forward whirl [8] and a small unbalance may lead to backward whirl at higher rotational speeds. The unbalance of the rotor can be determined using a balancing machine. Since this facility was not available, the unbalance was determined using the eddy current position signals to determine the orbit radius while the AMBs were operational. Using the constants of the AMBs, the force exerted by the AMBs can be calculated. Using this AMB force, the unbalance magnitude can be determined. The force exerted by the AMB (F_{AMB}) is determined using (4.3)

$$F_{AMB} = K \cdot r + C \cdot \dot{r} \tag{4.3}$$

with r the radius of the displacement of the geometric centre of the shaft away from the geometric centre of the AMB, K the equivalent linear stiffness of the AMB and C the equivalent linear damping constant of the AMB.

Since the relationship between the unbalance force and the rotational speed of the rotor is known from (4.4), a model is fitted to the data with that shape. The graphs representing the AMB forces against the rotational speed and the fitted models are shown in Figure 20.

$$F_{unbalance} = e \cdot \omega_{Rotor}^2 \tag{4.4}$$

The discrepancies between the measured data and the fitted models are attributed to the critical frequencies of the rotor, measurement errors and non-concentric sensing surfaces. The magnitude of the unbalance was found to be $163\ \text{g·mm}$ at the left bearing and $128\ \text{g·mm}$ at the right bearing. The unbalance at the left bearing location is larger than at the right bearing location.

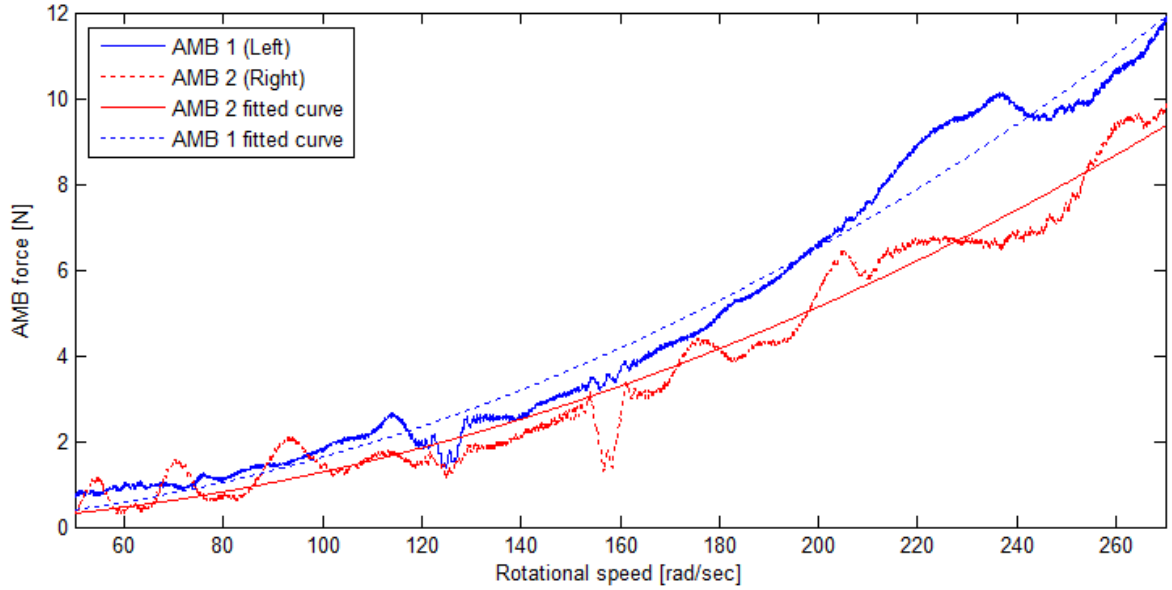

Figure 20: AMB force vs. rotational speed and fitted models

The unbalance magnitudes are now known but the angle between these two unbalances still needs to be determined. To determine the angle between the two unbalances, the difference in the phase angle between the two rotor orbits is investigated. The phase angle is investigated at low speed in order to minimise the effect that the phase shifts of the AMBs have on the result. This difference is found to be 29.71 degrees or 0.52 radians. This value is an approximation of the angle between the unbalance at the two bearing locations.

4.5 Windage and eddy current braking

The rotor speed is influenced by the aerodynamic losses of the rotor as well as the eddy current losses produced by the AMBs. The calculation of these losses is done by spinning the rotor down from a high speed and measuring the difference in the rotational speed per unit of time. This produces the deceleration of the rotor which can then be used to calculate the sum of the eddy current loss torque and aerodynamic torque in (4.5). This calculated aerodynamic and eddy current loss torque plotted against the rotational speed of the rotor is shown in Figure 21.

$$\tau_{air} = I_p \cdot \alpha_{levitated} \tag{4.5}$$

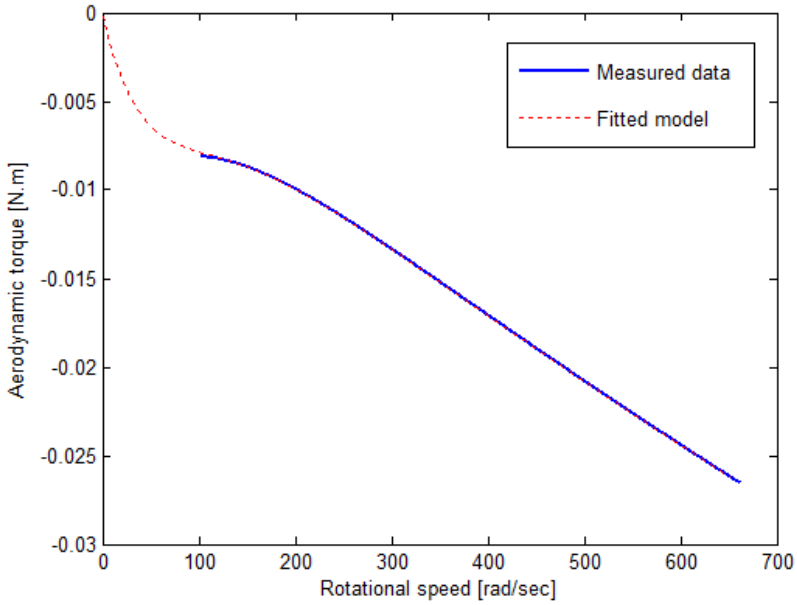

Figure 21: Aerodynamic and eddy current loss torque on rotor

Figure 21 also shows a model fitted to the data. Since it is known that the aerodynamic losses should be zero when the rotor is at a standstill, the model fitted is a ninth-degree polynomial given by (4.6)

$$\tau_{air} = I_p \cdot \left(p_1 \cdot \omega^9 + p_2 \cdot \omega^8 + p_3 \cdot \omega^7 + p_4 \cdot \omega^6 + p_5 \cdot \omega^5 + p_6 \cdot \omega^4 + p_7 \cdot \omega^3 + p_8 \cdot \omega^2 + p_9 \cdot \omega \right) \tag{4.6}$$

with $p_1 = -2.7\text{x}10^{-23}$, $p_2 = 9.8\text{x}10^{-20}$, $p_3 = -1.54\text{x}10^{-16}$, $p_4 = 1.38\text{x}10^{-13}$, $p_5 = -7.7\text{x}10^{-11}$, $p_6 = 2.76\text{x}10^{-8}$, $p_7 = -6.24\text{x}10^{-6}$, $p_8 = 8.27\text{x}10^{-4}$ and $p_9 = -6.16\text{x}10^{-2}$.

4.6 Bearing friction

The other factor that decelerates the rotor is the friction within the BBs. The bearing friction is determined by spinning the rotor down in the BBs. The rotor is secured to the bearings by fitting a sleeve over the rotor so that the rotor is making contact with the BBs at all times. The rotor is spun up to a certain speed and left to spin down while recording the rotor speed. The rotor speed is again used to determine the angular deceleration. The angular deceleration is used to determine the deceleration torque on the rotor. The deceleration torque is the sum of the bearing deceleration torque and the aerodynamic deceleration torque. This relationship is given by (4.7).

$$\tau_{braking} = \tau_{air} + \tau_{bearings} \tag{4.7}$$

The measured and fitted total deceleration torque curves are shown in Figure 22.

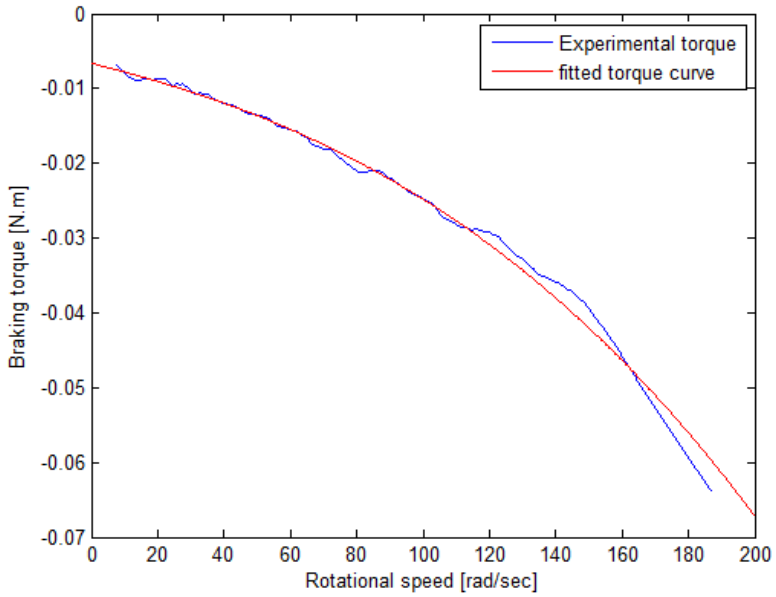

Figure 22: Total deceleration torque

In Figure 23, the deceleration torque curves for the bearing and the aerodynamic losses are shown together with the total deceleration torque curve. The bearing deceleration torque is determined by subtracting the aerodynamic deceleration torque from the total deceleration torque. The resultant torque curve is the bearing deceleration torque. The bearing deceleration torque is dependent on the rotational speed of the bearing. The formula for the bearing deceleration torque is shown in (4.8)

$$\tau_{bearing} = p_1 \cdot \omega^9 + p_2 \cdot \omega^8 + p_3 \cdot \omega^7 + p_4 \cdot \omega^6 + p_5 \cdot \omega^5 + p_6 \cdot \omega^4 + p_7 \cdot \omega^3 + p_8 \cdot \omega^2 + p_9 \cdot \omega + p_{10} \qquad (4.8)$$

with $p_1 = 1.05x10^{-25}$, $p_2 = -3.82x10^{-22}$, $p_3 = 6.02x10^{-19}$, $p_4 = -5.38x10^{-16}$, $p_5 = 3.01x10^{-13}$, $p_6 = -1.07x10^{-10}$, $p_7 = 2.18x10^{-8}$, $p_8 = -3.68x10^{-6}$, $p_9 = 1.3x10^{-4}$ and $p_{10} = -6.62x10^{-3}$.

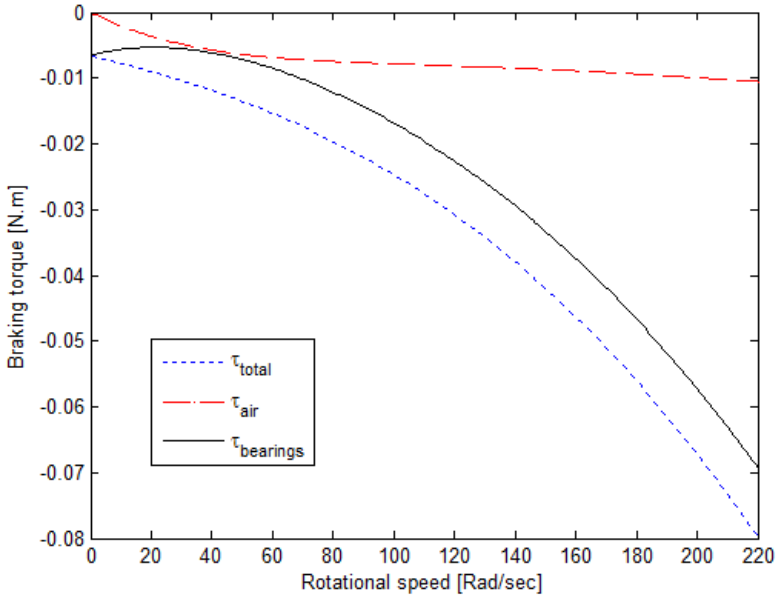

Figure 23: Bearing deceleration torque curve

The bearing deceleration torque is not equal to 0 at 0 rad/sec the reason for this is that in much the same way as that normal translational friction has a breakaway force, the bearings have a breakaway torque required to overcome static friction within the bearings.

4.7 Rotor circularity at sensor positions

Determining the circularity of the rotor is important for the BB simulation model to be an accurate representation of the true behaviour of the rotor during a simulated rotor delevitation event. The circularity of the rotor was determined using the eddy current position sensors. The sensing location of this particular AMB system is on the same surface where BB contact takes place. It is therefore assumed that the circularity of the rotor is the same at the bearing locations and the sensing locations.

The circularity was determined by measuring the position data of the rotor, rotating at low speed while delevitated and logging the angular position of the rotor. By plotting the displacement against the angular position of the rotor and fitting a spline through the data, the result in Figure 24 is obtained. Using these splines the cross-sectional circularity of the rotor is obtained as shown in Figure 12.

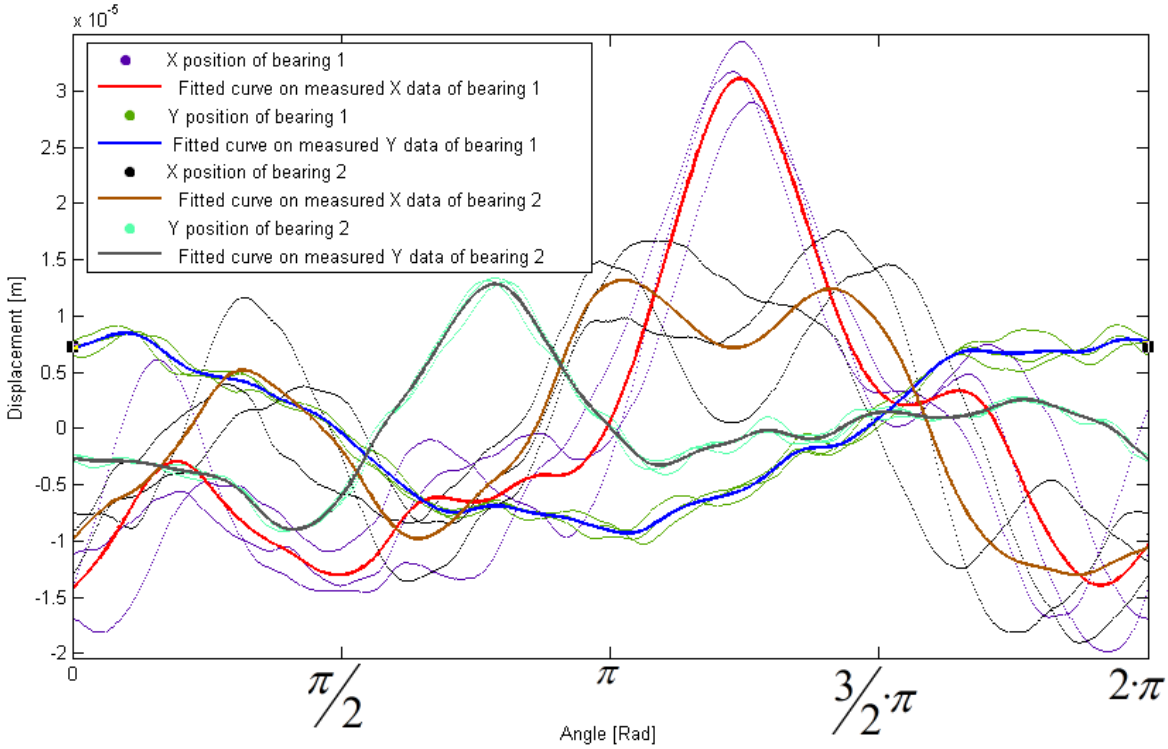

Figure 24: Measurement of sensing location circularity at both sensing locations

The variations in the experimental data are attributed to the fact that the rotor is free to move axially, and the variation in circularity with axial position. These changes in the surface are averaged using a spline fit through the data. The fitted spline for each axis on each of the bearings is used to create the lookup tables in the simulation to model the circularity of the rotor.

In order to model the circularity of the rotor with greater accuracy, a three dimensional lookup table should be created where the axial position is controlled and measured. Since this BB simulation model does not model the axial position of the rotor, the current approximation of the circularity is deemed sufficient.

4.8 Conclusion

This chapter dealt with the empirical studies employed to determine some of the parameters of the system that were unknown. These parameters were the bearing clearance, the friction factor between the rotor and the inner-race, the unbalance of the rotor, the aerodynamic deceleration of

the rotor, the bearing deceleration caused by the internal friction of the bearing and the circularity of the rotor at the sensing positions. With these parameters known, they can be implemented in the simulation model BBSim as proposed in Chapter 3.

Although all of the measurements used to determine the unknown parameters of the system includes some form of measurement error, the measurements are considered sufficiently accurate for use in the model. Some of the measurement techniques could be further developed to increase accuracy. The inclusion of the axial movement of the rotor in future simulation models would also require the implementation of a three dimensional lookup table of the circularity of the rotor.

In the next chapter three different methods of quantifying the severity of rotor delevitation events are discussed. The three methods are the impulse of the rotor during a delevitation event, the Rotor Drop Quality factor (RDQ) and the non-dimensionalised speed of the geometric centre of the rotor ($Vval$ and $Vvala$).

Chapter 5

Quantifying rotor delevitation severity

This chapter deals with the quantification of the severity of rotor delevitation events. With continued use, BBs tend to degrade depending on the severity of the rotor delevitation events that have occurred. The necessity to quantify the severity of these events is therefore paramount to enable active condition monitoring of the BBs. The quantification of the severity of rotor delevitation events could enable the end-user to have a preventative maintenance schedule for the system's BBs.

Three methods of quantification are presented namely the impulse of a rotor delevitation event, Rotor Drop Quality (RDQ) method and a method using the non-dimensionalised speed of the geometric centre of the rotor ($Vval$ and $Vvala$).

A method of quantification is needed that does not rely on the measurement of force, since the experimental test stand does not have force measurement capabilities. RDQ and $Vval$ are both determined using only position data. Since any AMB system already includes position sensors, these methods of quantification can be applied to any existing AMB system. A flowchart of the simulation based validation process for the quantification methods is shown in Figure 25.

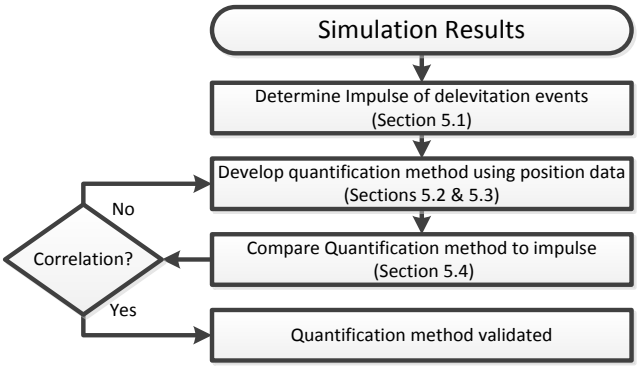

Figure 25: A flowchart of the validation process for the quantification methods

5.1 Impulse

Impulse is defined as the integral of force with respect to time as shown in (5.1). Impulse can also be determined using the mean value of force ($\overline{F}$) over a given period of time (Δt).

$$I = \int_{t_1}^{t_2} F \cdot dt \simeq \overline{F} \cdot \Delta t \tag{5.1}$$

Since most AMB systems are not fitted with force measurement equipment, the comparison of experimental and simulated forces (and impulse) is problematic. Although the impulse of a rotor delevitation event is a valid quantification method, the lack of force measurement equipment renders it an inappropriate method in most cases.

Calculation of the impulse of a rotor delevitation event is done by using the average of the force acting on the bearing over the total time of the delevitation event. This produces a singular value per bearing for a rotor delevitation event. This value can then be used to compare various rotor delevitation events to each other. It is important to note that when comparing rotor delevitation

events with varying durations, the value for the impulse should be normalized by dividing with the total time (t_{total}) of the delevitation event as shown in (5.2).

$$I_{perSecond} = \frac{\overline{F} \cdot \Delta t}{t_{total}} \tag{5.2}$$

Equation (5.2) produces a value with the unit of Newton or, stated in other terms, it is the impulse-per-second value of the rotor delevitation event.

5.2 Rotor drop quality (RDQ) factor

The RDQ factor is intended to be used to compare different rotor delevitation events to each other without the use of force measurements. The main causes of bearing degradation will be stated in the following paragraphs. These causes will then be integrated into a method to calculate the severity of rotor delevitation events. Most rotor delevitation events without force measurements are judged on a qualitative basis. This is not desirable since it can be very subjective. The need for a quantitative classification method is apparent.

5.2.1 Bearing degradation

Factors that contribute to the degradation of the bearings are the deformation of the bearing, the centripetal force, the bouncing of the rotor and the rated speed of the bearing.

It becomes necessary to include these factors in a quantification method for the severity of rotor delevitation events. The method used to quantify each of these factors is stated in the following paragraphs and then integrated into a RDQ factor.

5.2.1.1 Deformation of the bearing

The force generated by bearing deformation is described by (5.3). This shows that the force is dependent on the position of the rotor in relation to the BB, the stiffness and the damping of the BB.

$$F_{normal} = \begin{cases} 0 & if \quad s_{rotor} < R_{airgap} \\ K_{BB} \cdot (s_{rotor} - R_{airgap}) + C_{BB} \cdot \dfrac{d(s_{rotor} - R_{airgap})}{dt} & if \quad s_{rotor} \geq R_{airgap} \end{cases} \tag{5.3}$$

The inclusion of the stiffness and damping of the BB enables the ability to compare different bearings.

5.2.1.2 Centripetal force

Another force acting on the bearing is the centripetal force of the rotor. This force is dependent on the mass of the rotor, the radius at which the rotor is orbiting the midpoint of the BB and the rotational speed of the centre of mass of the rotor in the bearing clearance. The rotational speed referred to here is not the rotational speed of the rotor itself but the rotational speed of the orbit of the rotor. The equation for the calculation of the centripetal force is given in (5.4).

$$F_{centripetal} = m_{rotor} \cdot s_{rotor} \cdot \omega_{COM}^2 \tag{5.4}$$

with ω_{COM} the rotational speed of the centre of mass of the rotor within the backup bearing clearance, s_{rotor} the displacement of the centre of mass of the rotor from the centre of the BB clearance and m_{rotor} the mass of the rotor.

The centripetal forces also account for the whirling forces. Whirling is very important in the degradation of BBs since it creates enormous forces on the bearing. Backward whirl has the potential to have a higher frequency than that of forward whirl. This means that the centripetal forces have the potential to be larger during backward whirl.

5.2.1.3 Bouncing

Impact forces also degrade BBs. An impact occurs when the rotor goes from a non-contact state to a contact state. Furthermore, the RDQ factor should include a more severe penalty for rotor delevitation events that tend toward backward whirl even if backward whirl did not develop. The reason for this penalty is that backward whirl will eventually develop as the bearing degrades. This will also enable the comparison between different rotor delevitation events to determine whether the rotor is closer to going into backward whirl compared to previous rotor delevitation events. Should the RDQ value increase with consecutive rotor delevitation events, the bearings need to be replaced.

Both the impact forces and the tendency toward backward whirl are taken into account by assigning a weighting factor to the position of the rotor in the BBs. These factors are assigned higher values for larger bouncing- and backward-whirl-prone locations. To accomplish this, the bearing airgap area is divided into 6 different areas based on the angle of an imaginary line that connects the rotor location with the geometric centre of the BB. The airgap sectors and the accompanying weighting factors are shown in Figure 26. It is important to note that the weighting factors are estimated and only valid for horizontal machines and may be refined based on further studies. In vertical machines the bouncing factor (BF) should be set equal to 1.

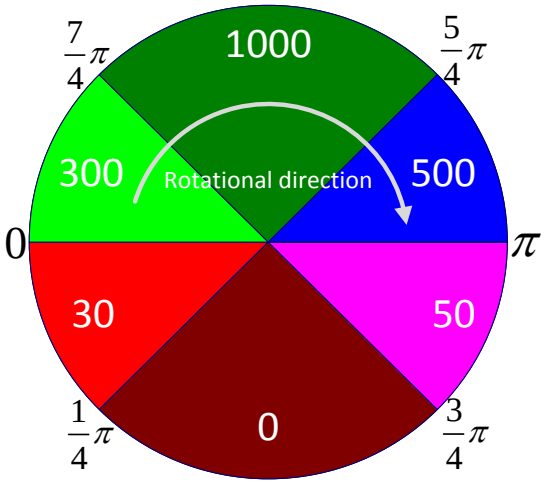

Figure 26: BB airgap area weighting sectors

The rotor position within these sectors determines the value of the bouncing factor (BF). The bouncing factor is determined using (5.5) and (5.6). The value is computed for each data point in the captured or simulated data. The mean of these values is calculated and results in the bouncing factor. The rationale behind the weighting factor values is that whirl and high bounces are the worst conditions and therefore the highest point has the largest weighting factor. Secondly, a rocking motion is ideal and means that the lowest point in the bearing airgap has the smallest weighting factor value. Thirdly, for a clockwise rotor rotation, a backward whirl motion will tend to climb the right side of the airgap. The right side sectors therefore have larger values when compared to the left side sectors. The weighting factor values have, for the purpose of this thesis, been chosen with

relative differences as shown in (5.5). Further study could include the refinement of the values of these weighting factors.

$$BF(i) = \begin{cases} 1000 & if \quad \frac{5}{4}\pi < \phi(i) < \frac{7}{4}\pi \\ 500 & if \quad \pi \le \phi(i) \le \frac{5}{4}\pi \\ 300 & if \quad \frac{7}{4}\pi \le \phi(i) \le 2\pi \\ 50 & if \quad \frac{3}{4}\pi \le \phi(i) < \pi \\ 30 & if \quad 0 \le \phi(i) \le \frac{1}{4}\pi \\ 0 & if \quad \frac{1}{4}\pi < \phi(i) < \frac{3}{4}\pi \end{cases} \tag{5.5}$$

$$BF = \frac{1}{n} \cdot \sum_{i=1}^{n} BF(i) \tag{5.6}$$

with n the total number of samples and i an index number.

5.2.1.4 *Rated speed of the bearing*

All rolling element bearings have a maximum rated speed. This maximum speed is the speed at which the bearing can operate continuously without being damaged. The RDQ factor should take into account the speed of the rotor and normalize the rotational speed of the rotor with regard to the rated speed of the bearing. This will create a speed factor and will enable the comparison of the severity between rotor delevitation events using different bearings. The speed factor (ω_{factor}) is defined in (5.7).

$$\omega_{factor} = \frac{\omega_{rotor}}{\omega_{BB_{rated}}} \tag{5.7}$$

5.2.2 Formulation of *RDQ* factor

To take the mentioned factors into account, (5.8) and (5.9) is formulated to determine the RDQ value. The $RDQ(i)$ is a vector of values. This needs to be simplified into a single number for ease of comparison between different rotor delevitation events. Simplification is achieved by adding the mean value of the $RDQ(i)$ vector and the maximum value of the $RDQ(i)$ vector.

$$RDQ(i) = BF \cdot \omega_{factor}(i) \cdot \frac{\left(F_{normal}(i) + F_{Centripetal}(i)\right)}{F_{max_{BB}}} \tag{5.8}$$

$$RDQ = \overline{RDQ(i)} + RDQ(i)_{max} \tag{5.9}$$

with $F_{max_{BB}}$ the maximum static rated load of the BB.

Using both the mean value and the maximum value obtained through (5.8) ensures that degradation caused by short periods of violent behaviour of the rotor is not overlooked.

5.2.3 The usefulness of *RDQ*

RDQ is a useful tool to compare different rotor delevitation events to each other, and to have a quantitative number to represent the severity of a rotor delevitation event. The *RDQ* value of rotor delevitation events can be used to determine the degradation on a particular set of bearings. The *RDQ* value can also be used to compare the severity of rotor delevitation events on different BB designs on the same system.

5.2.3.1 Determining the bearing degradation

The degradation of bearings is very important in determining when to replace the bearings. In certain situations, the replacement of bearings can be very costly due to downtime. A bearing inspection procedure should be compiled based on the *RDQ* values for pre-determined test delevitation events. These tests will be done periodically using controlled rotor delevitation events with the same initial values for each delevitation event. An upward trend in the *RDQ* values would indicate that the bearings are beginning to degrade and negatively influencing the behaviour of the rotor. Early identification of this upward trend could be used to schedule downtime of the plant to replace the BBs.

5.2.3.2 BB design comparison

The *RDQ* value can also be used to compare rotor delevitation events on different sets of BBs. These results can then be compared to make a decision between the different designs or bearing selections. Choosing a certain design over another design should be based on quantitative results. The use of *RDQ* values enables this quantitative comparison.

5.2.4 *RDQ* value classification

The classification of the value of the *RDQ* for a certain rotor delevitation event is necessary to determine how severely a rotor delevitation event deteriorated the BB health. The classification is based on the results of both simulated (found in Appendix C.5) rotor delevitation events and experimental (found in Appendix C.6) rotor delevitation events. It is important to note that these classification values should be refined using consecutive rotor delevitation events followed by in depth analysis of the bearing degradation.

Table 5: *RDQ* value classification

RDQ value	Rotor motion	Bearing degradation
0 - 1	Ideal rocking motion	Minimal
1 - 100	Rocking motion with minor bouncing	Very low
100 - 200	Low speed forward whirl (low whirl frequency)	Low
200 – 5 000	High speed forward whirl or low speed backward whirl	High
> 5 000	High speed backward whirl	Destructive

In Table 5, the *RDQ* values are classified according to their value. Any *RDQ* value lower than 200 is low enough that the bearings would be able to handle repeated rotor delevitation events. If the *RDQ* value is between 200 and 5 000, the bearings would not be able to indefinitely handle rotor delevitation events. If the *RDQ* value is more than 5 000, the bearings are being pushed to their limit and may fail during a rotor delevitation event.

5.3 Non-dimensionalised velocity of the geometrical centre of the rotor *(Vval)*

An alternative to measure the severity of a rotor delevitation event is to use a non-dimensionalised distance over time and produce a non-dimensionalised speed. The rationale behind the non-

dimensionalised velocity can be found in the well-known formulae for impulse (5.10) and average force (5.11)

$$I \simeq m \cdot \Delta v = \overline{F} \cdot \Delta t \tag{5.10}$$

$$\overline{F} = m \cdot \bar{a} = m \cdot \left(\frac{\Delta v}{\Delta t} \right) \tag{5.11}$$

with Δv and $\bar{a}$ the change in velocity and the average acceleration respectively, m the mass of the rotor and $\overline{F}$ the average force of the rotor delevitation event. From these equations, the hypothesis is made that there is a relationship between the distance travelled by the geometric centre of the rotor over time (*Vval*) and the average impulse of the rotor delevitation event as given in (5.12). This hypothesis is discussed and validated in Section 5.4.2.

$$Vval \propto \overline{F} \cdot \Delta t \tag{5.12}$$

The transverse motion is an indication of the energy that the BBs dissipate or transform during a certain rotor delevitation event and of the degradation of the bearing quality [55].

5.3.1 Formulation of *Vval*

The distance is non-dimensionalised by dividing with the airgap radius in order to produce a value that represents the number of times the rotor has travelled the entire distance of the airgap radius. The definition of the non-dimensionalised distance is shown in (5.13) [55].

$$Dval_k = \frac{\sum_{i=((k \cdot n)-n)+1}^{k \cdot n} \sqrt{\left(x_i - x_{i-1}\right)^2 + \left(y_i - y_{i-1}\right)^2}}{r_{airgap}} \text{ with } k = \left[1, \ldots, \frac{n_{total}}{n} \right] \tag{5.13}$$

with n the window size (number of samples), i the index number, r_{airgap} the radius of the BB clearance, x the position of the rotor centre in the x-direction, y the position of the rotor centre in the y-direction, k the index number for $Dval$ and n_{total} the total number of samples in the rotor delevitation event data

This non-dimensionalised distance is divided by the time over which it was calculated to produce an average non-dimensionalised speed with the unit of per-second. If the chosen window size is the same as the total number of samples in the rotor delevitation event's data, there is only one $Dval$ value. For this case, (5.14) is used to determine the $Vvala$ value with f_s the sampling frequency and n the window size [55].

$$Vvala = Dval_1 \cdot \left(\frac{f_s}{n_{total}} \right) \tag{5.14}$$

Should the window size be chosen smaller than the total number of samples in the data set, there is more than one $Dval$ value. Of these $Dval$ values, only the largest value is used to determine the $Vval$ value as shown in (5.15) [55].

$$Vval = \max\left(Dval_1 \cdot \left(\frac{f_s}{n} \right), \ldots, Dval_k \cdot \left(\frac{f_s}{n} \right) \right) \tag{5.15}$$

It is important to note that the maximum value for *Vval* does not necessarily occur directly after the rotor delevitation. The dynamics of the system could cause a critical frequency being traversed at a lower rotational speed than the delevitation rotational speed. When a critical frequency of the system is traversed, the behaviour of the rotor in the BBs can become much more violent. In these cases, the maximum value for *Vval* would occur at these critical frequencies.

Throughout this document *Vvala* is determined with a window size of 60 000 samples and a sampling frequency of 10 000 Hz due to the capabilities of the experimental system. Similarly, *Vval* is determined with a window size of 1 000 samples and a sampling frequency of 10 000 Hz [55]. The window size is chosen large enough for sufficient averaging of the results while still emphasising periods of destructive behaviour.

These values are then used to determine the severity of a rotor delevitation event when it is taking place, on previously captured data or on simulation results. The real-time calculation of this value could enable safe rotor delevitation tests where the rotor can be re-levitated once a safe threshold value has been reached or exceeded.

5.3.2 The usefulness of *Vval*

Although *Vval* poses the same usefulness as that of *RDQ* as stated in Section 5.2.3, *RDQ* is more suited to be used as a design tool and *Vval* is more suited to be used as a real-time condition monitoring tool during controlled experimental rotor delevitation events. This is due to the fact that *Vval* is much less computationally intensive than *RDQ*. Secondly, *Vval* is much more suited to validate simulation results with experimental results since the exact position of the BB is irrelevant for the calculation of the *Vval* values.

Using the *Vval* values of simulation results and comparing these to experimental results will give an indication to the similarity of the behaviour of the rotor between simulation and real-world results. This method empowers the researcher to use a quantitative value, instead of only a qualitative visual comparison, to measure the similarity between simulation and real-world results.

5.3.3 *Vval* value classification

The classification of the value of the *RDQ* for a certain rotor delevitation event has a clear breakaway value where the BBs start to degrade. This is not the case with *Vval*. The value of *Vval* is also dependent on the chosen value for n the sample window size. This makes the classification of *Vval* values a difficult task. The table below shows the values of *Vval* based on a window size of 1 000 samples at a sampling frequency of 10 000 Hz. The classification is again based on the results of both simulated (found in Appendix C.5) rotor delevitation events and experimental (found in Appendix C.6) rotor delevitation events. It is important to note that these classification values should be refined using consecutive rotor delevitation events followed by in depth analysis of the bearing degradation.

Table 6: *Vval* value classification

Vval value	Rotor motion	Bearing degradation
0 - 90	Ideal rocking motion	Minimal
90 - 170	Rocking motion with minor bouncing	Very low
170 - 250	Low speed forward whirl (low whirl frequency)	Low
250 - 500	High speed forward whirl or low speed backward whirl	High
>500	High speed backward whirl	Destructive

In Table 6, the *Vval* values are classified according to their magnitude. It is important to note that these values are only valid for a window size of 1 000 samples and at a sampling frequency of 10 000 Hz. The distinction between the different classifications is not as well defined as the classifications of *RDQ* values. The classification shown in Table 6 only serves as a guide.

5.4 Comparison of *RDQ*, *Vval* and *Vvala* to impulse of simulated rotor delevitation events

Based on the work presented in Section 5.2 and 5.3, it is necessary to indicate whether these quantification methods (*RDQ* and *Vval*) are valid quantification methods. The quantification methods are validated by the comparison of various simulated rotor delevitation events' impulse values to either the *RDQ* or the *Vval* values of the same simulated rotor delevitation events. If these comparisons have a relation to each other, it can be stated that the quantification method is validated since the quantification method based on position data (*RDQ* and *Vval*) correlates to quantification methods based on force data (Impulse).

5.4.1 Validation of *RDQ* quantification method

The data used to validate the *RDQ* quantification method was generated using the model described in Chapter 3 and Chapter 4. In total, 1 343 rotor delevitation events were simulated with varying system parameters. The system parameters that were varied are the bearing stiffness, the bearing damping, the friction factor between the rotor and the bearing inner-race, the inertia of the bearing inner-race and the rotational speed of the rotor. By varying these parameters over a wide range of values, it is ensured that the results are valid for a large range of system parameters.

Figure 27 shows the comparison between the impulse and the *RDQ* values for 1 343 simulated results. Plotting the impulse versus the RDQ values of both bearings for 1 343 delevitation simulations produces 2 686 data points. The figure shows a clear correlation between the *RDQ* values and the impulse values of the rotor delevitation events although the results bifurcate into two separate trend lines as given in Figure 27.

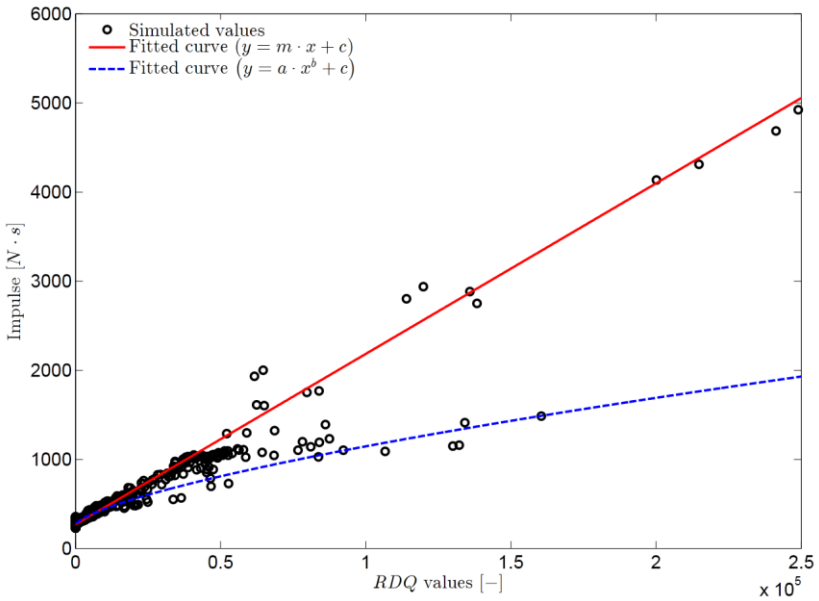

Figure 27: Comparison of impulse and *RDQ* values of 1343 simulated rotor delevitation events

The bifurcation can be explained by the fact that the *RDQ* method uses a combination of the average and maximum values of (5.8) as shown in (5.9) where the impulse value is determined using only the average force over the entire rotor delevitation event duration. The products are two

distinct tendencies when comparing *RDQ* to the impulse of rotor delevitation events. The bifurcation of the results can be explained by a rotor delevitation event where there is a short period of violent bouncing followed by a long period with a rocking motion. In this case the impulse value would be lower compared to the *RDQ* value because the *RDQ* value is based on both the average and the maximum value.

Although there is bifurcation of the results when comparing *RDQ* to the impulse of the simulated rotor delevitation results, the quantification method is validated. Refining the chosen parameters could possibly remove the bifurcation in the results. Since there is more than one relationship between the *RDQ* and impulse values, using the *RDQ* factor quantification method to validate the simulation model would not be ideal.

5.4.2 Validation of *Vval* and *Vvala* quantification methods

The same data used to validate the *RDQ* quantification method was used to validate the *Vval* and *Vvala* quantification methods. In this case 2 686 *Vval* values were calculated as well as their corresponding *Vvala* values to produce 5 372 data points. These values are correlated to the impulse-per-second values since *Vval* was calculated using 1 000 samples (0.1 seconds) and *Vvala* using 60 000 samples (6 seconds). The result is shown in Figure 28.

Figure 28 shows a clear correlation between the impulse and the *Vvala* and *Vval* values. Although the correlation between the impulse and the *Vvala* and *Vval* values is not exact, both *Vval* and *Vvala* produce an indication of the impulse produced during a rotor delevitation event without using any force data. An approximation of the impulse value for a certain *Vval* or *Vvala* value can be found using (5.16). It is important to note that this relationship is only valid for the specific system under investigation.

$$I_{perSecond} \simeq 1.217\times10^{-3}\cdot Vval^2$$
$$I_{perSecond} \simeq 1.217\times10^{-3}\cdot Vvala^2 \qquad (5.16)$$

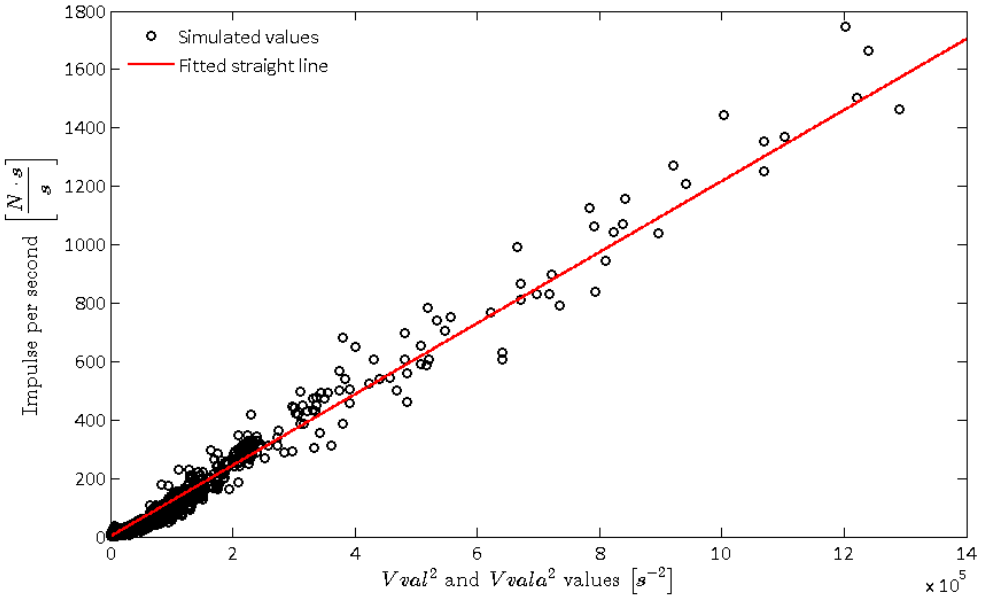

Figure 28: Comparison of *Vval*^{2} and *Vvala*^{2} to impulse-per-second of 1343 simulated rotor delevitation events

The hypothesis made in Section 5.3 is validated with the relationship being of a second order. The relationship between Vval and the impulse is given in (5.17) where K_q is a constant dependent on the system under investigation.

$$I_{perSecond} = K_q \cdot Vval^2$$
$$I_{perSecond} = K_q \cdot Vvala^2 \quad (5.17)$$

Since both *Vval* and *Vvala* can be directly related back to impulse, they are considered as validated quantification methods. Secondly, since there is a functional relationship between the impulse values and the *Vval* and *Vvala* values, this quantification method would be ideally suited to validate the simulation model based on experimental delevitation events.

5.5 Discussion on quantification methods

Both of the discussed quantification methods (*RDQ* and *Vval*) are validated using impulse data for 1 343 simulated rotor delevitation events. The validation enables the quantitative comparison of experimental and simulated results. The quantitative comparison of experimental and simulated results is critical in the validation of the simulation model.

Both *RDQ* and *Vval* quantification methods have advantages and disadvantages. While the *RDQ* method was found to be very useful when using simulation data, it was found that a small variation in the location of the BBs in experimental data produced widely varying results. This is problematic since the exact location of the BB cannot be determined with satisfactory tolerance when using experimental data. To this end and taking into account that the *RDQ* method does not produce a singular relationship to the impulse values, it was decided to validate the model using the *Vval* quantification method.

The *RDQ* method does produce a clear threshold between safe and unsafe rotor delevitation events. This threshold is not as clearly defined when using the *Vval* quantification method (refer to Table 5 and Table 6).

Since the calculation of the *Vval* and *Vvala* values are computationally not as intensive as the calculation of *RDQ* values, *Vval* and *Vvala* can be calculated in real-time on most commissioned AMB systems. The real-time calculation of these values enables condition monitoring of the BBs.

Due to the good correlation between impulse and *Vval* and *Vvala*, both the *Vval* and *Vvala* quantification methods are used to validate the rotor delevitation model.

5.6 Conclusion

In this chapter, three different methods of quantifying the severity of rotor delevitation events were described. The first method is to use the impulse of a rotor delevitation event. The *RDQ* method utilises various factors that influence bearing degradation to determine a value that indicates the severity of a rotor delevitation event. The *Vval* method makes use of the distance that the geometric centre of the rotor travels over time. This value is an indication of the energy transformed and absorbed by the BBs and also indicates the severity of a rotor delevitation event.

Both of the developed quantification methods utilize only position data to determine a value that indicates the severity of rotor delevitation events. After the discussion on the *RDQ* factor, the formulation and calculation of *Dval*, *Vvala* and *Vval* were discussed. The *RDQ* factor and *Vval* value

methods were compared using simulation data. With the RDQ factor method the separation between safe and unsafe rotor delevitation events is clear, while with the $Vval$ and $Vvala$ values this separation is not so clear. The advantage $Vval$ is real-time calculation.

In the next chapter, the validation of the BBSim model is discussed. The model is validated by comparing experimental results to simulated results. The comparison is made using three methods, $Vval$, visually and to a lesser extent, the RDQ factor.

Chapter 6

Model validation

In this chapter, the model BBSim is validated by comparing simulated results to experimental results. The comparison of these results is done by using the quantification method discussed in Chapter 5. The *Vvala* and *Vval* values of the experimental rotor delevitation events are compared to similar simulated rotor delevitation events. The simulated results were produced using a 3.2 GHz (12 core) CPU with 24 GB of RAM, simulation time varied between 1 and 2 hours per second of simulated rotor delevitation event when running 10 simulations in parallel.

A separate visual comparison of rotor orbits during simulated and experimental rotor delevitation events is performed. The comparisons focus on the shape and behaviour of the rotor orbits. Figure 29 shows a flowchart of the validation process for both the quantification methods and the simulation model.

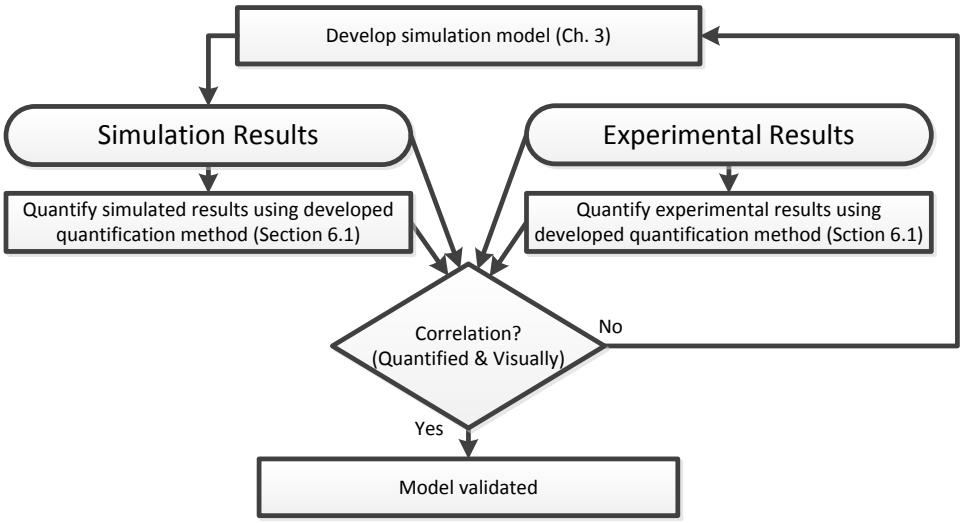

Figure 29: A flowchart of the validation process for the simulation model

6.1 Comparison of experimental and simulated *Vval* and *Vvala* values for different rotational speeds

Comparing the results of simulation models and experimental data obtained from AMB rotor delevitation events is a difficult task. To ease the comparison, the methods previously discussed in Section 5.3 are used. The *Vvala* and *Vval* values are used as a quantitative value to compare the results of the simulations to the experimental results. As with most theoretical results, there are discrepancies between the experimental and simulated results. These discrepancies are attributed to the stiff nature of bearing problems, the uncertainty of certain simulation parameters and the presence of noise in the experimental results.

All the experimental results were obtained using an AMB system [52] modified to work with rolling element BBs (Figure 18). Figure 30 shows the comparison between experimental and simulated *Vvala* values for bearing one. The black circles represent *Vvala* values for experimental rotor delevitation events lasting 6 seconds. Correspondingly the green squares represent the *Vvala* values for simulated rotor delevitation events lasting 6 seconds.

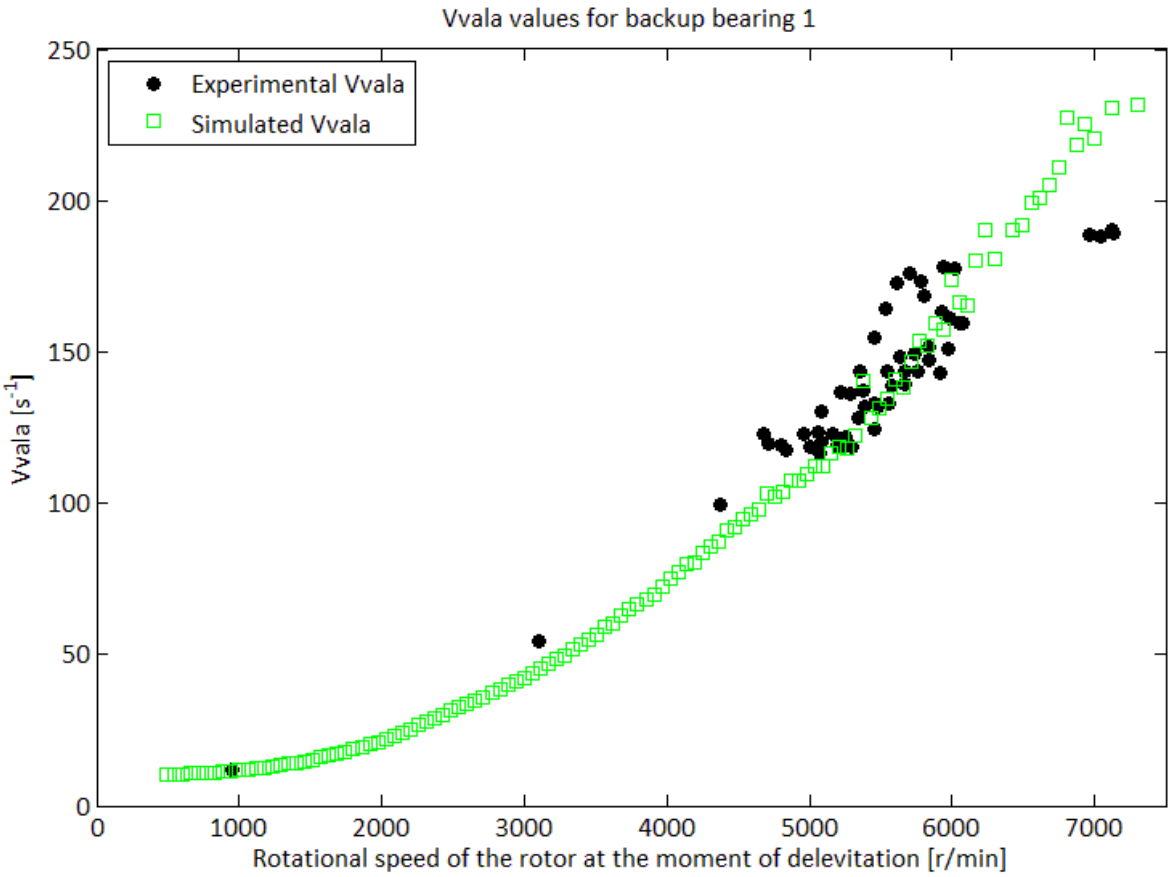

Figure 30: *Vvala* values compared between experimental and simulated results for bearing 1 (n = 60 000, f_s = 10 000 Hz)

The experimental and simulated data correlate well especially when considering that the stiffness and damping values for the bearing were not experimentally determined. The figure shows good correlation up to 6 000 r/min. The last data point taken at 7 000 r/min shows a lower *Vvala* value when compared to the simulated data. A possible explanation is that during the experimental spin-up of the rotor, the bearing inner-race of bearing one started to rotate with the rotor before the delevitation of the rotor due to an excessively large orbit. This spin-up of the inner-race caused the rotor and inner-race of the bearing to have the same rotational speed. The *Vvala* of this bearing would be less in the experimental results since there is no spin-up of the inner-race in the simulation.

When comparing the same results for bearing two (Figure 31) the correlation continues up to 7 000 r/min. This is to be expected since, in the experimental setup, bearing two does not spin up at higher speeds because there is not such a large rotor orbit as with bearing one.

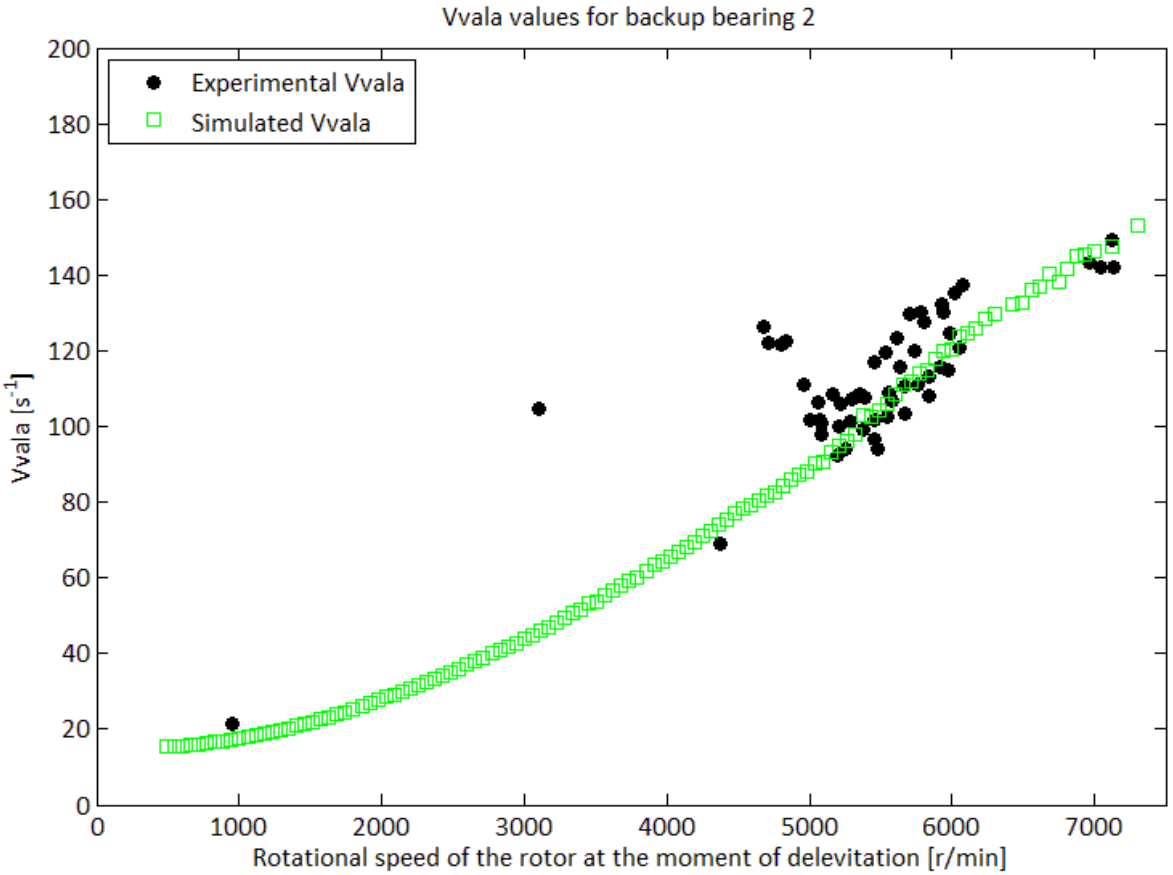

Figure 31: *Vvala* values compared between experimental and simulated results for bearing 2 (n = 60 000, f_s = 10 000 Hz)

Figure 32 shows the *Vval* values of experimental rotor delevitation events compared to those of simulated rotor delevitation events for bearing one. Similar to Figure 30, the experimental results show a lower *Vval* value for higher speeds when compared to the simulated results. This is, once again, due to the inner-race spin-up because of the excessively large rotor orbit in the experimental system at higher speeds.

Figure 33 shows the *Vval* values for bearing two for both experimental and simulated rotor delevitation events. The correlation between the values is better when compared to those of bearing one. In the experimental system, bearing two has a smaller rotor orbit than bearing one and consequently the bearing inner-race does not spin-up before the delevitation of the rotor.

It is interesting to note that the simulated results for both bearing one and bearing two show a wider spread in the results for *Vval* when compared to the narrow spread of the results for *Vvala*. The narrow spread of the results for *Vvala* is due to the fact that these values are averaged over 6 full seconds while the *Vval* values are calculated for 0.1 seconds.

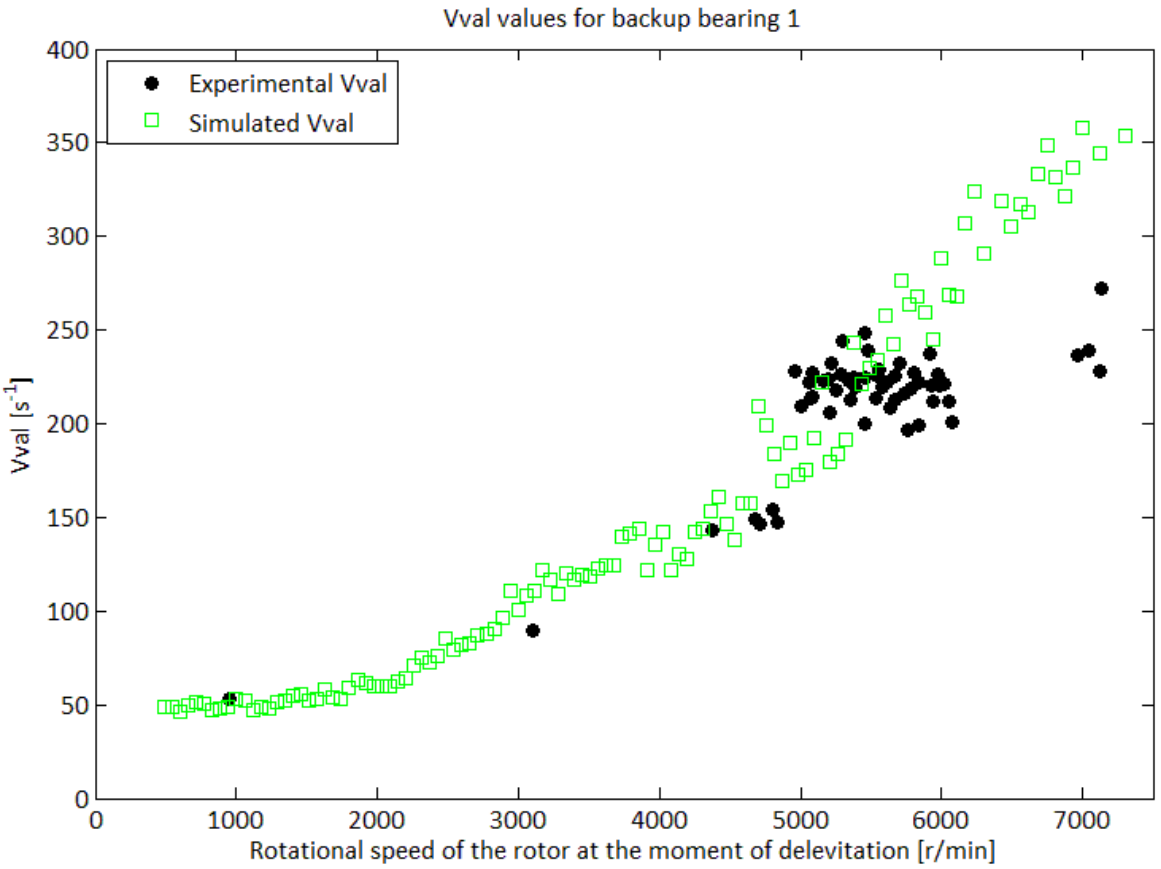

Figure 32: *Vval* values compared between experimental and simulated results for bearing 1 (n = 1 000, f_s = 10 000 Hz)

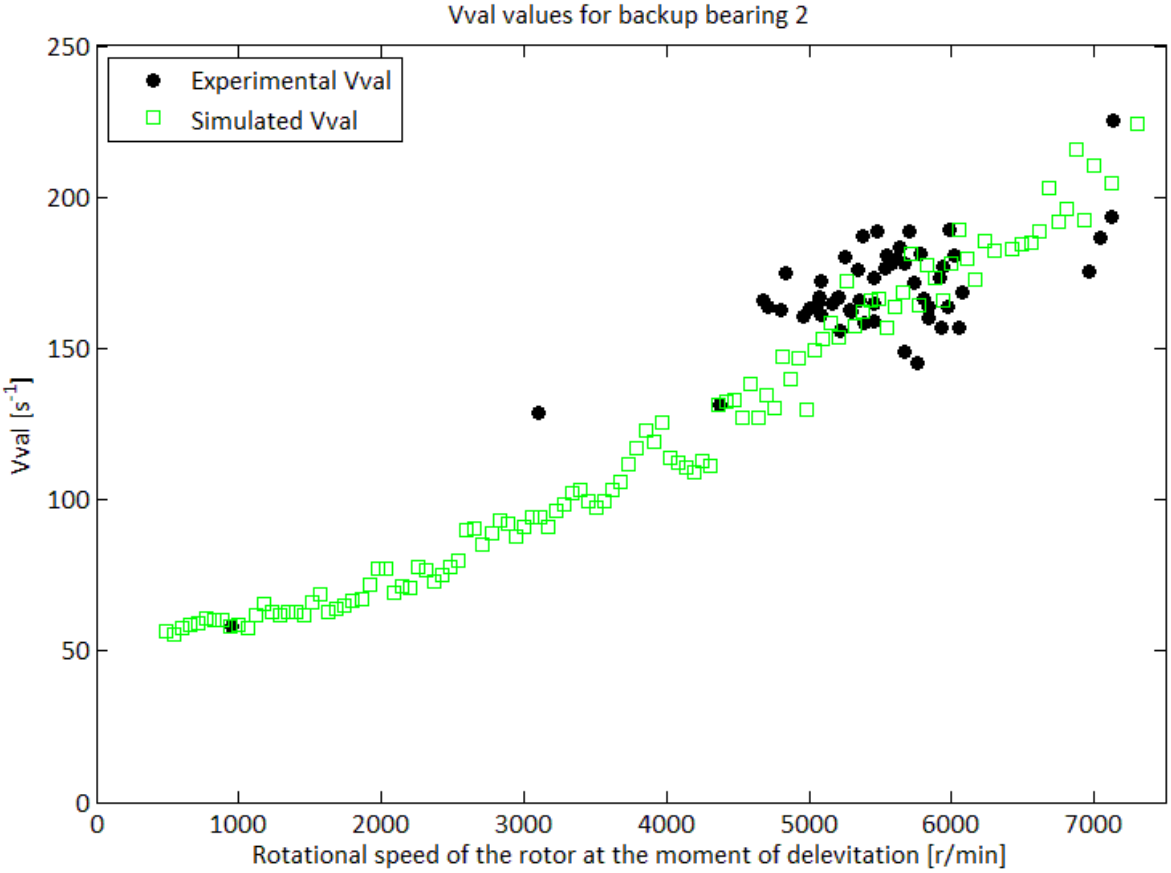

Figure 33: *Vval* values compared between experimental and simulated results for bearing 2 (n = 1 000, f_s = 10 000 Hz)

When using the validated quantification methods *Vval* and *Vvala* to compare simulated results to experimental results, the results show satisfactory correlation between the experimental and simulated results.

Before a statement can be made on the validation of the simulation model, a few of the experimental and simulated results are visually compared. The visual comparison of the rotor orbits during delevitation events ensures that the simulation model adequately predicts the correct rotor behaviour. The visual comparison of these rotor delevitation orbits is presented in the next section followed by a statement on the validation of the simulation model.

6.2 Visual comparison between experimental and simulation results

In this section, some selected results are presented showing different rotor behaviours during different initial conditions and compared to similar simulated results (also presented in [55]). The stiffness and damping of the bearing and bearing housing could not be measured accurately and therefore the experimental and simulated results do not correlate exactly. The behaviour of the rotor orbits is, however, important to note. The following case studies are done with experimental results obtained using an AMB system [52] modified to work with rolling element BBs (Figure 18).

Figure 34 shows the rotor orbit plot comparison for a rotor delevitation event where the rotational speed of the rotor at the moment of delevitation was $1\,173$ r/min. Comparing the simulated and experimental results for bearing one (the two plots on the left side of the figure), shows that the simulated and experimental results are similar. In particular, note the first bounce of the rotor. It is also important to note the presence of noise in the experimental results. Comparing the results for bearing two also reveals similar behaviour. After initial contact, the rotor bounces to the right of the clearance circle and then settles to a rocking motion with relatively small amplitude.

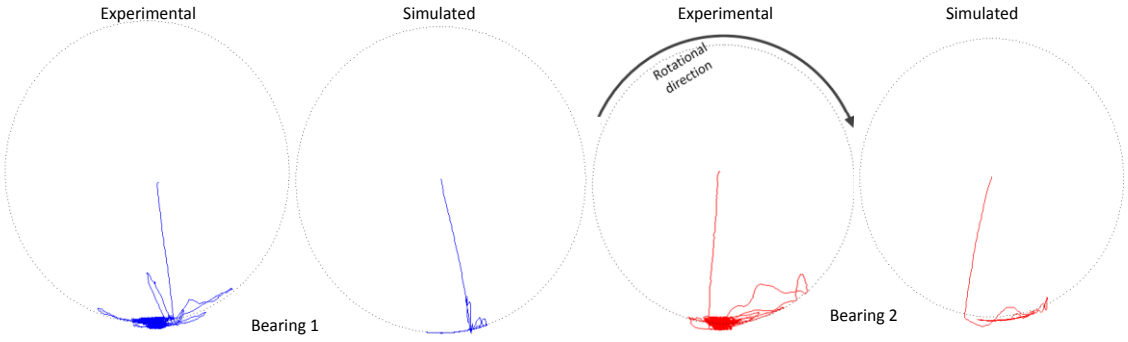

Figure 34: Orbit plot comparison for a rotor delevitation speed of 1 173 r/min (minimal rocking motion)

In Figure 35, similar results are shown with the exception that the initial rotational speed of the rotor delevitation event was higher ($2\,201$ r/min). Once again, note the presence of noise in the experimental results. The comparison between simulated and experimental results for bearing one displays very similar behaviour for the experimental and simulated rotor delevitation events, with the exception of the amplitude of the rocking motion. The difference in amplitude of the rocking motion is attributed to the fact that the bearing and bearing housing stiffness and damping values in the simulation differ from the real values. Secondly, the damping value present in the simulation of bearing two is too high. The excessively high damping value used for bearing two in the simulation not only affects the behaviour of bearing one, but also explains the lower amplitudes of the first bounce and the rocking motion present in bearing two. The bearing characteristics and rotor behaviour for bearing one influence the rotor behaviour at bearing two, and vice versa, due to cross-coupling.

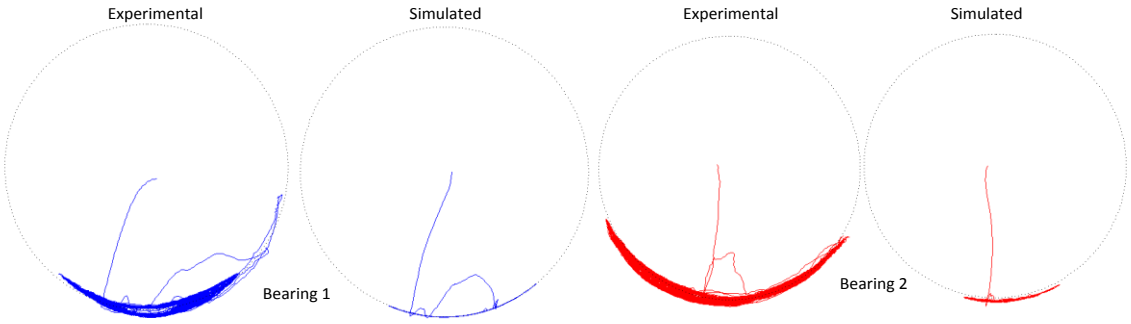

Figure 35: Orbit plot comparison for a rotor delevitation speed of 2 201 r/min (rocking motion)

A rotor delevitation event with an initial rotational speed of 4 589 r/min is shown in Figure 36. The experimental and simulated results of bearing one seems similar with the exception of the small bounces on the left side of the orbit plot of the simulated results. This is again attributed to the fact that the stiffness and damping characteristics of the simulated model do not exactly match those of the experimental setup. When examining the results of bearing two, it is once again clear that the amplitude of the experimental results' rocking motion is larger than that of the simulated results. This is assumed to be due to an excessively large damping present in the simulation model. The simulation and experimental results show a rocking motion for bearing one and two.

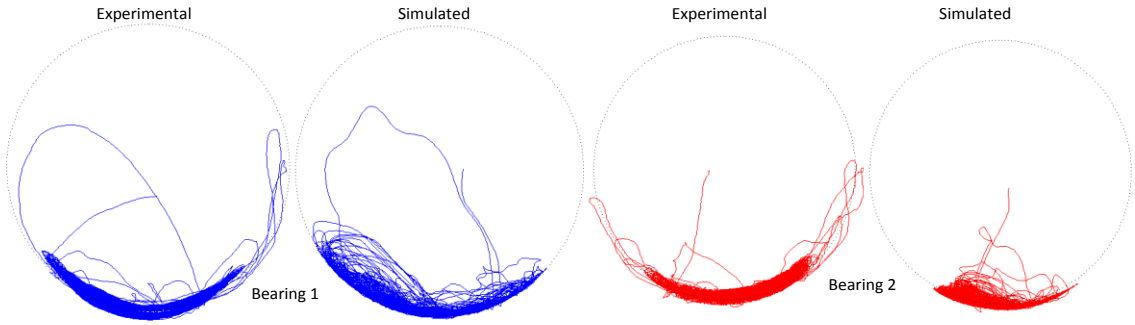

Figure 36: Orbit plot comparison for a rotor delevitation speed of 4 589 r/min (rocking motion with small bounces)

The results of a rotor delevitation event with an initial rotational speed of 5 097 r/min are shown in Figure 37. Comparing the rotor behaviour at bearing one clearly shows that both the simulation and the experimental results predict a tendency to go into a forward whirling motion, but both only experience a period of bouncing, and then settle to a rocking motion. An excessively large damping is again present in the simulation model of bearing two.

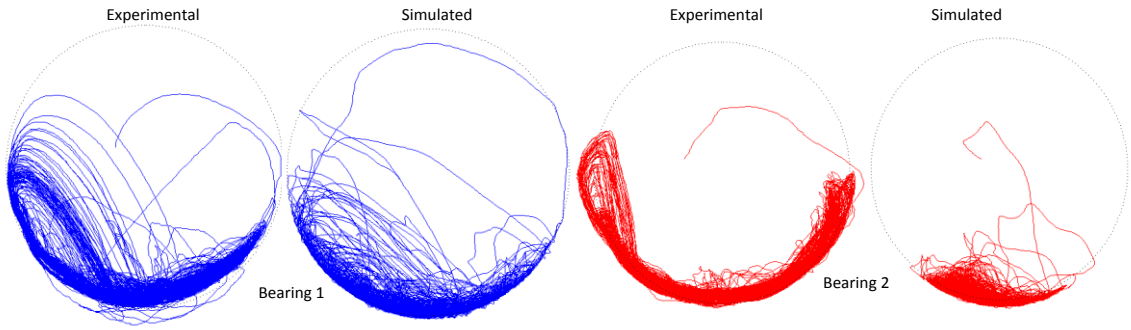

Figure 37: Orbit plot comparison for a rotor delevitation speed of 5 097 r/min (rocking motion leaning towards forward whirl)

Forward whirl occurs when the rotor orbit is in the same direction as the rotational direction of the rotor. If the rotor spins anti-clockwise, the rotor orbit is also anti-clockwise in direction. Backward whirl occurs when the rotor and the rotor orbit are moving in opposite rotational directions. The

rotor is rotating anti-clockwise but the rotor orbit is clockwise. The difference between forward and backward whirl is illustrated in Figure 38.

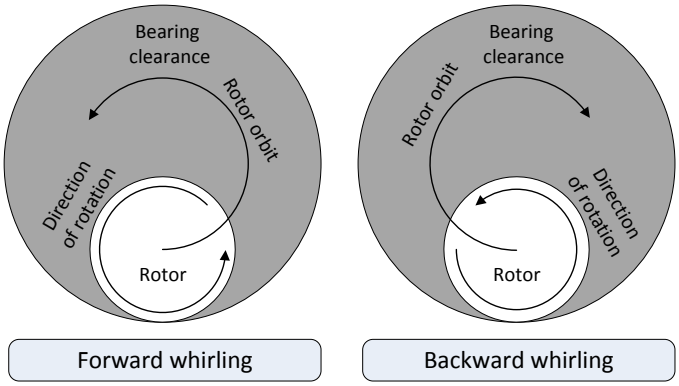

Figure 38: Illustration of forward and backward whirl

Forward whirl is not nearly as destructive as backward whirl. Although a forward whirl condition is not ideal, it remains better than a backward whirl condition. The orbit of a rotor delevitation event in a forward whirl regime is shown in Figure 39 (left bearing).

Figure 39 shows the orbit plots of the rotor behaviour of a rotor delevitation event at $5\,547$ r/min. The results of bearing one show that both simulated and experimental rotors experience a period of forward whirl, settling to a bouncing and then a rocking motion. The higher amplitude of the bouncing present in bearing two (when compared with the bouncing amplitude in Figure 37) indicates that the impact of the rotor at bearing one clearly influences the rotor behaviour at bearing two.

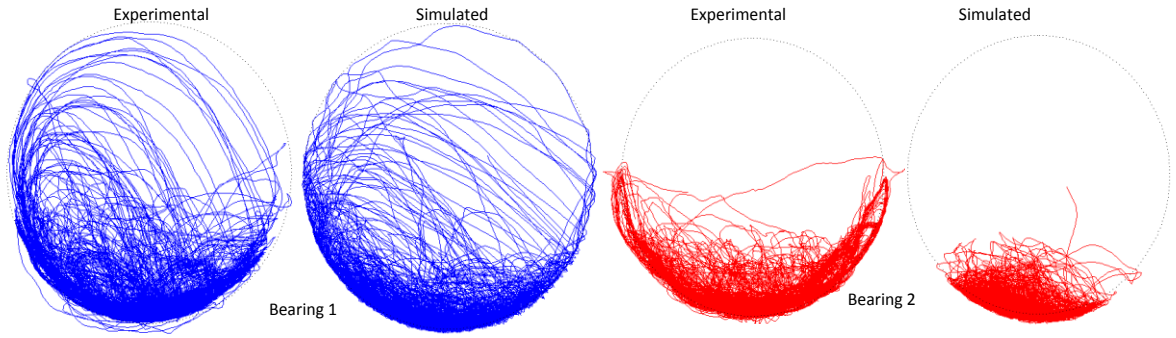

Figure 39: Orbit plot comparison for a rotor delevitation speed of 5 547 r/min (short duration forward whirl)

Figure 40 is similar to Figure 39 with the exception that the period of forward whirl in bearing one is longer and more pronounced than that for similar behaviour for the lower speed rotor delevitation event presented in Figure 39. When examining the results for bearing two it is clear that the impacts at bearing one have an influence on the rotor behaviour at bearing two as also seen in Figure 39.

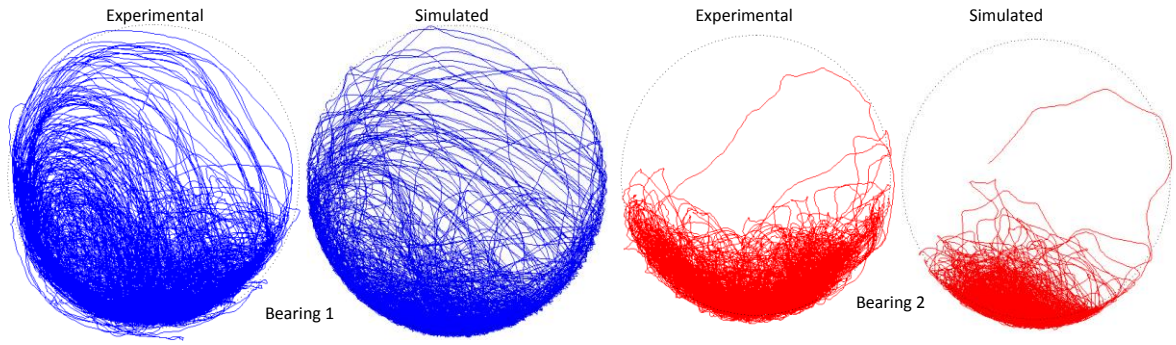

Figure 40: Orbit plot comparison for a rotor delevitation speed of 5 883 r/min (longer duration forward whirl)

6.3 Conclusion

This chapter focussed on the validation of the simulation model BBSim by means of the quantification method described in Section 5.3 and by visually comparing the rotor delevitation events' orbit plots.

The *Vval* and *Vvala* values correlated well up to a speed of $6\,000$ r/min for bearing one and up to $7\,000$ r/min for bearing two. The rotor has a higher level of unbalance at bearing location one and this caused a sufficiently large orbit to produce contact between the bearing inner-race and rotor. The contact between the inner-race and the rotor at bearing location one caused the bearing to spin-up prior to rotor delevitation. This premature spin-up of the bearing inner-race produced a less violent rotor delevitation event since the bearing was already rotating at the same speed as the rotor. This is clearly seen in the quantification plots for bearing one (Figure 30 and Figure 32). Bearing two did not have this problem and the correlation between the simulated and experimental results continued up to the maximum rotational speed of the system at $7\,000$ r/min (Figure 31 and Figure 33).

The figures presented in Section 6.2 show similar behaviour of the rotor for various rotor delevitation events. The rotor delevitation events produce various movement regimes and the movement regimes correlate well between the simulated and experimental rotor delevitation events. These results in conjunction with the results presented in Section 6.1, are sufficient to assume that the simulation model is valid.

The process of validation of the model is based on the delevitation rotational speed being varied and comparing the simulated results to the experimental results. This method was chosen due to financial constraints. The implication of varying only one parameter to validate the BBSim model is that the BBSim model might only be valid for this particular experimental system. The investigation into the validity of the simulation model on other systems is envisaged as future work (Section 8.4.2).

The validation of the simulation model enables a parametric study on the system in question [52]. A parametric study is important since it enables an investigation into the main influencing factors in the severity of rotor delevitation events. The results of this parametric study are presented in Chapter 7.

Chapter 7

BBSim parametric studies

In this chapter, selected parametric studies are done using the validated model. These results were also presented in [55]. The parametric study can be used as a guide when designing AMB systems and selecting BBs. The influencing parameters examined in this section include bearing stiffness, bearing damping, delevitation angle, friction, magnitude of unbalance and the inertia of the inner-race and balls of the bearing.

7.1 Bearing stiffness and damping

The parametric studies were done for three different initial speeds and varying bearing stiffness and damping characteristics. A total of 1 200 simulations, each simulation representing 7 seconds of real world time, were done. In the simulations, the AMBs are switched off after 1 second. This is done in order to let the transients of the AMBs settle. After the AMBs were switched off, there was a rotor delevitation event that was simulated for 6 seconds.

These 6-second simulation results were post-processed in order to produce the *Vvala* and *Vval* values for each rotor delevitation event. The *Vvala* and *Vval* values were then used to produce six different surface plots, one set of three (one for each speed) for the *Vvala* values and one set of three for the *Vval* values. The three axes of the plot are the stiffness, the damping and either the *Vvala* or the *Vval* value. These plots give some insight into how these parameters influence the rotor's behaviour and using these, a few design principles can be obtained.

The sensitivity of *Vval* to the bearing stiffness and damping is shown from Figure 41 to Figure 46. It is important to note that *Vval* values are the maximum value for a 0.1 second window size it emphasizes short periods of destructive behaviour. The higher the *Vval* value, the more destructive the behaviour.

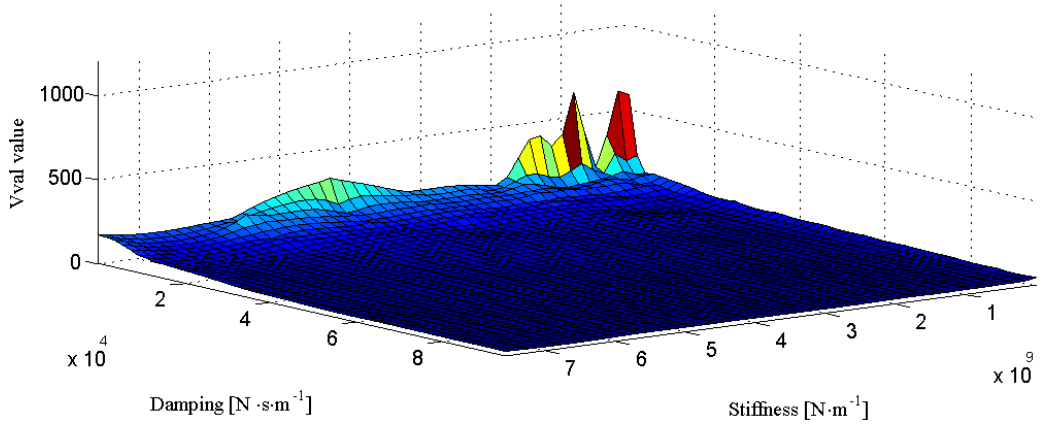

Figure 41: *Vval* for bearing one delevitated at 2 692 r/min

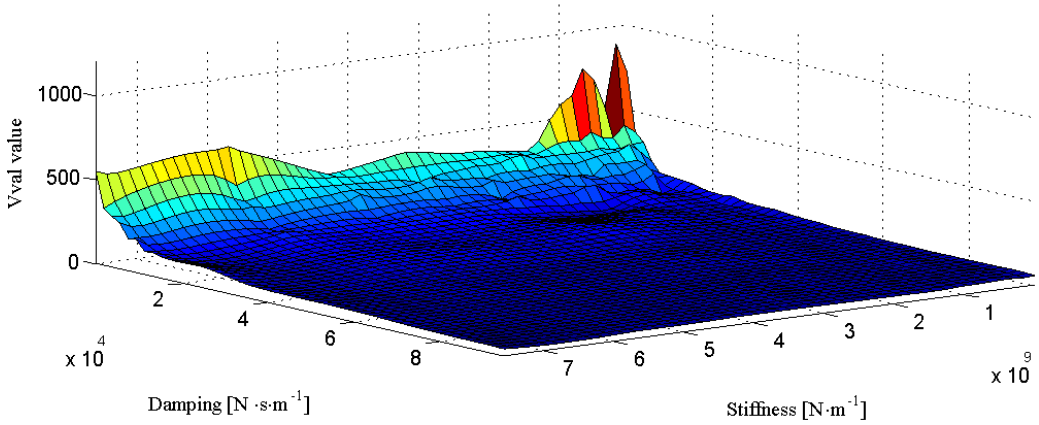

Figure 42: *Vval* for bearing one delevitated at 4 119 r/min

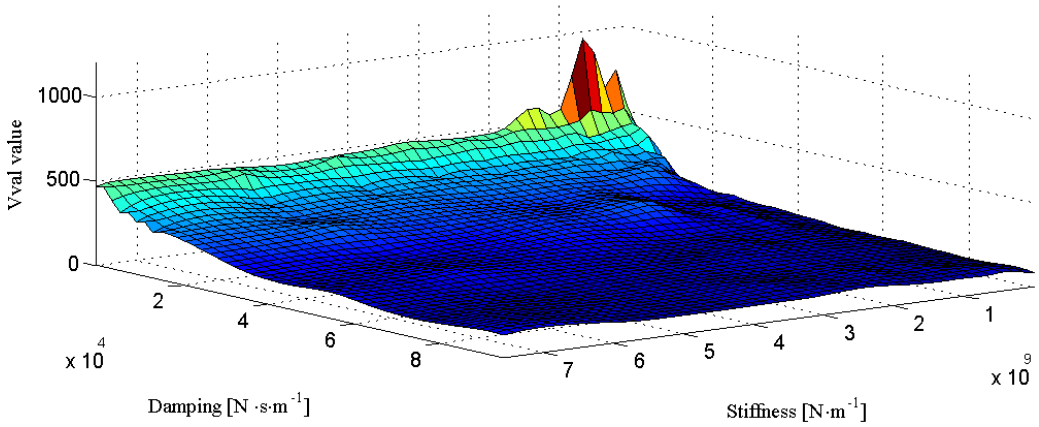

Figure 43: *Vval* for bearing one delevitated at 5 543 r/min

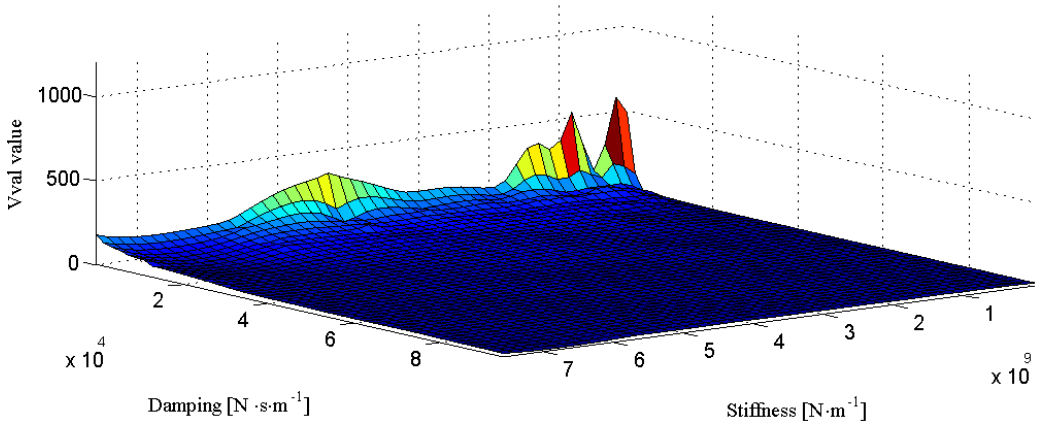

Figure 44: *Vval* for bearing two delevitated at 2 692 r/min

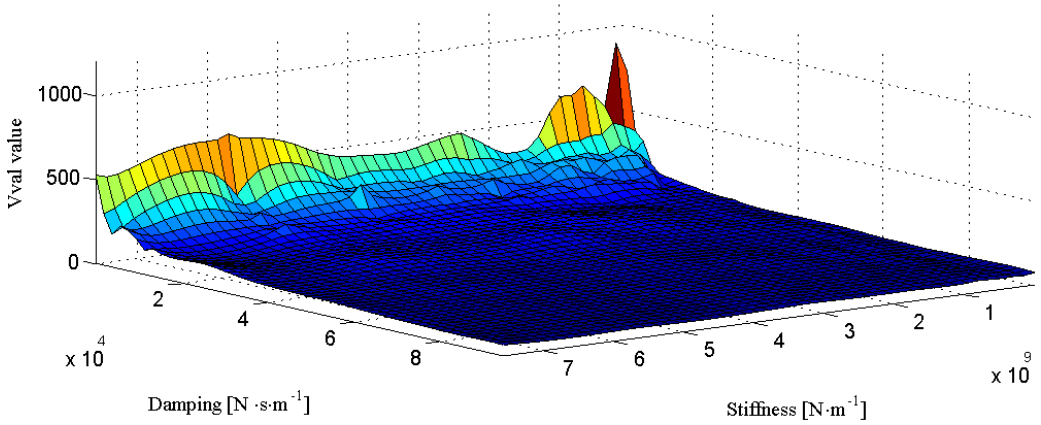

Figure 45: *Vval* for bearing two delevitated at 4 119 r/min

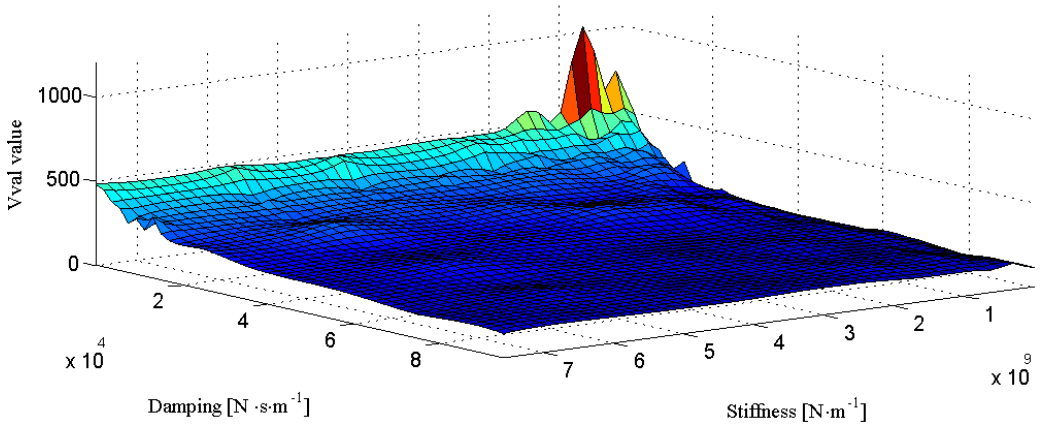

Figure 46: *Vval* for bearing two delevitated at 5 543 r/min

The graphs clearly show that the behaviour is more sensitive to the damping of the system compared to the stiffness of the system for higher damping values. The system is more sensitive to the stiffness at low damping values. While a higher damping is preferable, the stiffness of the system influences the behaviour of the rotor due to rotordynamic harmonics and is dependent on the rotor in question. A similar range statement cannot be made for the stiffness of the system since the ideal stiffness will vary depending on the rotordynamic characteristics of the rotor in question. Generally, it can be stated that excessively high and excessively low stiffness values should be avoided.

Figure 47 to Figure 52 show the same six surface plots as in Figure 41 to Figure 46 with the exception that *Vvala* was determined with a window size of 60 000 samples (at a sampling frequency of 10 000 Hz). From these plots, it is clear that the increased window size has an averaging effect. This means that the results obtained with a larger window size shows the average severity of a rotor delevitation event, averaging out short periods of violent rotor behaviour. From these results, it is once again clear that the rotor behaviour is more sensitive to the system damping than the stiffness. The rotordynamic harmonics due to the variation of the stiffness of the system are also less visible in these results since the rotor speeds down through the critical frequency and the result of the behaviour of the rotor during this period is averaged out by the rest of the rotor behaviour not near critical frequencies.

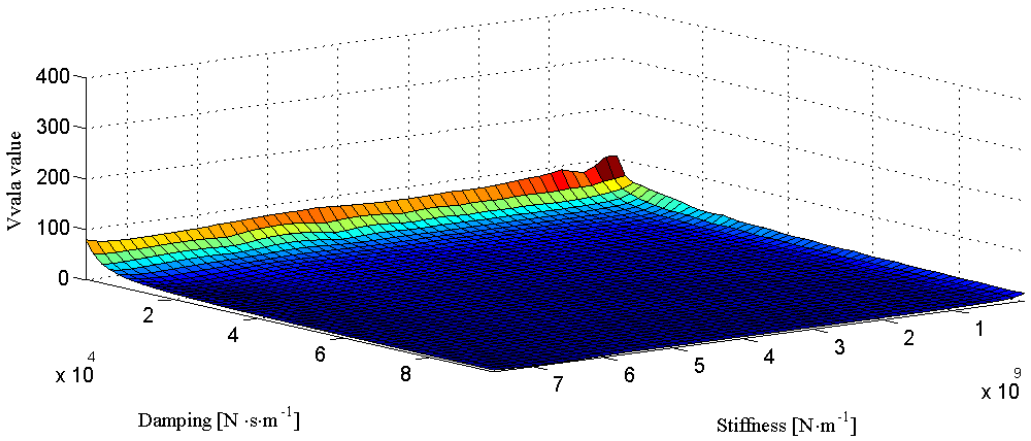

Figure 47: *Vvala* for bearing one delevitated at 2 692 r/min

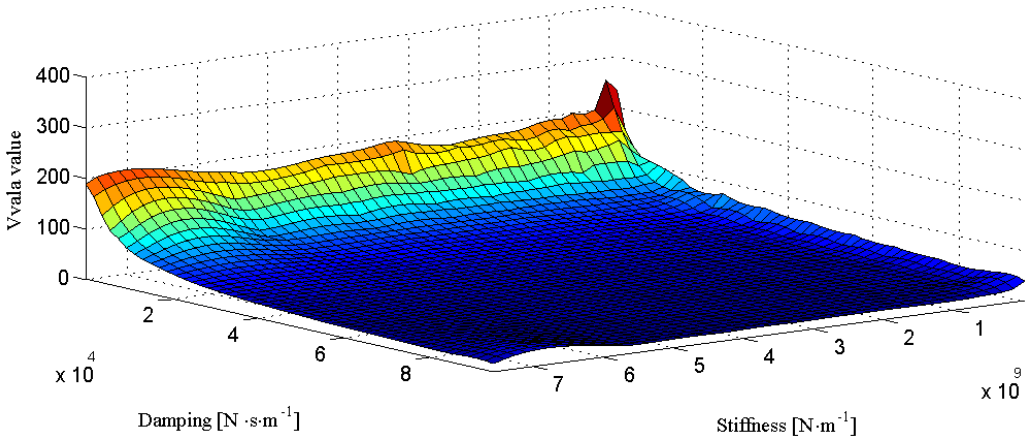

Figure 48 *Vvala* for bearing one delevitated at 4 119 r/min

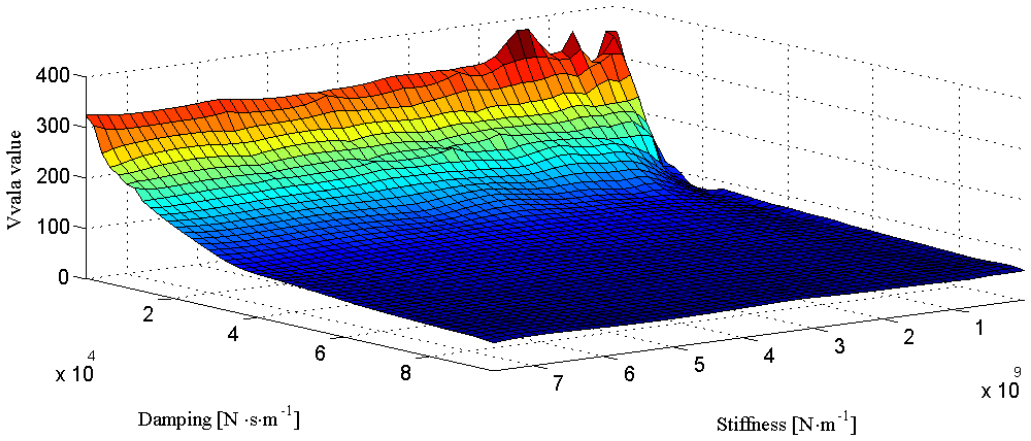

Figure 49 *Vvala* for bearing one delevitated at 5 543 r/min

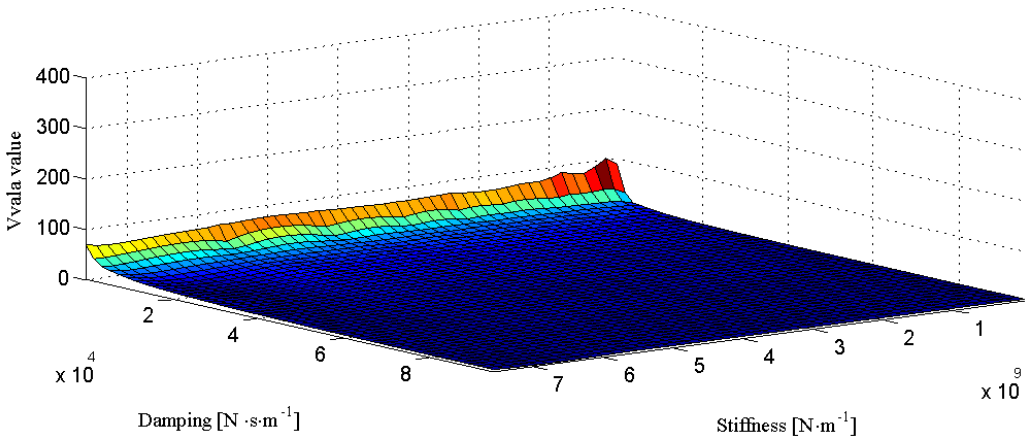

Figure 50: *Vvala* for bearing two delevitated at 2 692 r/min

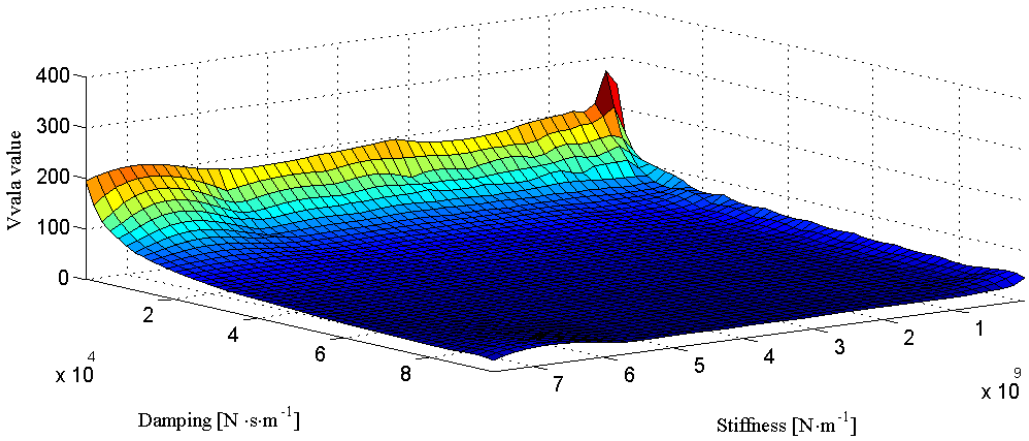

Figure 51 *Vvala* for bearing two delevitated at 4 119 r/min

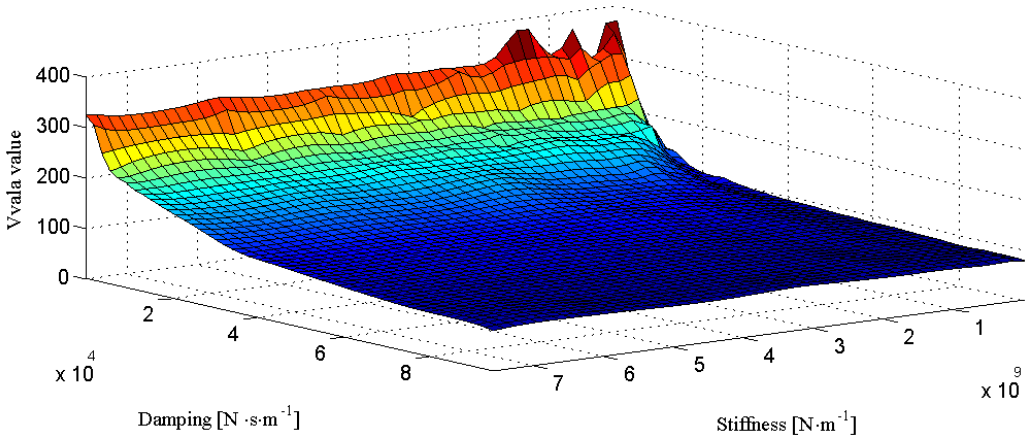

Figure 52 *Vvala* for bearing two delevitated at 5 543 r/min

The results from both these sets of figures are important when determining the optimal bearing stiffness and damping. The smaller window sized *Vval* (Figure 41 to Figure 46) is important in choosing the appropriate bearing stiffness and the larger window sized *Vvala* (Figure 47 to Figure 52) is important in determining an appropriate bearing damping.

7.2 Delevitation angle

The delevitation angle is the angle of the centre of mass of the rotor relative to the geometric centre of the BB clearance at the moment of delevitation as illustrated in Figure 53. This parametric study is

included to determine the impact that the location of the rotor, relative to the geometric centre of the BB clearance, has on the behaviour of the rotor.

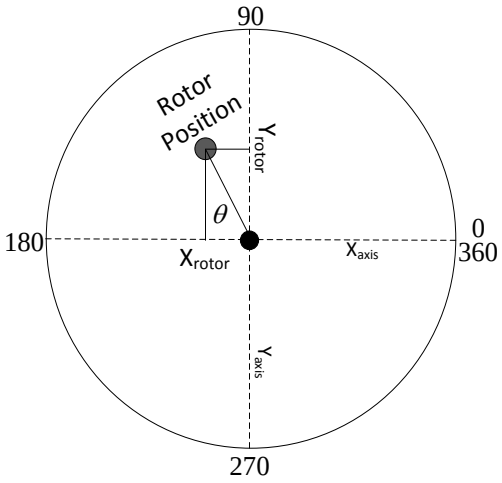

Figure 53: Illustration of the delevitation angle

Shown in Figure 54 to Figure 57 are four surface plots showing the sensitivity for the angle of delevitation and rotational speed of the rotor. Figure 54 and Figure 55 are once again for the smaller window size of 1 000 samples, while Figure 56 and Figure 57 are for a window size of 60 000 samples.

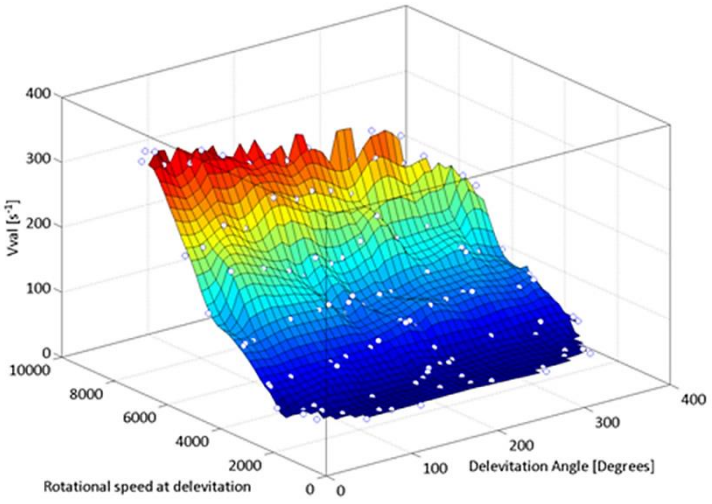

Figure 54: Rotor delevitation event severity (*Vval*) sensitivity for rotational speed and delevitation angle for bearing one

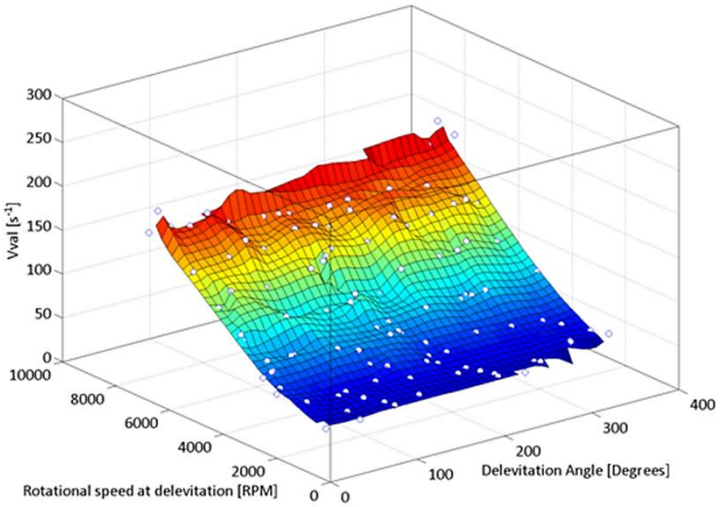

Figure 55: Rotor delevitation event severity (*Vval*) sensitivity for rotational speed and delevitation angle for bearing two

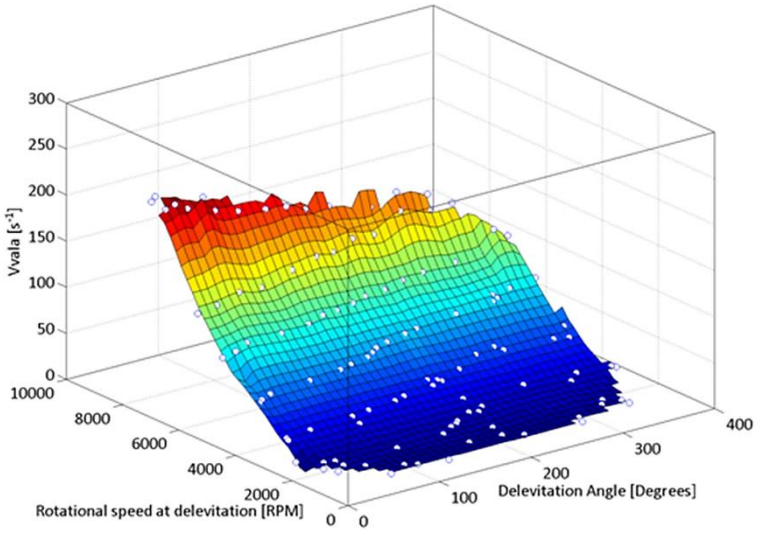

Figure 56: Rotor delevitation event severity (*Vvala*) sensitivity for rotational speed and delevitation angle for bearing one

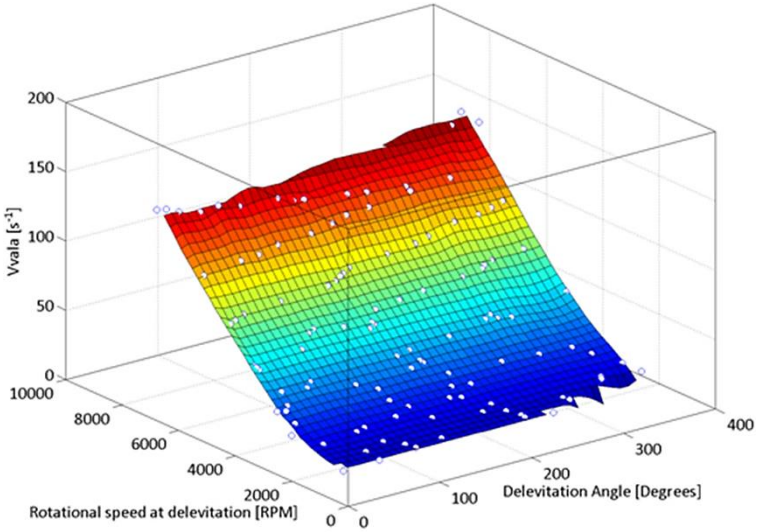

Figure 57: Rotor delevitation event severity (*Vvala*) sensitivity for rotational speed and delevitation angle for bearing two

From Figure 54 and Figure 55, it appears that the rotor behaviour is independent of the delevitation angle. It is however clear that the rotational speed has a large influence on the behaviour of the rotor, where higher speeds produce more destructive behaviour, as is expected. When examining Figure 56 and Figure 57, a small but noticeable effect on the behaviour is noted. If the rotor is delevitated near 0 or 360 degrees, larger *Vval* and *Vvala* values are produced.

7.3 Friction between inner-race of the bearing and the rotor

Shown in Figure 58 is the sensitivity of the rotor behaviour to the friction factor between the rotor contact surface and the inner-race of the rolling element bearing. The multiplication factor is simply the factor by which the parameter under investigation is multiplied and in this case, it is the friction factor.

Figure 58 shows that the rotor is relatively insensitive toward changes in the friction between the rotor inner-race and the BB. It is however important to note that this is only valid for rolling element bearings since the increased friction factor between the surfaces in contact causes the rotor and bearings to reach the same rotational speed in a shorter time period. The increased friction factor

also slows down the rotor faster until the rotor and the inner-race reach the same rotational speed. Thus the rotor is initially braked faster to produce a slightly less violent reaction when observing the *Vvala* value.

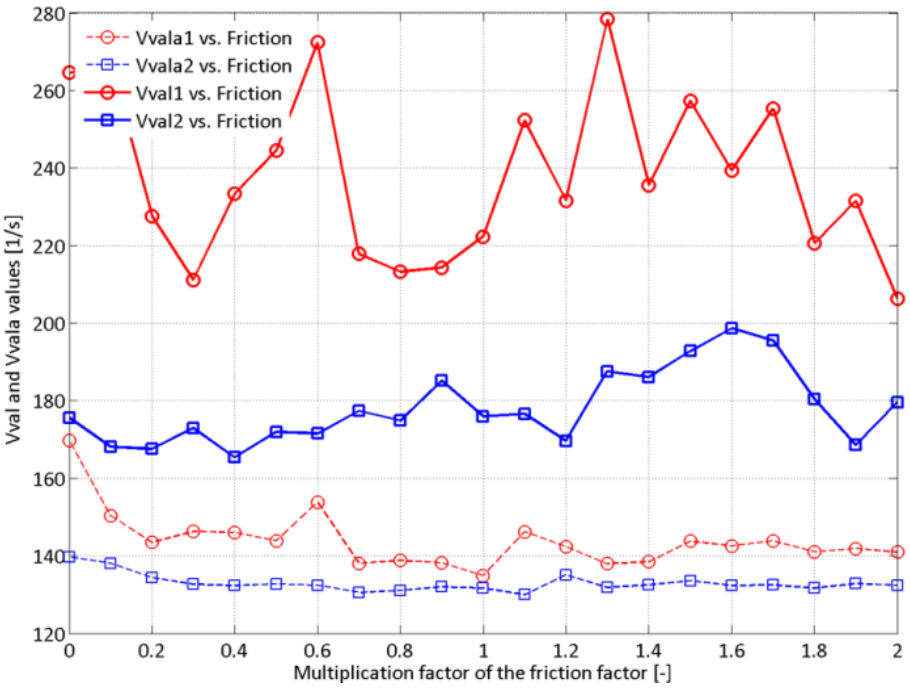

Figure 58: Rotor delevitation severity sensitivity to friction between inner-race of BB and rotor surface

The *Vvala* value for both bearings decreases slightly as the friction factor increases. This slight decrease can be attributed to the fact that the rotor and the inner-race reach the same rotational speed earlier in the delevitation event. With the rotor and the inner-race at the same speed, the behaviour of the rotor is essentially a rolling motion with minimal impacts.

The *Vval* values seem to contradict the *Vvala* values with a slight increase as the friction factor increases. The initial behaviour of the rotor will be more violent with increased friction between the surfaces in contact. With *Vval* only having a window size of 1 000 samples and only the maximum value for *Vval* plotted in the graph, the plotted values show that the initial behaviour of the rotor is more violent with increased friction. The more violent behaviour is due to the rotor being forced to climb the walls of the bearing clearance which produces a bouncing motion while the inner-race speeds up to the rotor speed. The danger in using materials with a high friction factor is that the rotor can be forced into a backward whirling motion with destructive consequences.

It can be concluded from these results that the friction between the rotor and the inner-race should not be excessively high or low. A too low friction factor would cause the rotor to be more prone to forward whirl (compare orbit plots of bearing one in Appendix C.5 on page 1803 and 1822) while an excessively large friction factor could induce backward whirl.

7.4 Inertia of the bearing inner-race and balls

In Figure 59, the rotor sensitivity to the inertia of the inner-race and balls of the rolling element bearing is shown. The sensitivity is similar to that of the friction factor, with the exception that the smaller window size *Vval* values seem insensitive to the variation in inertia of the rolling element bearing. This decreased sensitivity is because even though the bearing takes longer to reach the same rotational speed as the rotor, the friction factor remains constant, preventing an initial bouncing motion of the rotor.

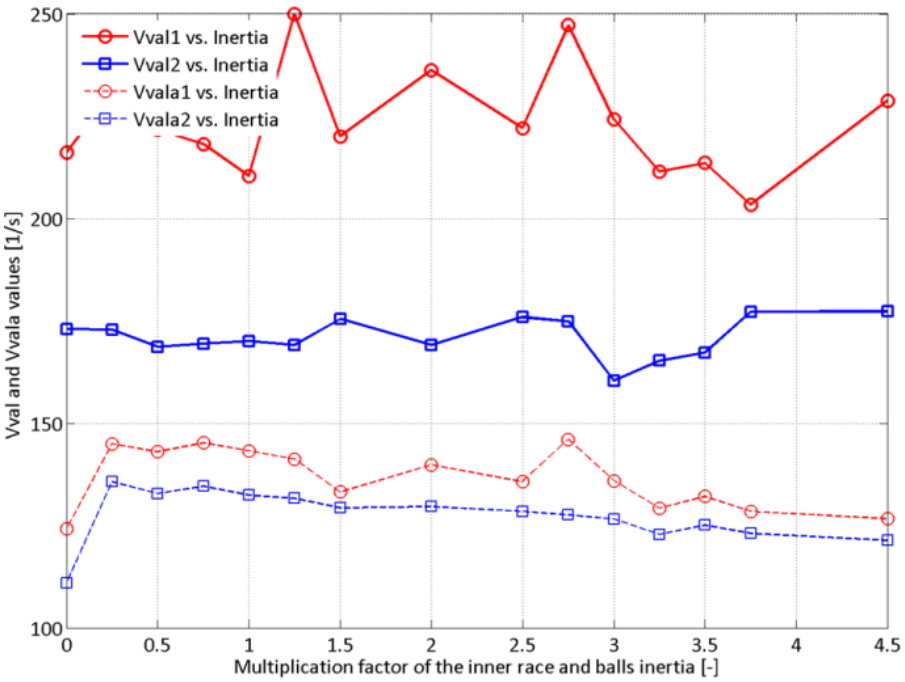

Figure 59: Rotor delevitation severity sensitivity to inertia of the inner-race and balls (size) of the BB

When investigating the results from the larger window sized *Vvala* values, it would appear that an ideal value for the inertia of the rolling element bearing would be zero, but this is not feasible. Another possible conclusion is that it would be ideal if the rotor and the bearing inner-race had the same rotational speed at the moment of delevitation, but this is also not feasible.

The inertia of the rolling element bearing is, in effect, causing a braking action on the rotor. With larger inertia, the bearing takes longer to reach the same rotational speed as the rotor. This means that the braking action is present for a longer time. This prolonged braking action causes the rotor to speed down quicker and the rotor behaviour is generally less destructive.

Due to the braking action applied to the rotor, a bearing with a higher inertia seems to be better. The risk of using a bearing with an excessively large inertia is that the rotor could develop backward whirl should the friction force be sufficient. This risk is higher when the rotor traverses a critical speed.

These results are important when considering a rotor that is not actively braked in the event of a magnetic bearing failure. Should the rotor be actively braked, the advantages of using a bearing with higher inertia is negated by the risk of causing backward whirl. In these cases, it would be preferential to use a bearing with a small inertia to ensure that the bearing and rotor reach the same speed faster, negating the possibility of developing backward whirl.

7.5 Unbalance of the rotor

In Figure 60, the sensitivity of the rotor behaviour to the unbalance of the rotor is shown. From the results plotted in the graph, it is clear that the rotor behaviour is sensitive to the magnitude of the unbalance of the rotor. While the plot shows that a lower unbalance would be preferential, this might not always be the case.

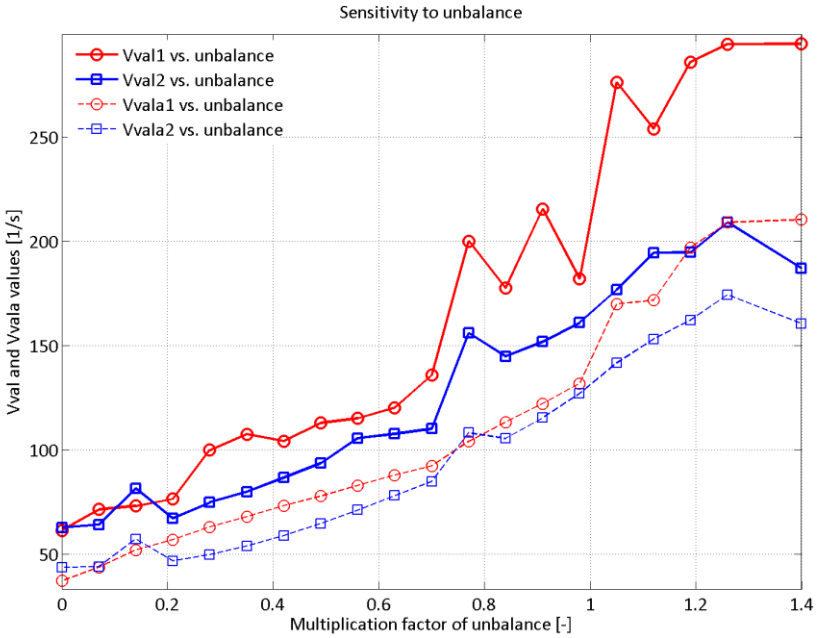

Figure 60: Rotor delevitation severity sensitivity to unbalance of the rotor

Unbalance of a rotor has been shown to prohibit backward whirl of the rotor [8,10,37], while higher unbalance magnitudes tend to cause forward whirl [1,8,10,12,74,75]. Having a low unbalance, in combination with a high friction factor and a bearing with a large inertia, might lead to the development of backward whirl. In general, however, a better-balanced rotor is preferential given that the BBs are rolling element type bearings, with neither an excessively large friction factor present between the surfaces in contact nor excessively large inertia.

7.6 Final thoughts on BBSim

The BBSim model is an integration of many simple models to produce a complex model. The model doesn't use any complex mathematical equations or solution techniques. This helps to reduce the solution time. The model includes more phenomena than any other model in the current literature. The effect of each of these phenomena on each other and the system as a whole is taken into account to produce a result that resembles the real world data better than any of the previous models were able to do.

7.7 Conclusion

The simulation model presented in Chapter 3 (BBSim) was used to perform parametric studies. The parametric studies revealed that the rotor behaviour is determined by various parameters. The results of the parametric studies were analysed and the following conclusions were made:

- Rotor behaviour is less sensitive to bearing stiffness and more sensitive to the bearing damping. A higher damping is preferred with neither an excessively large nor small bearing stiffness.
- Rotor behaviour is found to be slightly sensitive to the delevitation angle where the rotor behaviour is adversely affected when the rotor is delevitated near the right side of the BB clearance for a rotor rotating anti-clockwise, and near the left side for a rotor rotating clockwise.
- Rotor behaviour is moderately sensitive to the friction factor between the surfaces in contact, where the friction factor should neither be too high nor too low. The friction factor

for steel-on-steel of 0.2– 0.25 should be sufficient. This make the need for extra surface lubrication unnecessary.

- A higher inertia for the bearing is preferential for free running (not actively braked) rotors, where the speed-up of the bearing acts as a brake on the rotor. The opposite is preferred for actively braked rotors where a lower inertia is preferred due to the possibility of developing backward whirl.
- Unbalance plays an important role in the behaviour of the rotor. A well-balanced rotor is preferred, given that the bearing inertia and the contact friction are not excessively large.

In the next chapter, conclusions are made from the research presented, the contributions of the research are highlighted and future work is discussed.

Chapter 8

Conclusions and recommendations

This chapter gives the conclusions on the results of the presented body of work. The contributions of this research are highlighted and future work is recommended.

8.1 Conclusions

Various conclusions can be made from the presented research. Some of these conclusions are presented in this section. The conclusions of the research can be categorized in three sub-sections, namely, conclusions about the developed simulation model (BBSim), conclusions about the quantification methods presented and conclusions about the method of validation of the simulation model.

A model for an AMB/BB system is a complex problem but the problem can be divided into less complex sub-problems. The sub-problems can then be modelled relatively easily and be integrated into a whole.

The model presented addresses most of the shortcomings of the simulation models currently in the literature identified in Chapter 2. For the parameters of the AMB/BB system that could not be analytically determined or measured directly, empirical methods were used to determine the values. These parameters were: the bearing clearance, the friction factor between the rotor and the inner-race, the unbalance of the rotor, the aerodynamic deceleration of the rotor, the bearing deceleration caused by the internal friction of the bearing and the circularity of the rotor at the sensing positions. After these parameters were determined, they were implemented in the BBSim simulation model.

The validation of the simulation model was problematic since most AMB/BB systems do not have force measurement capabilities. Alternative quantification methods were developed that do not require force measurement values. Both of the developed quantification methods correlated well with the impulse value for various rotor delevitation events. Because of this correlation between the impulse and the two developed quantification methods, the quantification methods were validated.

The validation of the quantification methods enabled the quantitative comparison of experimental and simulated results. The experimental and simulated quantities also correlated well. Various simulated and experimental rotor delevitation events were qualitatively compared and it was found that the rotor orbits of the simulated and experimental rotor delevitation events were similar. Since both the quantitative and qualitative experimental and simulated results compare well, the model is considered valid.

The RDQ factor method provided a clear distinction between safe and unsafe rotor delevitation events while the $Vval$ and $Vvala$ methods could not. The advantage of $Vval$ is real-time calculation.

8.2 Future work made possible by the development of BBSim

A validated simulation model for AMB/BB systems enables future investigations into problems that were previously not possible. These problems are discussed in the following sections.

8.2.1 Studies into load-sharing

The simulation model developed during this study enables an investigation into the behaviour of the rotor during load-sharing operation. Load-sharing occurs when the AMB is operational but it is being overloaded. The behaviour of the rotor during this operating regime should be investigated in order to optimise the control of AMBs during overload. Similar to the experimental investigation presented in [76] and as stated in [7], this investigation is largely missing from the literature.

8.2.2 Separate AMB failure studies

An investigation into the behaviour of the rotor when only one of the AMBs fails should be completed. An integrated simulation model including the rotor, AMBs and the BBs enables a study into the effect on rotor behaviour should only one of the AMBs fail and the other AMB remain operational. This investigation will enable the development of emergency shutdown procedures for AMB systems where the system is operational but one of the AMBs has failed.

8.2.3 Investigation of rotor behaviour for all AMB failure modes

An investigation into the rotor behaviour for all the failure modes described in [77] (Table 8) should be completed. The integrated model BBSim enables the investigation into all of these failure modes as well as the effect that load-sharing between the AMB and the BB has on the behaviour of the rotor during these failure modes.

An investigation into all the stated failure modes on a simulation model enables the development for emergency shutdown procedures for all of the various failure modes where the shutdown procedure would endeavour to minimise the severity of the rotor and BB interaction.

8.2.4 Effect of circularity on control and stability of AMBs

The effect that the rotor circularity and sensor run-out has on the stability of the rotor needs to be investigated. The sensor run-out can induce synchronous frequencies and higher harmonics on the rotor and may lead to power amplifier saturation and can cause instability. The BBSim simulation model enables an investigation into the frequencies excited because of various non-circular sensor surfaces on the rotor.

Most machining processes do not leave a surface perfectly circular and the discontinuities in the magnetic properties of the shaft material causes sensor run-out. This sensor run-out could cause a super-synchronous error on the position signal of up to $100\ \mu m$. This is not an insignificant value when considering that the total airgap of the system is typically $250\text{-}1\ 000\ \mu m$.

8.2.5 Further investigation into forward whirl

It is proposed that, with the help of BBSim, an in depth investigation should be done on the causes of forward whirl. This investigation could yield important conclusions about what causes forward whirl as well as the driving force behind the frequency of the forward whirl.

8.3 Future work to improve BBSim

The capabilities and limitations of BBSim are given in Appendix A in Table 7. Some of these limitations and how they could be addressed are now discussed.

8.3.1 Modify BBSim to enable the simulation of other BB types

The current version of BBSim in this thesis is only capable of simulating rolling element bearings but the model could be relatively easily modified to also simulate plain BBs. The inclusion of hydro-dynamic bearings poses larger challenges but would also be possible. This would enable the

comparison of using various BB types for the same system and when used in conjunction with the quantification methods presented in this thesis, an objective choice between bearing types could be made.

8.3.2 Include the simulation of axial BBs and AMBs

At the moment, BBSim only simulates the radial AMBs and BBs. The inclusion of an axial AMB and BB is deemed important since a recent publication attributes the formation of forward whirl to the interaction at the axial BBs [48]. Secondly, the inclusion of an axial model would enable an investigation into the axial natural frequencies during levitation and the effect these frequencies has on the stability of the rotor.

8.3.3 Thermal modelling

One of the major limitations of the BBSim simulation model is the lack of thermal modelling. A thermal model should be developed that determines the amount of heat generated by the contact dynamics and the dissipation of this heat through the rotor and the BBs. The heat generated by repeated rotor delevitation events could alter the heat treatment condition of the rotor and cause bearing failure.

8.4 Future experimental work

Through the completion of this research, the following experimental work was identified to improve current knowledge of BBs.

8.4.1 The development of a method for repeatable experimental rotor delevitations

A major issue with experimental work is that the results of experimental tests vary widely for similar rotational speeds. The reason behind this is speculated to be the initial conditions of the rotor during a delevitation event playing a large role in the final behaviour of the rotor. The method used to obtain the repeatable results used in this research should be investigated further.

8.4.2 Compare results to more real-world simulations of larger systems

The experimental results obtained for this research were obtained on a 4-axis suspended rotor with a relatively small mass (approximately $7\ \mathrm{kg}$). The results obtained in this study need to be repeated for a larger mass rotor to determine whether the simulation model BBSim also produces valid results for larger AMB systems.

8.4.3 Refining the threshold values of $Vval$ and RDQ

By examining more experimental results, the threshold values for both $Vval$ and RDQ should be refined. RDQ and $Vval$ values should be an indication of the level of safety during a delevitation event. These values could also be used to classify AMB systems according to the severity should the rotor be delevitated at operating speed.

8.5 Contributions of this research towards BB knowledge

The main contribution of this research is the development of the simulation model BBSim [53] which integrates previous work and new work in a novel way to produce a new simulation model. This model can be used to determine the system behaviour and make improvements to the design based on simulation results.

In the literature behaviour of a rotor in a BB has been stated as being chaotic since widely differing results are obtained for rotor delevitation events at the same rotational speed [2,22,24,27,60]. The

problem is that the behaviour is not only dependent on the initial rotor speed, but also the initial point of contact on the BB.

When the rotor is delevitated at the same phasor angle and at the same rotational speed, the resulting rotor behaviour is repeatable. The method used to obtain repeatable results proves that the system is not chaotic since results can be repeated for the same initial values [54]. The statement that the behaviour of the rotor is not chaotic is also supported by the results obtained in [68]. The delevitation of the rotor at the same phasor angle but at different rotational speeds enables a better comparison between different rotor delevitation events, since the first contact on the bearing is in the same or similar location and not arbitrary. The proposed method also enables the comparison of rotor delevitation events at different phasor angles but at the same rotational speed. These experimental results show whether the rotor behaviour is sensitive to the initial contact point during a rotor delevitation event.

The proposed method to quantify the rotor delevitation event severity in [54,55] creates a way to compare rotor delevitation events of different systems to each other and indeed different delevitation events on the same system to each other. This method can also be used to determine the replacement schedule for bearings currently used in industry.

Although forward whirl has been successfully simulated in [48] the behaviour of the rotor is fully attributed to the interaction of the rotor with the axial BB. While BBSim does not include an axial BB, the model still successfully predicts forward whirl. Although forward whirl is observed in experimental rotor-delevitations, most simulations up to date have predicted the more destructive backward whirl to occur. BBSim can successfully simulate forward and backward whirl depending on the system parameters.

To summarize the contributions of this research:

- A more comprehensive model of a cross-coupled flexible rotor-AMB-BB system [53];
- A method to obtain repeatable experimental results [54];
- Two methods for quantifying the severity of a rotor delevitation event (RDQ and $Vval$) [54,55];
- Simulation of forward whirl [53].

8.6 Closure

The goal of this research was to enable the simulation of a rotor delevitation event and to quantify the resulting motion of the rotor within the BB clearance. This has been accomplished. The presented research could be used in various ways to minimize the uncertainty when working with BBs and to further the application of AMB technology.

Bibliography

[1] R. G. Kirk and T. Ishii, "Transient Rotor Drop Analysis of Rotors Following Magnetic Bearing Power Outage," in *MAG'93 Magnetic Bearings, Magnetic Drives and Dry Gas Seals Conference and Exhibition*, Alexandria, VA, USA, 1993, pp. 53-61.

[2] G. Schweitzer, "Applications and Research Topics for Active Magnetic Bearings," in *IUTAM Symposium on Emerging Trends in Rotor Dynamics*, Delhi, India, 2011, pp. 263-273.

[3] D. E. Bentley, "In pursuit of better bearings," *Orbit*, vol. 2, pp. 33-42, 2000.

[4] G. Schweitzer, "Safety and Reliability Aspects for Active Magnetic Bearing Applications - A Survey," *Proceedings of the Institution of Mechanical Engineers, Part I: Journal of Systems and Control Engineering*, vol. 219, no. 6, pp. 383-392, 2005.

[5] J. C. Ji, C. H. Hansen, and A. C. Zander, "Nonlinear Dynamics of Magnetic Bearing Systems," *Journal of Intelligent Material Systems and Structures*, vol. 19, no. 12, pp. 1471-1491, September 2008.

[6] J. W. Zu and Z. Ji, "An Improved Transfer Matrix Method for Steady-State Analysis of Nonlinear Rotor-Bearing Systems," *Journal of Engineering for Gas Turbines and Power*, vol. 124, no. 2, pp. 303-311, 2002.

[7] E. N. Cuesta, L. U. Medina, V. R. Rastelli, N. I. Montbrun, and S. E. Diaz, "A Simple Kinematic Model for the Behaviour of a Magnetically Levitated Rotor Operating in Overload Regime," in *Proceedings of ASME Turbo Expo*, Atlanta, Georgia, USA, 2003.

[8] J. Schmied and J. C. Pradetto, "Behaviour of a One Ton Rotor Being Dropped Into Auxiliary Bearings," in *Proceedings of Third International Symposium on Magnetic Bearings*, Alexandria, VA, USA, 1992.

[9] L. P. Tessier, "The Development of an Auxiliary Bearing Landing System for a Flexible AMB Supported Hydrogen Process Compressor Rotor," in *Proceedings of MAG '97, Industrial Conference & Exhibition on Magnetic Bearings*, Alexandria, VA, USA, 1997.

[10] M. T. Caprio, B. T. Murphy, and J. D. Herbst, "Spin Commissioning and Drop Tests of a 130 kW-Hr Composite Flywheel," in *Proceedings of the ninth International Symposium on Magnetic Bearings*, Lexington, KY, USA, 2004.

[11] A. Kärkkäinen, M. Helfert, B. Aeschlimann, A. Mikkola, and J. Sopanen, "Effect of Misalignment of Retainer Bearings on Dynamic Responses of Rotor System during Emergency Stop," in *Proceedings of the ASME 2007 International Design Engineering Technical Conferences & Computers and Information in Engineering Conference*, Las Vegas, NV, USA, 2007.

[12] L. Hawkins, A. Filatov, S. Imani, and D. Prosser, "Test Results and Analytical Predictions for Rotor Drop Testing of an Active Magnetic Bearing Expander/Generator," *Journal of engineering for gas turbines and power*, vol. 129, no. 2, pp. 522-529, April 2007.

[13] M. Chen, J. Walton, and H. Heshmat, "Test of a Zero Clearance Auxiliary Bearing," in *Proceedings of the MAG '97 Industrial Conference and Exhibition on Magnetic Bearings*, Alexandria, VA, 1997.

[14] H. M. Chen, J. Walton, and H. Heshmat, "Zero clearance auxiliary bearings for magnetic bearing systems," in *ASME Turbo Expo*, Orlando, FL, USA, 1997.

[15] D. Ransom, A. Masala, J. Moore, G. Vannini, and M. Camatti, "Numerical and Experimental Simulation of a Vertical High Speed Motorcompressor Rotor Drop onto Catcher Bearings," in *11th International Symposium on Magnetic Bearings*, Nara, Japan, 2008, pp. 136-143.

[16] R. Markert and G. Wegener, "Transient Vibration of Elastic Rotors in Retainer Bearings," in *Proceedings of ISROMAC-7*, Hawaii, Honolulu, 1998, pp. 764-774.

[17] H. Olsson, K. J. Åström, C. Canudas de Wit, M. Gäfvert, and P. Lischinsky, "Friction Models and Friction Compensation," *European Journal of Control*, vol. 4, no. 3, pp. 176-195, 1998.

[18] P. Dietl, J. Wensing, and G. C. Nijen, "Rolling Bearing Damping for Dynamic Analysis of Multi-body Systems—Experimental and Theoretical Results," *Proceedings of the Institution of Mechanical Engineers, Part K: Journal of Multi-body Dynamics*, vol. 214, no. 1, pp. 33-43, September 1999.

[19] J. Sopanen and A. Mikkola, "Dynamic Model of a Deep-Groove Ball Bearing Including Localized and Distributed Defects. Part 1: Theory," *Proceedings of the Institution of Mechanical Engineers, Part K: Journal of Multi-body Dynamics*, vol. 217, no. 3, pp. 201-211, 2003.

[20] J. Sopanen and A. Mikkola, "Dynamic Model of a Deep-Groove Ball Bearing Including Localized and Distributed Defects. Part 2: Implementation and Results," *Proceedings of the Institution of Mechanical Engineers, Part K: Journal of Multi-body Dynamics*, vol. 217, no. 3, pp. 213-223, 2003.

[21] J. Jiang, H. Ulbrich, and A. Chavez, "Improvement of rotor performance under rubbing conditions through active auxiliary bearings," *International Journal of Non-Linear Mechanics*, vol. 41, no. 8, pp. 949-957, 2006.

[22] J. C. Ji and C. H. Hansen, "Approximate Solutions and Chaotic Motions of a Piecewise Nonlinear-Linear Oscillator," *Chaos, Solitons & Fractals*, vol. 20, no. 5, pp. 1121-1133, 2004.

[23] C. V. S. Villa, J. Sinou, and F. Thouverez, "The Invariant Manifold Approach Applied to Nonlinear Dynamics of a Rotor-Bearing System," *European Journal of Mechanics A/Solids*, vol. 24, no. 4, pp. 676-689, 2005.

[24] Y. A. Amer and U. H. Hegazy, "Resonance Behaviour of a Rotor-Active Magnetic Bearing with Time-Varying Stiffness," *Chaos, Solitons & Fractals*, vol. 34, no. 4, pp. 1328-1345, 2007.

[25] C. V. S. Villa, J. Sinou, and F. Thouverez, "Investigation of a Rotor- Bearing System with Bearing Clearances and Hertz Contact by Using a Harmonic Balance Method," *Journal of the Brazilian Society of Mechanical Sciences & Engineering*, vol. 29, no. 1, pp. 14-20, 2007.

[26] G. von Groll and D. J. Ewins, "The harmonic balance method with arc-length continuation in rotor/stator contact problems," *Journal of Sound & Vibration*, vol. 241, no. 2, pp. 223-233, 2001.

[27] G. T. Flowers, H. Xie, and S. C. Sinha, "Dynamic Behaviour of a Magnetic Bearing Supported Jet Engine Rotor with Auxiliary Bearings," in *First Industry/Academy Symposium on Research for Future Supersonic and Hypersonic Vehicles. Applications, Design, Development, and Research*, Greensboro, NC, USA, 1994, pp. 399-401.

[28] P. S. Keogh, M. O. T. Cole, M. N. Sahinkaya, and C. R. Burrows, "On the Control of Synchronous Vibration in Rotor/Magnetic Bearing Systems Involving Auxiliary Bearing Contact," *Journal of Engineering for Gas Turbines & Power*, vol. 126, no. 2, pp. 366-372, 2004.

[29] M. N. Sahinkaya, A. G. Abulrub, and P. S. Keogh, "On the Modelling of Flexible Rotor/Magnetic Bearing Systems when in Contact with Retainer Bearings," in *Proceedings of the Ninth International Symposium on Magnetic Bearings*, Lexington, KY, USA, 2004.

[30] A. G. Abulrub, M. N. Sahinkaya, P. S. Keogh, and C. R. Burrows, "Effective Model Reduction for Magnetically Levitated Flexible Rotors Including Contact Dynamics," in *ASME 2005 International Design Engineering Technical Conferences and Computers and Information in Engineering Conference*, Long Beach, CA, 2005.

[31] G. Sun, "Rotor drop and following thermal growth simulations using detailed auxiliary bearing and damper models," *Journal of Sound & Vibration*, vol. 289, no. 1, pp. 334-359, 2006.

[32] A. Kärkkäinen, J. Sopanen, and A. Mikkola, "Transient Simulation of AMB Supported Electric Motor during Rotor Drop on Retainer Bearings," Lappeenranta University of Technology, Lappeenranta, Research Report 2006.

[33] A. Kärkkäinen, "Dynamic Simulations of Rotors During Drop on Retainer Bearings," Lappeenranta University of Technology, Lappeenranta University of Technology, Lappeenranta, Finland, PhD Thesis 2007.

[34] S. Braut et al., "Dynamic Analysis of the Rotor-Stator Contact due to Blade Loss," in *proceeding of the Twelfth World Congress in Mechanism and Machine Science*, Besançon, France, 2007.

[35] N. Bachschmid, P. Pennacchi, and A. Vania, "Thermally Induced Vibrations due to Rub in Real Rotors," *Journal of Sound & Vibration*, vol. 299, no. 4, pp. 683-719, 2007.

[36] M. N. Sahinkaya, A. G. Abulrub, and P. S. Keogh, "Performance of Synchronous Controllers for Rotor Magnetic Bearing Systems Under Retainer Bearing Contact," in *The Seventh International Conference on Motion and Vibration Control (MOVIC'04)*, St. Louis, MO, USA, 2004, pp. 8-11.

[37] G. Sun, A. B. Palazzolo, A. Provenza, and G. Montague, "Detailed Ball Bearing Model for Magnetic Suspension Auxiliary Service," *Journal of Sound & Vibration*, vol. 269, no. 3, pp. 933-963, 2004.

[38] L. Půst, "Weak and strong nonlinearities in magnetic bearings," *Mechanism & Machine Theory*, vol. 39, no. 7, pp. 779-795, 2004.

[39] A. Kärkkäinen, J. Sopanen, and A. Mikkola, "Dynamic Simulation of a Flexible Rotor during Drop on Retainer Bearings," *Journal of Sound & Vibration*, vol. 306, no. 3, pp. 601–617, July 2007.

[40] S. Popprath and H. Ecker, "Nonlinear Dynamics of a Rotor Contacting an Elastically Suspended Stator," *Journal of Sound & Vibration*, vol. 308, no. 3, pp. 767-784, 2007.

[41] R. G. Kirk, K. V. S. Raju, and E. E. Swanson, "Evaluation of AMB Turbomachinery Auxiliary Bearings," *Journal of vibration & acoustics*, vol. 121, no. 2, pp. 156-161, 1999.

[42] A. A. Younan, T. W. Dimond, and P. E. Allaire, "Transient Drop Analysis of Auxiliary Bearings in Fluid Film/Magnetic Bearing Supported Rotor," in *11th International Symposium on Magnetic Bearings*, Nara, Japan, 2008, pp. 160-167.

[43] Y. Ishida and T. Inoue, "Vibration Characteristics of a Rotor System in Contact with a Backup Bearing: Cases with Various Failure Patterns of the Active Magnetic Bearing," *Journal of Vibration and Control*, vol. 14, no. 4, pp. 571-589, 2008.

[44] L. Xie, R. Nordmann, and B. Aeschlimann, "Numerical Investigation of AMB Supported Rotor Interaction with Auxiliary Bearing," in *11th International Symposium on Magnetic Bearings*, Nara, Japan, 2008, pp. 406-411.

[45] M. Orth and R. Nordmann, "ANEAS, a Modelling Tool for Nonlinear Analysis of Active Magnetic Bearing Systems," in *Proceedings of the IFAC Conference of Mechatronic Systems*, Berkeley, CA, USA, 2002.

[46] L. E. Stacke, D. Fritzson, and P. Nordling, "BEAST-a Rolling Bearing Simulation Tool," *Proceedings of the Institution of Mechanical Engineers, Part K: Journal of Multi-body Dynamics*, vol. 213, no. 2, pp. 67-71, 1999.

[47] L. E. Stacke and D. Fritzson, "Dynamic Behaviour of Rolling Bearings: Simulations and Experiments," *Proceedings of the Institution of Mechanical Engineers, Part J: Journal of Engineering Tribology*, vol. 215, no. 6, pp. 499-508, 2001.

[48] J. Wilkes, J. Moore, D. Ransom, and G. Vannini, "An improved catcher bearing model and an explanation of the forward whirl/whip phenomenon observed in active magnetic bearing transient drop experiment," in *Proceedings of ASME Turbo Expo 2013: Turbine Technical Conference and Exposition*, San Antonio, TX, USA, 2013.

[49] Mathworks. (2010, August) Matlab Central. [Online]. http://www.mathworks.com/matlabcentral/fileexchange/28563-rotor-dynamics-toolbox-rotfe

[50] I. Bucher, "RotFE The finite element rotor analysis package," Faculty of mechanical engineering, Technion, Haifa, User manual 2000.

[51] S. Myburgh, G. van Schoor, and E. O. Ranft, "A Non-linear Simulation Model of an Active Magnetic Bearings Supported Rotor System," in *International Conference on Electrical Machines*, Rome, Italy, 2010.

[52] E. O. Ranft, "The development of a flexible rotor active magnetic bearing system," North West University, Potchefstroom, Masters' thesis 2005.

[53] J. J. Janse van Rensburg, G. van Schoor, and P. A. van Vuuren, "Delevitation modelling of an active magnetic bearing supported rotor," in *Proceedings of the 12th International Symposium on Magnetic Bearings (ISMB12)*, Wuhan, China, 2010.

[54] C. Vanek, F. Worlitz, J. J. Janse van Rensburg, and G. van Schoor, "Experimentelle und theoretische Untersuchungen zum Rotorabsturz in Wälzlager," in *Workshop Magnetlagertechnik Zittau-Chemnitz*, Zittau, 2011, pp. 97-101.

[55] J. J. Janse van Rensburg, G. van Schoor, and P. A. van Vuuren, "The characterization of the severity of rotor delevitation events - A parametric study," in *Proceedings of the 13th International Symposium on Magnetic Bearings (ISMB13)*, Arlington, VA, USA, USA, 2012.

[56] S. Myburgh, "The development of a fully suspended AMB system for a high-speed flywheel application," North West University, Potchefstroom, Masters' thesis 2007.

[57] SKF. (2006, April) Magnetic bearings. [Online]. http://www.skf.com/group/products/magnetic-systems/technology-key-benefits/active-magnetic-bearings/index.html

[58] R. Larsonneur, "Design and control of active magnetic bearing systems for high speed rotation," Swiss Federal Institute of Technology, Zurich, Ph. D thesis 1990.

[59] J. J. Janse van Rensburg, "Development of a flywheel energy storage system –uninterrupted power supply (FLY-UPS)," North-West University, Potchefstroom, Masters' thesis 2007.

[60] E. N. Cuesta, V. R. Rastelli, L. U. Medina, N. I. Montbrun, and S. E. Diaz, "Non-Linear Behaviours in the Motion of a Magnetically Supported Rotor on the Catcher Bearing During Levitation Loss, an Experimental Description," in *Proceedings of the ASME Turbo Expo*, Amsterdam, The Netherlands, 2002.

[61] T. Ishii and R. G. Kirk, "Analysis of Rotor Drop on Auxiliary Bearings Following AMB Failure," in *ROMAG 91. Conference on Magnetic Bearings and Dry Gas Seals*, Washington, DC, USA, 1991.

[62] T. Ishii and R. G. Kirk, "Transient Response Technique Applied to Active Magnetic Bearing Machinery During Rotor Drop," *ASME Journal of Vibration and Acoustics*, vol. 118, no. 2, pp. 154-163, April 1996.

[63] Y. Guojun, W. Li, Z. Lei, and Y. Suyuan, "Preliminary Scheme Design and Analysis of Catcher Bearing for HTR-10GT," in *Proceedings of the Second International Meeting on High Temperature Reactor Technology*, Beijing, China, 2004.

[64] M. Helfert, M. Ernst, R. Nordmann, and B. Aeschlimann, "High-Speed Video Analysis of Rotor-Retainer-Bearing-Contacts due to Failure of Active Magnetic Bearings," in *Proceedings of the 10th International Symposium on Magnetic Bearings*, Martigny, Switzerland, 2006.

[65] S. R. Penfield and E. Rodwell, "Auxiliary Bearing Design Considerations for Gas-Cooled Reactors," International Atomic Energy Agency, Palo Alto, USA, Report of a technical committee meeting (TCM) on Gas Turbine Power Conversion Systems for Modular HTGRs 2001.

[66] J. M. Vance, *Rotordynamics of Turbomachinery*. New York, NY, USA: WILEY, 1988.

[67] P. McMullen, V. Vuong, and L. Hawkins, "Flywheel Energy Storage System with AMB's and Hybrid Backup Bearings," in *Tenth International Symposium on Magnetic Bearings*, Martigny, Switzerland, 2006.

[68] E. V. Karpenko, M. Wiercigroch, and M. P. Cartmell, "Regular and Chaotic Dynamics of a Discontinuously Nonlinear Rotor System," *Chaos, Solitons & Fractals*, vol. 13, no. 6, pp. 1231-1242, 2002.

[69] R. G. Kirk, E. J. Gunter, and W. J. Chen, "Transient Rotor Drop Evaluation of AMB Machinery," in *NEDO-ISO Joint Workshop*, Ibaraki, Japan, 2004.

[70] P. S. Keogh and M. O. T. Cole, "Contact Dynamic Response With Misalignment in a Flexible Rotor/Magnetic Bearing System," *Journal of Engineering for Gas Turbines and Power*, vol. 128, no. 2, pp. 362-369, 2006.

[71] M. Kotzalas, *Advanced concepts of bearing technology: rolling bearing analysis*, 5th ed. New York, USA: Taylor & Francis, 2006.

[72] American Society for Metals, *ASM Handbook: Volume 18: Friction, Lubrication, and Wear Technology*, 10th ed., Peter J Blau, Ed. New York, NY, USA: ASM International, 1992.

[73] P. J. Blau, *Friction Science and Technology: From Concepts to Applications*, 2nd ed. New York, NY, USA: CRC Press, 2008.

[74] E. E. Swanson, R. G. Kirk, and J. Wang, "AMB rotor drop initial transient on ball and solid bearings," in *Proceedings of MAG '95: Magnetic Bearings, Magnetic Drives, and Dry Gas Seals Conference & Exhibition*, Alexandria, VA, USA, 1995, pp. 207-216.

[75] S. Zeng, J. Q. Zhang, and H. N. Wang, "Transient response of active magnetic bearing rotor during rotor drop on backup bearings," *Proceedings of the Institution of Mechanical Engineers, Part C: Journal of Mechanical Engineering Science*, vol. 220, no. 6, pp. 785-794, February 2006.

[76] M. Orth, R. Erb, and R. Nordmann, "Investigations of the Behaviour of a Magnetically Suspended Rotor during Contact with Retainer Bearings," in *Proceedings of the Seventh International Symposium on Magnetic Bearings*, Zurich, Switzerland, 2000.

[77] E. E. Swanson and H. Heshmat, "Oil Free Foil Bearings as a Reliable, High Performance Backup Bearing for Active Magnetic Bearings," *Journal of Engineering for Gas Turbine and Power*, vol. 124, no. 2, pp. 375-381, 2002.

Appendix A

Table of the capabilities of BBSim

In this appendix, the detail of each of the capabilities and limitations of BBSim is discussed and explained. A short description of the principles on which each of the capabilities operate is given. In Table 7, the description of the capability is given in the first column, the second and third column is marked with an 'X' depending on whether that specific capability is included or not and the forth column describes the detail regarding that specific capability.

Table 7: Model capabilities and limitations

Capability description	Included in the model	Excluded from the model	Comments
Flexible rotor	X		Use RotFE for the rotor model
Rigid rotor		X	Could be implemented but deemed unnecessary
Unbalance	X		Unbalance is modelled as a force vector in phase with the rotational speed of the rotor. Within RotFE the unbalance can be of any magnitude at any location on the rotor (more than one unbalance can be specified at different locations on the rotor).
Friction	X		Coulomb friction $\left(F_{Friction} = \mu_{material} \cdot F_{normal}\right)$ is used since all of the current literature relevant to this research suggests that Coulomb friction is a sufficient approximation of reality. Friction is used to cross-couple the different axis of a BB, and to calculate the inner-race speed-up and rotor speed-down.
Rotor braking (resistor bank)	X		The active braking of the rotor is modelled by applying a constant torque on the rotor at the motor location decelerating the rotor. (The model does not yet include the UMP – unbalance magnetic pull).
Rotor braking (friction)	X		Passive braking due to the friction on the inner-race and rotor as well as the rolling friction of the BB itself. The friction force is converted to a torque that is applied to the rotor. This is a non-linear braking torque and depends on the magnitude of the normal force and the current speed of the BB.
Rotor braking (Windage)	X		Windage (aerodynamic) braking is included in this simulation although it needs to be determined using empirical methods as described in Section 4.5.
Stator dynamics	X		The dynamics of the stator is included by using all of the masses and stiffnesses between the contact area and the rigid connection to the ground.(Still needs to be implemented).

Inner-race acceleration	X		The inner-race acceleration is calculated by using the moment of inertia of the rotor and the inner-race and balls. The moment of inertia of the inner-race and balls are significantly smaller than the inertia of the rotor the inner-race accelerates significantly more than the rotor decelerates due to the contact.
Non-linear damping (elastomeric)	X		Elastomeric damping is simulated by approximating the elastomer characteristics by using a representative model. Here either a combination of stiffnesses and dampers in parallel and series are used or a sample piece, characterized using simple impact tests and deducing an LTI-model from the experimental data.
Non-co-location (AMB)	X		Co-location is the effect of sensing the rotor position at another location than where the AMB's is situated, not measuring the true displacement on the actuator location. The model has the ability to sense the position at a certain location and use this position data to determine the force necessary to correct the position, and then apply this force in another location.
Non-linear AMB model	X		The AMB model included in this simulation is a non-linear model that was previously developed by S. Myburgh [51].
Linear AMB model	X		A linear AMB-model can also be used to speed up the simulation process (the linear model is simply a stiffness and damping coupled in parallel).
Load-sharing (AMB/BB)	X		Using either of the above mentioned models load sharing between the AMB and the BB can be simulated. The AMB is still trying to control the rotor position but the force needed is higher than the AMB is capable of exerting on the rotor. The rotor makes contact with the BB and the BB exerts a force on the rotor.
Any number of BBs	X		Some systems in the industry uses 3 or 4 BBs but all of the rotor-drop models only simulates one or two BBs this model can simulate any number of BBs.
Non-identical BBs	X		The BBs can be identical or non-identical, the model can also model different stator characteristics (stiffness damping and mass of the unit) at each of the BB locations.
Identical BBs	X		Identical BBs can also be modelled.
Thermal analysis		X	A detailed thermal analysis is not included. An increase in temperature would cause thermal growth increasing the preload on the BBs, the effect of this thermal growth is neglected because it is foreseen that this will not have a great effect on the rotor-bearing behaviour and for computational effectiveness.
Transient	X		The model is transient and speed-up and speed-down tests can be done on either the BBs or the AMBs or both.
Steady-state	X		Steady-state simulations can be done on only the AMBs by keeping the rotational speed constant for a sufficiently long time.

Frequency domain simulation		X	This model is not a frequency-domain simulation, but some frequency domain data can be obtained by some post-processing.
Plain BBs	X		The model can simulate the behaviour of plain (bush-type) BBs by setting the inner-race inertia to infinite or by setting the inner-race speed to zero.
Rolling element BBs	X		Rolling element BB is simulated as stated earlier.
Impact analysis	X		The impact of the rotor onto the BBs and all the associated forces are modelled.
Simulating contacting state	X		The model allows for a contact and non-contact state of the rotor or a high frequency chattering between these 2 states.
Simulating non-contacting state	X		
BB-misalignment	X		Work still needed to achieve this in the model.
BB defects		X	BB defects such as brinelling, pitting and ball-sliding are not modelled.
Air-gap modelling	X		The airgap is modelled by using a non-linear stiffness and damping (for a certain displacement the stiffness and damping is set to zero).
Sudden unbalance (blade-loss simulation)	X		Sudden unbalance or blade-loss simulation is achieved by adding to the unbalance at a predefined point in time. Thus simulating the effect of a piece of the rotor breaking free and causing a sudden unbalance.
Axial BB modelling		X	The axial BB is not included in this model, a simple impact model could be included but the cross-coupling of the axial BB to the radial BB is foreseen as a problem area, for a first iteration the rotor is assumed to be axially static during a rotor drop. This assumption is close to the real life situation that occurs in a horizontally mounted machine with no axial load.
Vertical machine	X		The gravitational acceleration is set to zero although the effect of the axial BB and its associated forces on the rotor behaviour would be absent, the model would still be useful for estimation purposes.
Horizontal machine	X		The simulation of a vertical machine is done by setting the gravity acceleration in the direction of the gravity force to g.

Appendix B

The failure modes of AMBs

Table 8: Failure modes of AMBs as defined in [77]

Failure Mode	Description
1	Vertical AMB position signal goes to full scale. This simulates a malfunction wherein the vertical sensor electrical continuity is lost through damage to the cable or sensor thus causing an erroneous full scale output from the sensor signal conditioner.
2	Horizontal AMB position signal goes to full scale. This simulates a malfunction wherein the AMB's horizontal sensor electrical continuity is lost through damage to the cable or sensor causing an erroneous full-scale output from the sensor signal conditioner.
3	Both vertical and horizontal position signals go to full scale. This simulates a malfunction wherein the electrical continuity is disrupted to both the vertical and horizontal control sensors causing an erroneous full-scale output from both sensor signal conditioners.
4	Vertical position signal goes to zero. This simulates any malfunction where the vertical position feedback becomes zero.
5	Horizontal position signal goes to zero. This simulates any case where the horizontal position feedback to the AMB controller becomes zero
6	Horizontal and vertical position signals go to zero. This simulates any case where both position feedbacks to the AMB controller becomes zero causing both the vertical and horizontal position feedback signals to become zero.
7	Horizontal left PWM amplifier is disabled (no current to the two left coils). This simulates any malfunction that results in disruption of current to this coil as well as loss of continuity in the coil.
8	Both horizontal PWM amplifiers (left and right) are disabled (no current to any horizontal coil). This simulates any malfunction that results in disruption of current to these coils as well as loss of continuity in the coils.
9	Vertical top PWM amplifier is disabled (no current to the two top coils). This simulates any malfunction that results in disruption of current to this coil as well as loss of continuity in the coil.
10	Top and bottom vertical PWM amplifiers are disabled (no current to any vertical axis coil). This simulates any malfunction that results in disruption of current to these coils as well as loss of continuity in the coils.
11	Bias PWM amplifier is disabled (no current to the bias coil). This simulates any malfunction that results in disruption of current to this coil as well as loss of continuity in the coil.
12	All four control amplifiers (no current to any control coil) are disabled but bias remains active. This simulates any malfunction that results in disruption of current to these coils as well as loss of continuity in the coils.
13	All four PWM amplifiers and the bias current are disabled (no current to any coil). This simulates any malfunction that results in disruption of current to these coils as well as loss of continuity in the coils.

Appendix C

Appendix DVD

The following is included in the accompanying DVD. Unfortunately, the data from the simulations could not be included since these files amount to a size of 850 GB. Should the data be required, please send an e-mail to 12297348@nwu.ac.za and request the applicable data.

C.1 PhD Thesis including Appendix C.5 and C.6
C.2 Simulink models
C.3 Empirical studies code
C.4 *RDQ* and *Vval* code
C.5 Results of simulated rotor delevitation events
- C.5.1 Simulation results with varying stiffness and damping delevitated at 2 692 r/min (Page 41 – 440)
- C.5.2 Simulation results with varying stiffness and damping delevitated at 4 119 r/min (Page 442 – 841)
- C.5.3 Simulation results with varying stiffness and damping delevitated at 5 534 r/min (Page 843 – 1 762)
- C.5.4 Simulation results with varying delevitation r/min, inertia, friction and unbalance (constant stiffness and damping) (Page 1 764 – 1 862)
- C.5.5 Simulation results with varying delevitation r/min (constant inertia, friction, unbalance stiffness and damping) (Page 1 864 – 1 978)

C.6 Results of experimental rotor delevitation events
- C.6.1 Non-lubricated (page 1-55)
- C.6.2 Lubricated (Page 56-105)
- C.6.3 Plain bearings (Page 106-111)

C.7 Published articles
- C.7.1 J. J. Janse van Rensburg, G. van Schoor, and P. A. van Vuuren, "Delevitation modelling of an active magnetic bearing supported rotor," in *Proceedings of the 12th International Symposium on Magnetic Bearings (ISMB12)*, Wuhan, China, 2010.
- C.7.2 C. Vanek, F. Worlitz, J. J. Janse van Rensburg, and G. van Schoor, "Experimentelle und theoretische Untersuchungen zum Rotorabsturz in Wälzlager," in *Workshop Magnetlagertechnik Zittau-Chemnitz*, Zittau, 2011, pp. 97-101.
- C.7.3 J. J. Janse van Rensburg, G. van Schoor, and P. A. van Vuuren, "The characterization of the severity of rotor delevitation events - A parametric study," in *Proceedings of the 13th International Symposium on Magnetic Bearings (ISMB13)*, Arlington, VA, USA, USA, 2012.

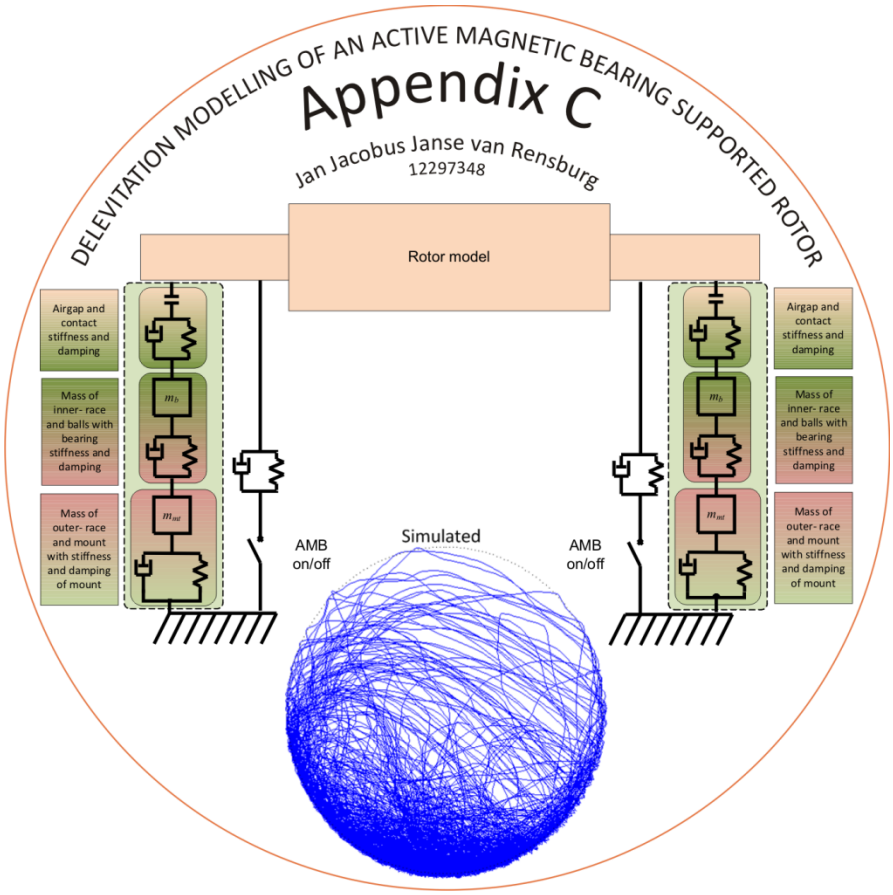
DELEVITATION MODELLING OF AN ACTIVE MAGNETIC BEARING SUPPORTED ROTOR
Appendix C
Jan Jacobus Janse van Rensburg
12297348
Rotor model
Airgap and contact stiffness and damping
Mass of inner- race and balls with bearing stiffness and damping
Mass of outer- race and mount with stiffness and damping of mount
AMB on/off
Simulated
AMB on/off
Airgap and contact stiffness and damping
Mass of inner- race and balls with bearing stiffness and damping
Mass of outer- race and mount with stiffness and damping of mount